DISSERTATION

REG3β limits lymphatic drainage of cardiac leukocytes and improves resolution of myocardial inflammation

Inauguraldissertation zur Erlangung des Grades eines Doktors der Humanbiologie
des Fachbereichs Medizin
der Justus-Liebig-Universität Gießen

vorgelegt von
Almeida Góes, Maria Elisa

aus Rio de Janeiro, Brasilien

Gießen (2024)

Aus dem Fachbereich Medizin der Justus-Liebig-Universität Gießen

Eingereicht am Fachbereich Medizin der Justus-Liebig-Universität Gießen

Erstgutachter/in: Prof. Dr. Jochen Pöling

Zweitgutachter/in: Prof. Dr. Susanne Rohrbach

Tag der Disputation: 06.02.2025

TABLE OF CONTENTS

1. INTRODUCTION

1.1 Cardiovascular diseases: epidemiology and relevance

Cardiovascular diseases lead to approximately one third of all deaths globally (D. Mozaffarian et al., 2016, as cited in Khan et al., 2020). They constitute a major socioeconomic burden, with 1.7 million annual deaths (2021) in the European Union, and an estimated € 282 billion cost every year (Luengo-Fernandez et al., 2023).

The most prevalent cardiovascular disease, myocardial infarction (MI), results from accumulation of oxidized lipids and cholesterol in arterial walls, triggering inflammatory processes, which lead to formation of atherosclerotic plaques. Subsequent rupture of unstable atherosclerotic lesions and subsequent formation of thrombi affects arterial circulation (Palasubramaniam et al., 2019). The interruption of blood flow in coronary arteries can limit nutrient and oxygen delivery to heart tissue, causing rapid cardiomyocyte death (D. Mozaffarian et al., 2016).

The probability of survival of MI patients who are rapidly hospitalized and treated is above 90 % (S. Mozaffarian, et al. 2021a; Smolina et al., 2012). However, the degree of burden that can subsequently lead to heart failure and death varies based on the pathophysiological progression of the disease. Altogether, the molecular, cellular and interstitial changes happening in the heart after an ischemic event lead to cell death and loss of contractile function (Cohn et al., 2000, as cited in Azevedo et al., 2016). Consequently, the infarcted tissue is replaced with a scar, and the left ventricle undergoes changes in size, shape and function (Frantz et al., 2022; Cohn et al., 2000, as cited in Leancă et al., 2022). Among the many factors, which contribute to myocardial healing or heart failure, is an effective immune-inflammatory response (Halade & Lee, 2020; Shirazi et al., 2017).

1.2 Inflammation in the infarcted heart

Cardiac remodeling typically takes place over weeks and is initiated by a chain of inflammatory events, which allows removal of dead tissue and enables reparative pathways, such as revascularization and formation of a granulation tissue and a fibrotic scar (Frangogiannis, 2014, 2018; Frantz et al., 2022).

Currently, researchers define three stages of cardiac remodeling following MI. The inflammatory phase initiates acutely, hours after the ischemic event, and lasts for 4-7 days,

being followed by the proliferative phase, which is concluded after approximately 14 days. These two phases are marked by a dynamic interplay between short-lived leukocytes, while the third (maturation phase) can extend throughout weeks and involves the re-emergence of the inflammatory response (Forte et al., 2018; Prabhu & Frangogiannis, 2016; Weil & Neelamegham, 2019). The experimental work done in this thesis spans the inflammatory and maturation phases of cardiac healing.

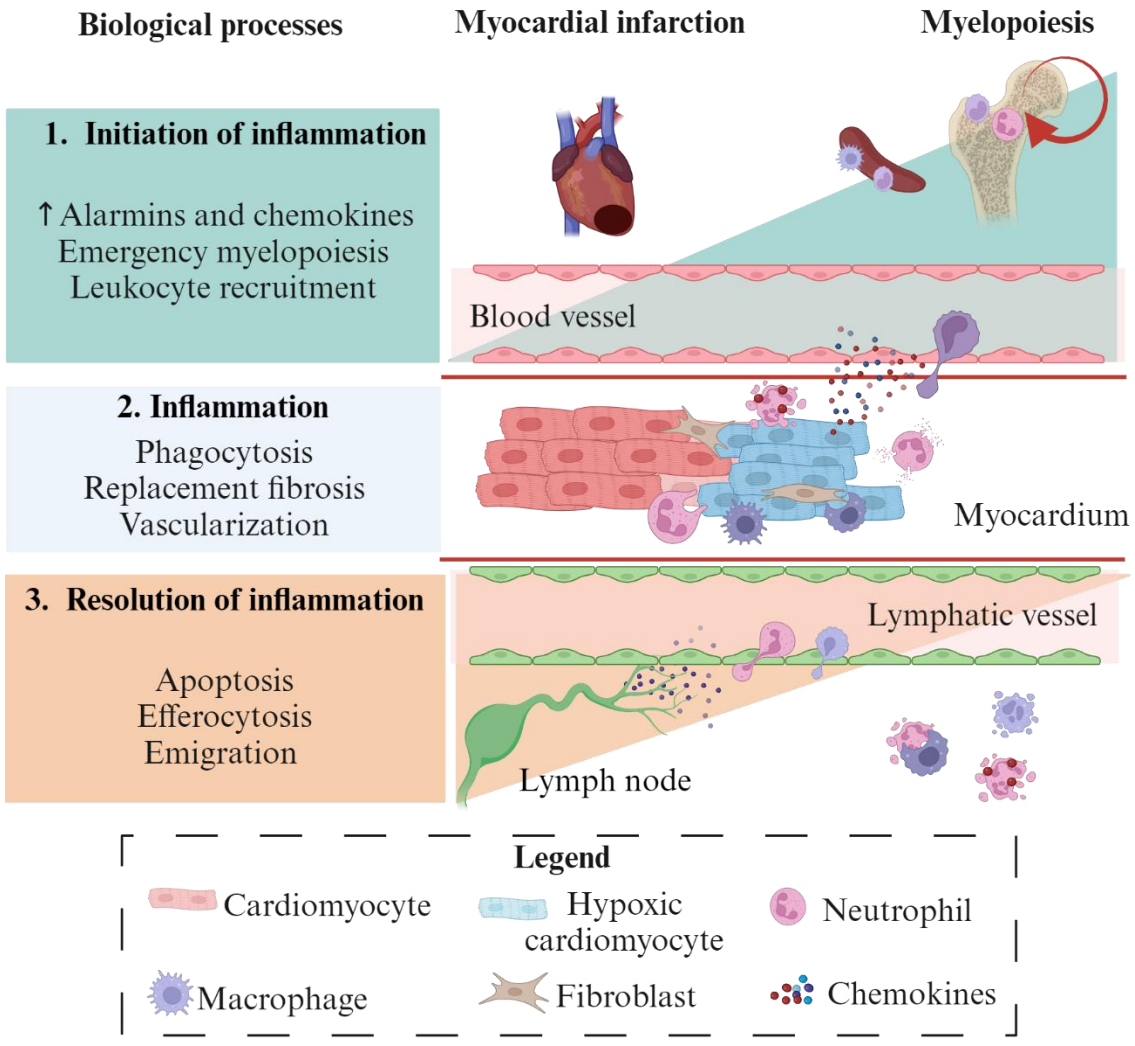

Figure 1. Distinct inflammatory processes after myocardial infarction. Hypoxic cardiomyocytes, tissue-resident immune and non-immune cells initiate inflammation by secreting pro-inflammatory mediators, such as alarmins, chemokines and DAMPs. These factors attract circulating leukocytes to the tissue, which phagocytose dead cardiomyocytes and promote cardiac inflammation. Elevated leukocyte levels are constantly supplied by spleen reservoirs and by the bone marrow, which is undergoing emergency myelopoiesis.

The inflammatory phase must be temporally restricted in order to avoid nonspecific tissue degradation and deleterious remodeling. In the phase of resolution of inflammation, immune cells undergo apoptosis, can be efferocytosed by other phagocytes or leave the site of inflammation through afferent lymphatics, in the direction of mediastinal lymph nodes. Illustration created with "BioRender.com".

Directly after the onset of MI, hypoxic cardiomyocytes release pro-inflammatory mediators, such as alarmins, chemokines and endogenous danger-associated molecular patterns (DAMPs), thereby initiating an immune-inflammatory response **(Fig. 1)** (Forte et al., 2018). In the first few hours after injury, the spleen serves as the primary leukocyte reservoir, providing about 50 % of the immune cells which reach the heart (Swirski et al., 2009, as cited in Sager et al., 2015 and in Poller et al., 2020). Shortly after, the bone marrow (BM) initiates an emergency myelopoiesis programme, generating increased numbers of immune cells, which support the healing process of the infarcted heart (Dutta et al., 2015).

Leukocytes infiltrate from the circulation in waves, and different subsets are preferentially recruited at specific stages of myocardial healing. Innate immune cells – particularly neutrophils and macrophages – massively infiltrate the heart in the first days after onset of MI and coordinate the initial steps of subsequent acute inflammation (Frangogiannis, 2014, 2018).

Neutrophils, although not numerous, are present in the healthy heart tissue and are recruited from the blood upon tissue injury (Ballesteros et al., 2020; Lafuse et al., 2021). Despite being the most abundant circulating leukocytes, neutrophils have a half-life of only 24h in mice (Casanova-Acebes et al., 2018). Therefore, they are constantly produced de novo in the bone marrow through a process called granulopoiesis (Puhl & Steffens, 2019).

Infiltrating neutrophils have a phagocytic nature, important to clear dead cells. Additionally, they release a plethora of inflammatory mediators and proteolytic enzymes, which promote remodeling of the infarcted tissue (Puhl & Steffens, 2019). Despite the traditional belief that neutrophils are detrimental to cardiac healing *per se*, it is now understood that their pro-inflammatory action is needed in timely and spatially-restricted ways, and that they can also have additional anti-inflammatory and pro-reparative effects (Ma, 2021; Puhl & Steffens, 2019; Vafadarnejad et al., 2020).

In contrast to neutrophils, distinct cardiac macrophage populations exist in the resting heart (Epelman et al., 2014). In fact, macrophage functions vary according to their origin

(Epelman et al., 2014; Moskalik et al., 2022). Resident cardiac macrophages mostly derive from the yolk-sac or fetal liver mononuclear progenitors and proliferate locally (Epelman et al., 2014; Lafuse et al., 2021; Y. H. Li et al., 2022; Moskalik et al., 2022). These macrophages typically lack C-C motif chemokine receptor 2 (CCR2), express the glycoprotein Ly6C at low levels ($Ly6C^{lo}$) (Y. H. Li et al., 2022) and are traditionally regarded as cardioprotective (Epelman et al., 2014; Lafuse et al., 2021).

In pro-inflammatory contexts, resident macrophages can be partially replaced by monocyte-derived macrophages, which express Ly6C at high levels ($Ly6C^{hi}$) (Epelman et al., 2014; Moskalik et al., 2022). Monocytes bear the CCR2 receptor and infiltrate the tissue following classic chemokine gradients, such as C-C motif chemokine ligand 2 (CCL2) (Y. H. Li et al., 2022). $CCR2^{+}$ $Ly6C^{hi}$ monocyte-derived macrophages tend to show a proinflammatory cytokine secretion profile, phagocytosing cardiomyoyte debris and promoting collagen deposition (Lafuse et al., 2021; Moskalik et al., 2022).

Monocyte-derived $CCR2^{+}$ $Ly6C^{hi}$ macrophages can also decrease Ly6C expression over time, converting into $CCR2^{+}$ $Ly6C^{lo}$ macrophages (Y. H. Li et al., 2022). Such macrophages foster anti-inflammatory processes by secreting anti-inflammatory cytokines and thereby promoting angiogenesis and collagen deposition (Lafuse et al., 2021; Y. H. Li et al., 2022). $Ly6C^{lo}$ macrophages are therefore predominantly active during the reparative phase, in which they orchestrate revascularization of the infarcted tissue, ensuring that the healing tissue will receive oxygen and nutrient supply (Forte et al., 2018; Frangogiannis, 2014, 2018; Moskalik et al., 2022).

Although acute inflammation is indispensable for stimulating myocardial fibrosis and maintaining cardiac homeostasis, exacerbated responses can have negative consequences for the stability of newly formed fibrotic scars (Puhl & Steffens, 2019). One potential explanation for the sustained inflammatory response in chronic stages of myocardial healing is that innate immune cells promote further inflammatory processes for as long as necessary to restore tissue homeostasis (para-inflammation). If such a process continues beyond a reversible point, restoration of left ventricular function becomes compromised, giving way to collateral tissue damage and heart failure (Adamo et al., 2020).

For instance, neutrophil activity depends largely on the degranulation and release of a plethora of enzymes and complement factors, which induce the proteolytic breakdown of

necrotic cardiomyocytes. However, prolonged neutrophil activity can cause maladaptive remodeling, due to excessive release of reactive oxygen species (ROS), cytokines and enzymes. Combined, these can promote infarct expansion, cardiac rupture and death (Puhl & Steffens, 2019; K. Sun et al., 2021). Therefore, (especially, but not only) neutrophil activity must be mitigated in order to ensure myocardial healing with minimal adverse remodeling.

Different mechanisms ensure that the inflammation subsides within a limited period of time, enabling the transition from the inflammatory to the proliferative phase of cardiac healing (Prabhu & Frangogiannis, 2016). In fact, most leukocytes have a relatively short half-life, undergoing programmed cell death (apoptosis) after a few days (Halade & Lee, 2022). Apoptosis may take place in the scar itself, or in other organs. For example, neutrophils can undergo apoptosis in the heart tissue and be removed by other phagocytes, such as macrophages, in a process called efferocytosis (Y. Li et al., 2021; Sansonetti et al., 2020). Alternatively, senescent neutrophils may be drained from the heart and migrate ("home") to the bone marrow in a CXCR4 (C-X-C motif chemokine receptor 4)-dependent manner. The C-X-C motif ligand 12 (CXCL12), which is expressed in high levels in the bone marrow stroma (Eash et al., 2009), plays an important role in this process. Once in the bone marrow, senescent neutrophils are removed by resident stromal macrophages (Eash et al., 2009; Martin et al., 2003; Suratt et al., 2004, as cited in Casanova-Acebes et al., 2013).

Immune cell homing to the bone marrow not only ensures their clearance but also serves as an important communication bridge between the infarcted heart and the bone marrow (Puhl & Steffens, 2019). Parabiosis studies have shown that inflammasome-activated neutrophils migrate from the infarcted heart towards the bone marrow and directly amplify myelopoiesis/granulopoiesis through the local delivery of cytokines (primarily interleukin-1β, or IL-1β) (Sager et al., 2015; Sreejit et al., 2020, 2022). IL-1β binds to its receptor on myeloid precursors and stimulate myelopoiesis, ensuring that the heart demands for leukocytes will be met, or, alternatively, downregulated, when the acute inflammatory phase is over (Sreejit et al., 2022). Besides IL-1β, other inflammatory mediators, such as granulocyte-macrophage colony-stimulating factor (G-CSF, or CSF-3) and CCL2 also act on hematopoietic progenitors to promote myelopoiesis and release leukocytes into the circulation (Anzai et al., 2017; Dutta et al., 2015; Poller et al., 2020).

Beyond that, one further mechanism ensuring timely resolution of inflammation is the spatial removal of leukocytes from the site of inflammation, through afferent lymphatics. In the last decades, different studies have independently shown that lymphatic vessels respond to injury and actively enable resolution of inflammation (Henri et al., 2016; Shimizu et al., 2018; Vieira et al., 2018). In order for this to happen, lymphatic vessels present in the hypoxic myocardium secrete chemokines (e.g. C-C motif chemokine ligand 21, or CCL21) which attract leukocytes expressing the corresponding C-C motif chemokine receptor 7 (CCR7) into their lumen and towards the mediastinal lymph nodes (Vieira et al., 2018).

1.3 The lymphatic system

The lymphatic system is a part of the immune system, as well as a complementary component of the circulatory system. Structurally, it is composed of lymphatic capillaries, lymphatic collecting vessels and lymphoid organs, such as the lymph nodes, spleen, thymus, bone marrow and mucosa-associated lymphoid tissue (Olszewski, 2003).

The main function of lymphatic vessels is to collect interstitial extravasated plasma, macromolecules and cells, which were not recovered by venous capillaries. In humans, this volume adds up to 3 liters every 9 hours (Levick & Michel, 2010, as cited in Harris et al., 2023). Once inside lymphatic vessels, this rich mixture is called lymph, and it is returned to the blood via venous circulation in the subclavian and jugular veins (Aspelund et al., 2014, 2016). Accordingly, lymphatic malfunction causes lymphedema – an abnormal interstitial fluid accumulation –, which stresses the importance of lymphatics in keeping tissue homeostasis (Rockson, S.G. 2021).

Accumulation of interstitial fluid, or edema, is a hallmark of inflammation and results from leaky blood endothelial vessels (Hellenthal et al., 2022). The increase in interstitial fluid pressure and the accumulation of inflammatory mediators stimulate proliferation of lymphatic vessels, which in turn ensures tissue fluid homeostasis and immune cell clearance (S. Liao & Von Der Weid, 2014; Schwager & Detmar, 2019). In analogy to the name given to blood vessel proliferation (angiogenesis), de novo formation of lymphatic vessels is called lymphangiogenesis.

The molecular pathways promoting lymphangiogenesis in homeostasis and disease have been thoroughly dissected in the last decades. Seminal studies performed by Dr. Kari

Alitalo and his research group enabled the current understanding on this topic. Among the most important achievements was the identification of vascular endothelial growth factor C (VEGF-C) (Joukov et al., 1996, 1997) and vascular endothelial growth factor D (VEGF-D) (Achen et al., 1998) as the most potent pro-lymphangiogenic factors.

These factors belong to the VEGF family of ligands and bind to receptor tyrosine kinases with cognate names (VEGFRs) **(Fig. 2)**. VEGF-A – the most well-known factor of this family – drives, together with VEGF-B, vascular endothelial proliferation (Ferrara et al., 1992). However, VEGF-C and VEGF-D mostly act on VEGFR3 (highly expressed in lymphatic endothelial cells), whereas VEGF-A and -B have strong affinity for VEGFR1 and VEGFR2 (rather expressed on blood endothelial vessels) (Pandey et al., 2018).

With additional years of research, genetic, biotechnological and pharmacological tools to block or stimulate VEGFR3 activity were developed. For example, mouse lines with a conditional genetic deletion of *Vegfr3 (Prox1-Cre^{ERT2} Vegfr3$^{fl/fl}$), Vegfc (Prox1-Cre^{ERT2} Vegfc$^{fl/fl}$)*, and germline deletion of *Vegfd (Vegfd$^{-/-}$)* allow the spatial and temporal blockage of lymphangiogenesis, without impacting developmental stages (Aspelund et al., 2014; Baldwin et al., 2005; Haiko et al., 2008). Pharmacologically, the inhibitors MAZ51 and SAR131675 selectively inhibit VEGFR3 activity with little off-targets (Alam et al., 2012; Kirkin et al., 2004). Moreover, overexpression of a soluble VEGF-C trap (sVEGFR3) limits the availability of this ligand, resulting in impaired lymphangiogenesis (Antila et al., 2017).

Furthermore, selective stimulation of VEGFR3 can be obtained by local or systemic delivery of VEGF-C$_{C165S}$, an engineered isoform, which has negligible affinity for VEGFR2 (Joukov et al., 1996). Alternatively, AAV-VEGF-C$_{C165S}$ delivery allows overexpression of this ligand and enhanced receptor stimulation (Saaristo et al., 2002).

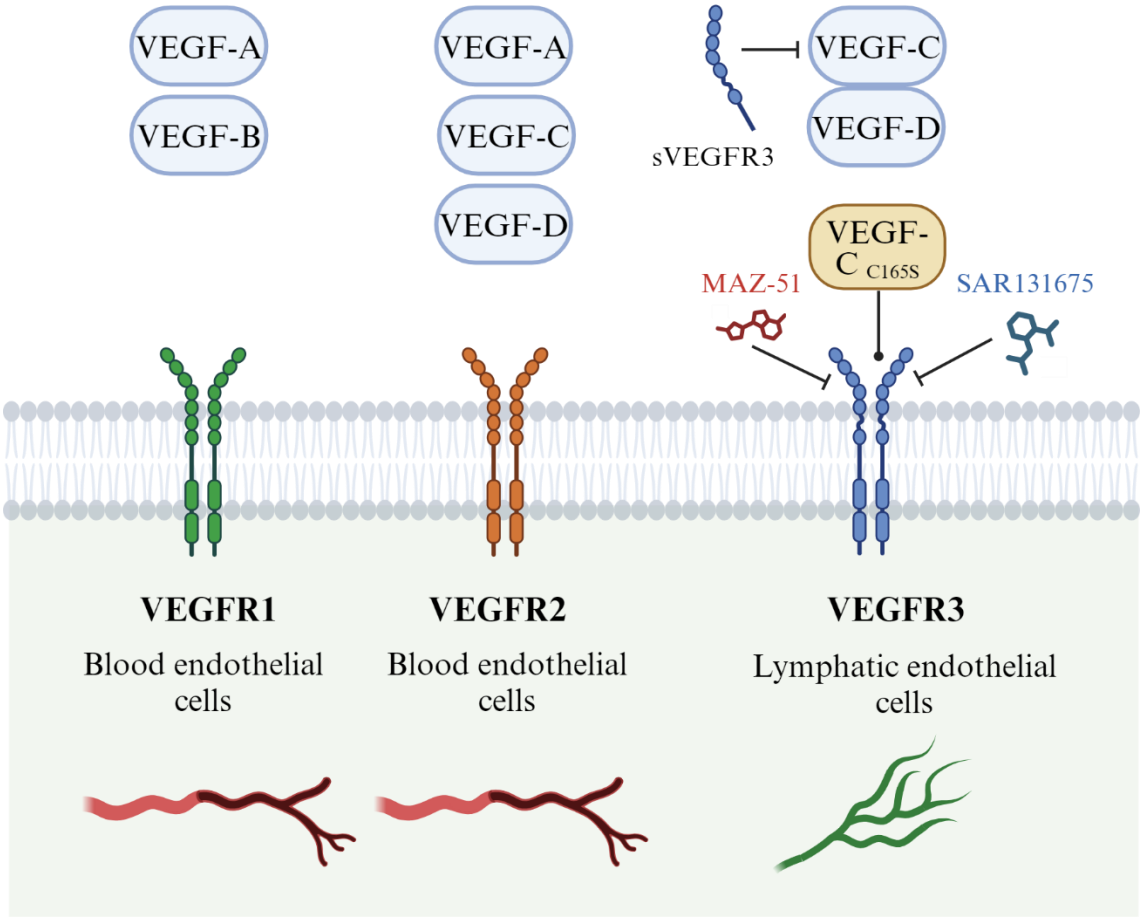

Figure 2. VEGF-C and VEGF-D drive lymphatic endothelial proliferation via VEGFR3 signaling. The most studied members of the family of VEGF ligands are VEGF-A, VEGF-B, VEGF-C and VEGF-D. These ligands bind, with different degrees of affinity, to the tyrosine kinase receptors VEGFR1, VEGFR2 and VEGFR3. Whereas VEGFR1 and VEGFR2 are largely expressed by blood endothelial cells, VEGFR3 is almost exclusively expressed by lymphatic endothelial cells. VEGF-C and VEGF-D thus promote lymphatic expansion via VEGFR3 activation, although they bind with lesser affinity to VEGFR2, thereby having minor effects on blood vessel proliferation. A genetically engineered soluble version of VEGFR3 can also bind VEGF-C and VEGF-D, working as a trap, which blocks lymphangiogenesis in interventional studies. In addition to that, the MAZ51 and SAR131675 are selective pharmacological VEGFR3 inhibitors. Illustration created with "BioRender.com".

The lymph system has also been thoroughly studied on a systemic level. Similar to most other organs, cardiac lymphatics ensure fluid homeostasis by draining the interstitial fluid from the endocardium in the direction of the epicardium, where pre-collectors are located (Brakenhielm & Alitalo, 2019; Huang et al., 2017). Superficial lymphatic pre-collectors are present on the anterior and posterior walls of the heart. These vessels are

located next to the lateral coronaries, and run from the apex towards the base, where they drain into mediastinal lymph nodes (Brakenhielm & Alitalo, 2019). Whereas cardiac lymphatics from bigger mammals (including humans) cover all layers of the heart, murine lymphatics are predominantly located in the epicardium and subepicardial regions (Brakenhielm & Alitalo, 2019; Loukas et al., 2013). Still, lymphatics can be found in atria, valves, septum and ventricles, where they are most dense (Huang et al., 2017). Interestingly, cardiac lymphatic collectors lack a smooth muscle cell coverage (Harris et al., 2023; Houssari et al., 2020). Instead, it is widely accepted that the cardiac lymph is propelled forward by the heart muscle contraction in each cycle of systole (Harris et al., 2022, 2023).

1.3.1 Lymphangiogenesis in infarcted hearts

In 2007, Ishikawa and collaborators described the expansion of the lymphatic vasculature in the context of acute cardiac remodeling. They examined human postmortem histological sections of infarcted hearts and reported a pronounced sprouting of lymphatic vessels from non-damaged parts into the infarcted area. A few years later, Klotz and collaborators (2015) confirmed that enhanced cardiac lymphangiogenesis takes place within ischemic regions of mice after MI.

Subsequent studies have reported lymphangiogenesis in the first three weeks after the onset of MI (Glinton et al., 2022; Houssari et al., 2020; Shimizu et al., 2018; Vieira et al., 2018; Vuorio et al., 2018). Genetic and pharmacological manipulation of the VEGFR3-VEGF-C signaling axis allows inhibition and stimulation of cardiac lymphangiogenesis **(Fig. 3)**. For instance, mice overexpressing a soluble decoy of VEGFR3 (sVEGFR3) shows impaired lymphangiogenesis (Vuorio et al., 2018). Similarly, intramyocardial delivery of the VEGFR3 pharmacological inhibitor MAZ51 to infarcted hearts also impairs expansion of lymphatic vessel (Glinton et al., 2022; Shimizu et al., 2018). Finally, infarcted *Prox1-Cre^{ERT2} Vegfr3$^{fl/fl}$* and *R26-Cre^{ERT2} Vegfc$^{fl/fl}$ Vegfd$^{f-/-}$* mice consistently show restricted lymphatic vessel expansion (Keller et al., 2021).

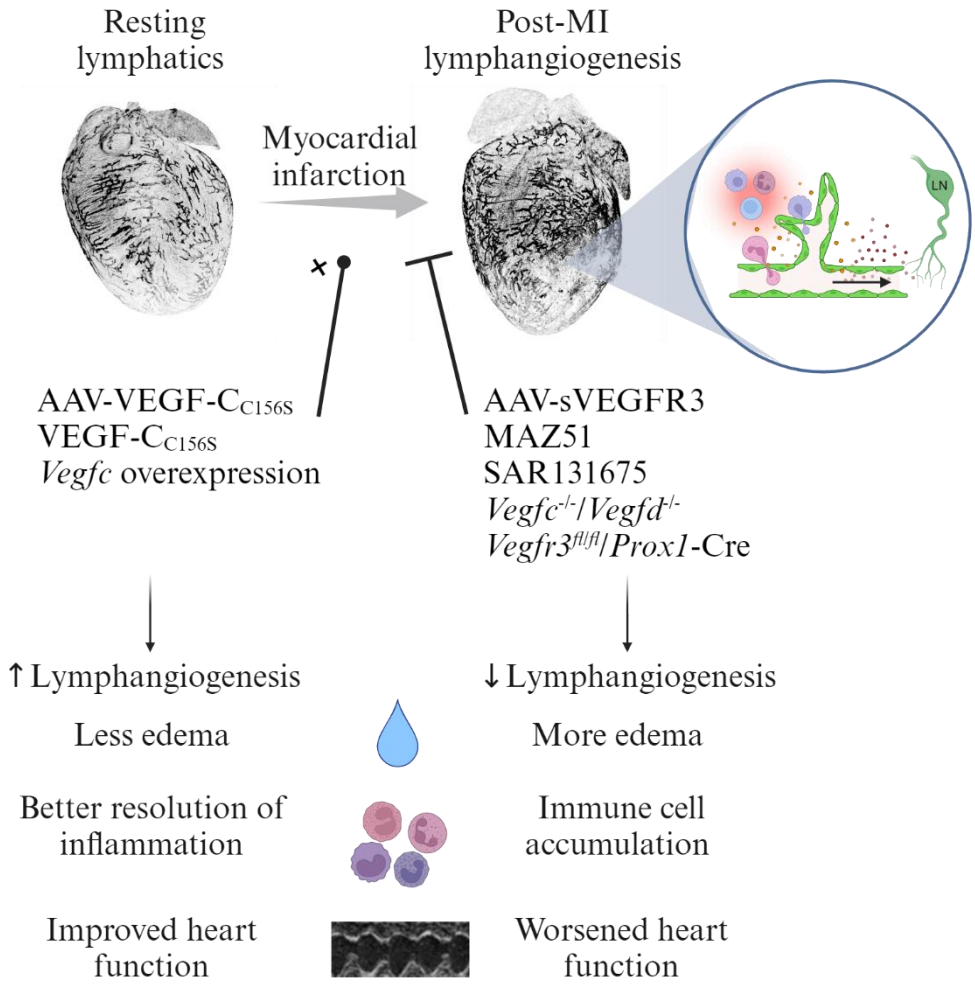

Figure 3. Effects of lymphangiogenesis on infarcted hearts. De novo lymphangiogenesis occurs in the infarcted heart and is most pronounced in the border zone. The process of lymphatic vessel expansion can be stimulated by means of VEGF-C delivery or genetic overexpression. Conversely, lymphangiogenesis can be blocked using pharmacological agents (MAZ51 and SAR131675), conditionally knocking out *Vegfr3* and *Vegfc/Vegfd* or employing a soluble VEGFR-3 decoy, which sequesters circulating VEGF-C/VEGF-D. In the classical view, stimulation of lymphangiogenesis leads to less edema, overall better resolution of inflammation and improved heart function, and vice-versa, although controversy exists in the field (Houssari et al., 2020; Keller et al., 2021). Illustration created with "BioRender.com".

Table I presents an overview on the techniques and outcomes of studies investigating activation or inhibition of cardiac lymphangiogenesis after MI. Based on the classic paradigm of the roles of lymphatic vessels in fluid homeostasis and immune cell clearance, researchers hypothesized that enhancing cardiac lymphangiogenesis may improve heart function after damage. Initial studies have indeed supported this hypothesis (Henri et al., 2016; Shimizu et

al., 2018; Vieira et al., 2018), although recent reports have questioned their results and introduced controversy in the field (Houssari et al., 2020; Keller et al., 2021).

On one hand, Vieira et al. (2018) showed that post-MI lymphangiogenesis supports a time-controlled immune cell clearance from the infarcted area, limiting adverse effects of an overactive and prolonged inflammatory response. Similarly, VEGF-C therapies led to decreased edema and diminished presence of immune cells in the infarcted tissue (Glinton et al., 2022; Henri et al., 2016; Shimizu et al., 2018). Conversely, intramyocardial delivery of the VEGFR3 pharmacological inhibitor MAZ51 impaired lymphatic vessel expansion, compromising resolution of edema resolution and of the inflammatory response, leading to worsened heart function (Shimizu et al., 2018).

On the other hand, disrupted VEGFR3 signaling and reduced lymphatic coverage altered activity of regulatory T lymphocytes, culminating in improvements in the heart function of infarcted mice (Houssari et al., 2020). Furthermore, a subsequent study has employed three different genetic approaches to block lymphangiogenesis. In all three scenarios, no striking decline in heart function was observed, despite a strong reduction in lymphatic vessel density, questioning beneficial effects of lymphangiogenesis in improving heart functionality (Keller et al., 2021).

These paradoxical observations regarding the correlation of lymphangiogenesis and heart function questioned if de novo assembled lymphatic vessels are able to resolve cardiac inflammation, and whether they are cardioprotective at all. Of note, existing studies on cardiac lymphangiogenesis have only superficially assessed which immune cell types are attracted to the lumen of cardiac lymphatic vessels or where these cells go after leaving the infarcted heart. Anatomically, cardiac lymphatic collectors drain into mediastinal lymph nodes, and evidence exists that phagocytes transport cardiomyocyte debris to these organs (Vieira et al., 2018). To date, there is little or no evidence to say that mediastinal lymph nodes would be the final destination of these cells – or if, alternatively, lymphatics enable a systemic response to the very complex cardiac inflammatory dynamics.

Table I: Comparative literature review of studies investigating cardiac lymphangiogenesis in infarcted rodents. Abbreviations: I/R, ischemia-reperfusion; i.p., intraperitoneal; i.mc., intramyocardial; rec, recombinant; ECs, endothelial cells; LECs; lymphatic endothelial cells.

Author	Year	Journal	Rodent strain	Cardiac intervention	Time point(s)	Strategy	Lymphatic vessel density	Heart function	Edema	Resolution of inflammation	Survival	Others
Klotz	2015	Nature	C57Bl/6J	LAD ligation	1, 2, 3, 7, 14, 21, 28, 35 days	rec. VEGF-C i.p. delivery	Increased	Improved	-	-	-	-
Henri	2016	Circulation	Wistar rats (males)	LAD ligation and I/R	4 weeks, 12 weeks	rec. VEGF-C i.mc delivery	Increased	Improved	Improved	Improved	-	Less fibrosis
Vuorio	2018	Scientific Reports	C57Bl/6J	LAD ligation	8 days	sVEGFR3 overexpression	Decreased	Unaltered	-	Unaltered	Worsened	Hemorrhagia
Vieira	2018	JCI	C57Bl/6J	LAD ligation	7 days	rec. VEGF-C i.p. delivery	Increased	-	-	Improved	-	-
Shimizu	2018	JAHA	C57Bl/6J	LAD ligation and I/R	7 days	rec. VEGF-C i.mc delivery	Increased	Improved	Improved	Improved	-	Smaller scar
						MAZ-51 i.mc delivery	Decreased	Worsened	Worsened	Worsened	-	Bigger scar
Houssari	2020	ATVB	C57Bl/6J and Wistar rats	LAD ligation	7, 28 days	AAV9-*Vegfc* i.p. delivery	Increased	Improved	-	-	-	Unaltered scar size
						AAV9-*sVegfr3* i.p. delivery	Decreased	Improved	-	-	-	Bigger scar
Keller	2021	JCI	C57Bl/6J	LAD ligation	3, 7, 14 days	*Vegfr3* deletion ECs	Decreased	Unaltered	Slightly worsened	Unaltered	-	-
						Vegfr3 deletion LECs	Decreased	Unaltered	-	-	-	-
						Vegfc/d deletion global	Decreased	Unaltered	-	-	-	-
Glinton	2022	JCI	C57Bl/6J	LAD ligation	0, 3, 6, 9, 28 days	*Vegfc* deletion myeloid cells	Decreased	Worsened	-	Worsened	-	Bigger scar
						Vegfc overexpression	Increased	Improved	-	-	-	-

1.3.2 VEGF-C-based preclinical therapies for myocardial infarction

Pre-clinical studies employing gene therapy and local VEGF-C delivery have restored, to a certain degree, the immune cell balance and edema observed in the infarcted myocardium (Henri et al., 2016; Houssari et al., 2020). The promising but limited success of VEGF-C-based therapies in rodents suggests that activation of VEGF-C-mediated signaling cascades alone is not sufficient to promote cardiac lymphangiogenesis, completely resolving cardiac inflammation and thereby preventing cardiac dysfunction (Keller et al., 2021). Therefore, an urgent need exists to identify and characterize mechanisms regulating pathophysiological lymphangiogenesis during cardiac remodeling more deeply (Hu et al., 2019).

1.4 REG proteins expression and biological effects

1.4.1 REG family: locus and interspecies differences

Regenerating islet-derived (REG) proteins are a family of proteins first identified 45 years ago as constituent factors of pancreatic stones and promoting regeneration of pancreatic islets after pancreatectomy (De Caro et al., 1979; Terazono et al., 1988). The members of the REG family can be divided, based on their structural similarity, into four groups, which are numbered sequentially (1, 2, 3 and 4). Whereas mice express seven different members of this family (*Reg1, Reg2, Reg3a, Reg3b, Reg3g, Reg3d* and *Reg4*), humans only express five members (REG1A, REG1B, REG3A, REG3G and REG4). With exception of REG4 (*Reg4* in mice), which is present on chromosome 1p11 (3F3 in mice), all *REG* genes can be found on the same human chromosome locus 2p12 (6C3 in mice) (**Fig. 4**) (Chen et al., 2019).

The members of this superfamily share a high degree of similarity among themselves, and between species (Chen et al., 2019). Structurally, they possess a C-type-like lectin domain, which can bind various carbohydrates, including and in particular those present on the bacterial cell surface – conferring bactericidal properties to some members of this family (Mukherjee et al., 2014; C. Sun et al., 2021).

The expression of REG proteins is most prominent in organs of the gastrointestinal system – with emphasis on the pancreas and the intestine. Indeed, REG proteins have been linked with diabetes (Hou et al., 2011; B. Li et al., 2010; X. Xiong et al., 2011), pancreatic

cancer (Q. Li et al., 2016), pancreatitis (LaFonte et al., 2013) and hepatocellular carcinoma (R.-H. Yuan et al., 2005) (**Fig. 4**). Because of these organ associations, several aliases have been given to members of the REG3 group, including hepatocarcinoma-intestine-pancreatic protein (HIP) and pancreatic-associated protein (PAP).

Of note, one strong limitation in the study of the biological effects of REG proteins in physiology and disease is that their mode of action (e.g. receptor activation and signaling pathway) is unknown – or at least not consensually accepted. For instance, the glycosyltransferase EXTL3 was spatially and functionally linked to REG1α in rat PC12 neuron cells (Van Ba et al., 2012). However, conclusive experiments showing effective interaction between EXTL3 and REG1α still lack (Chen et al., 2019). Besides, EXTL3 is an intracellular enzyme with no known signaling roles, which argues against its putative role as the receptor for REG proteins (Wilson et al., 2022). An alternative explanation of the REG proteins mode of action is that they bind directly saccharide motifs on the bacterial cell wall and on the mammalian cell membrane via the lectin domain, rather than a classical receptor-ligand binding (Lehotzkya et al., 2010).

Biologically, REG proteins' effects are diverse: REG3 proteins are upregulated in acute stages of pancreatitis, REG1 stimulates proliferation of beta cells under inflammatory conditions and REG1 and REG3β ameliorate streptozotocin-induced diabetes in mice (Aida et al., 2018; Hou et al., 2011; LaFonte et al., 2013; B. Li et al., 2010; Unno et al., 2002; X. Xiong et al., 2011). Tumor cells in human pancreatic cancer also highly express REG1A, REG1B, REG3A – enabling their use as early markers for the detection of pancreatic cancer (Q. Li et al., 2016). Similar to the pancreas, REG proteins, such as REG1A and REG1B, seem to stimulate proliferation in intestinal cells in inflammatory bowel disease (IBD) (Van Beelen et al., 2013) and ulcerative colitis neoplasia (Tanaka et al., 2011; Van Beelen et al., 2013). REG3A, conversely, reduces apoptosis of epithelial cells in IBD (Van Beelen et al., 2013).

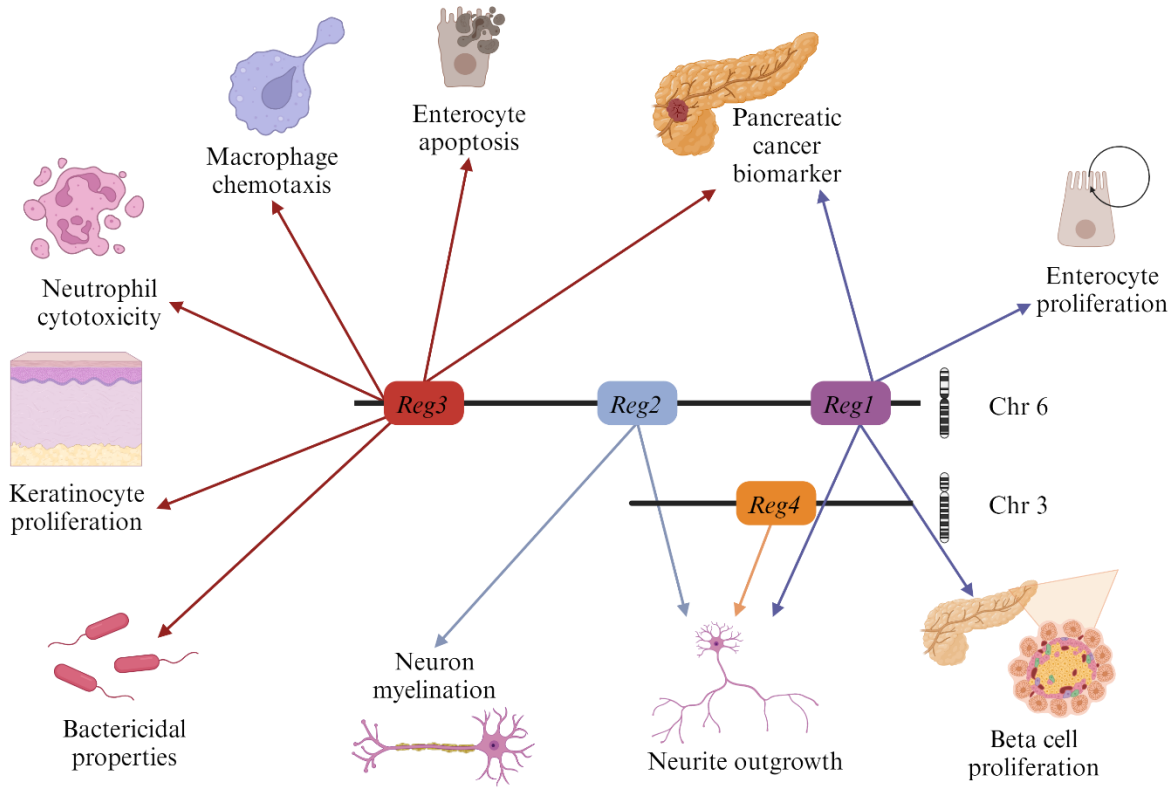

Figure 4. Biological effects associated with different members of the murine REG protein family. Members of REG1, REG2 and REG3 families cluster on the 63C murine chromosome, whereas REG4 is on 3F3. All REG regulate proliferation and survival of different cell types in the gastrointestinal system (beta cell proliferation, enterocyte proliferation and apoptosis), immune system (macrophage chemo-attraction, neutrophil cytotoxicity), central nervous system (neuron myelination and outgrowth) and skin (keratinocyte proliferation). Besides, members of REG3 family also share bactericidal properties. Illustration created with "BioRender.com".

Beyond the gastrointestinal system, *Reg1*, *Reg2* and *Reg4* are upregulated in injured motor neurons, stimulating neurite outgrowth (Namikawa et al., 2005, 2006). Moreover, rat *Reg2* promotes myelinization of injured neurons, human REG3A enhances keratinocyte proliferation after skin injury, and REG3β coordinates inflammation dynamics (e.g. macrophage chemo-attraction and neutrophil survival) in infarcted hearts (Lörchner, Pöling et al., 2015; Lörchner, et al., 2018). Altogether, most of the described biological effects of REG proteins revolve around cell proliferation and survival, being strongly associated with inflammatory conditions.

1.4.2 REG3β as a modulator of inflammation dynamics in the infarcted heart

In 2015, my group identified one member of the family of REG proteins – REG3β – as an essential regulator of cardiac healing, which orchestrates and balances immune-regulatory responses after experimental MI in mice (Lörchner, Pöling et al., 2015). More precisely, they demonstrated that cardiomyocytes challenged with the cytokine Oncostatin M secrete REG3β, which triggers at least two different biological effects in infarcted hearts (**Fig. 5)**. First, REG3β directly induces accumulation of macrophages in acute stages of the proinflammatory phase. (Lörchner, Pöling et al., 2015; Lörchner, et al., 2018). Second, REG3β directly restricts accumulation of neutrophils within the infarcted heart via inducing a rapid lysosomal-mediated cell death (Detzer, 2020). Here it was shown that REG3β efficiently and directly kills activated (older) neutrophils, but not young neutrophils, present in the circulation or bone marrow. Therefore, mice with a global genetic deletion of *Reg3b* (*Reg3b*$^{-/-}$) show an imbalanced acute immune response, poorer survival and higher incidence of cardiac rupture after MI due to impaired clearance of neutrophils (Lörchner, Pöling et al., 2015). Such impaired removal of neutrophils from infarcted hearts of *Reg3b*$^{-/-}$mice may not solely depend on attenuated killing but potentially also on reduced emigration of neutrophils via the lymphatic system.

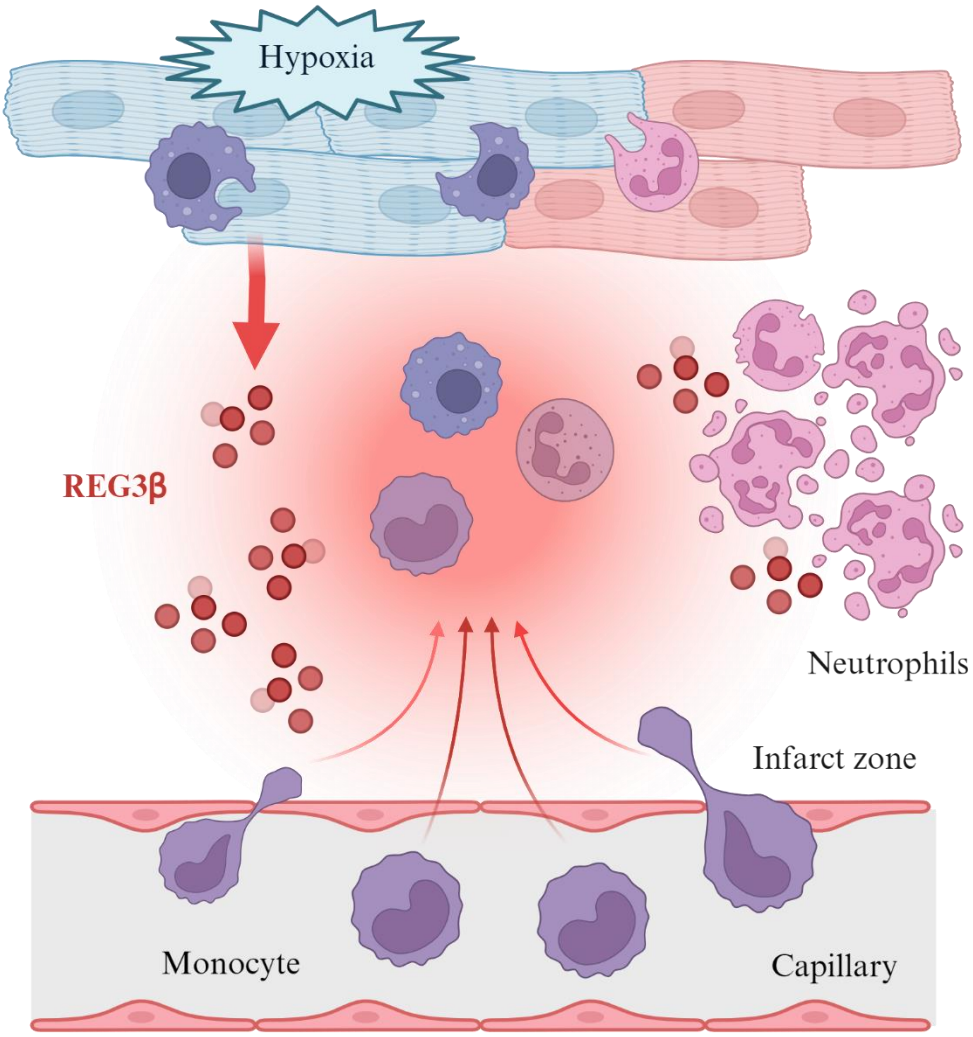

Figure 5. Known effects of REG3β in infarcted hearts. REG3β is secreted by cardiomyocytes after MI and modulates the initiation and resolution of inflammation by two modes of action: (i) it attracts monocytes/macrophages, recruiting them from the circulation into the inflamed tissue; and (ii) it directly binds to neutrophils and promotes their cell death through a lysosomal-dependent cell mechanism, limiting their life span in the infarcted heart. Illustration created with "BioRender.com".

2. OBJECTIVES

Initiation and resolution of immune-inflammatory processes are instrumental for efficient structural remodeling after myocardial infarction. Given the regulatory role of REG3β for a balanced immune-inflammatory response during the acute phase of myocardial healing, this work aimed to identify and characterize underlying mechanisms in REG3β-mediated resolution of cardiac inflammation. Besides REG3β-mediated chemoattraction of macrophages and killing of neutrophils, other mechanisms may contribute to myocardial healing. A series of studies point out the newly assembled cardiac lymphatic vasculature as an important regulator for resolution of inflammation and edema. Therefore, I evaluated whether REG3β affects the expansion of the cardiac lymphatic vascular network, thereby regulating leukocyte drainage, with a potential systemic feedback to distal organs controlling inflammation (e.g. bone marrow).

The project intended to mechanistically examine REG3β's influence on inflammation dynamics under a systemic approach – by (i) modulating the accumulation of distinct immune cell populations; (ii) regulating leukocyte emigration from the infarcted tissue through the lymphatic vasculature and (iii) affecting de novo immune cell production in the bone marrow and recruitment to the infarcted heart.

The specific objectives of this work can be summarized as:

1. Profile kinetics of individual leukocyte subpopulations within infarcted hearts of WT and *Reg3b*$^{-/-}$ mice at different time points of cardiac repair.
2. Characterize lymphatic vessel expansion within infarcted hearts of WT and *Reg3b*-deficient mice during cardiac repair, taking into account spatial and temporal changes.
3. Monitor leukocyte drainage in WT and *Reg3b*$^{-/-}$ mice after myocardial infarction.
4. Analyze systemic effects of emigrated cardiac tissue-derived leukocytes on cardiac inflammation in WT and *Reg3b*-deficient mice after myocardial infarction.

3. MATERIALS AND METHODS

3.1 Materials

3.1.1 Chemical reagents

Chemical	Catalogue Number	Company
1,4- Dithiothreitol (DTT)	6908.1	Carl Roth
4′,6-Diamidin-2-phenylindol (DAPI)	D1306	ThermoFisher Scientific™
4-(2-hydroxyethyl)-1- Piperazineethanesulfonic acid (HEPES)	6763.3	Carl Roth
5-Bromo-2′-deoxyuridine (BrdU)	B5002	Sigma-Aldrich
Agarose	A9539	Sigma-Aldrich
Amersham™ Protran™ 0.45 µm NC nitrocellulose blotting membranes	10600002	GE Healthcare Life Sciences®
Aprotinin	A6106	Sigma-Aldrich
AutoMACS rinsing solution	130-091-222	Miltenyi Biotec
BenchMark™ protein ladder	10747012	Invitrogen
Bicine	B3876	Sigma-Aldrich
Bis-Tris	A1025,0500	PanReac AppliChem
Bovine serum albumin (BSA) (for IHC)	A9576	Sigma-Aldrich
Bovine serum albumin (BSA) (for WM)	A7906	Merck
Bromophenol blue	114391	Merck
Dimethylsulfoxide (DMSO)	D8418	Sigma-Aldrich
Ethanol, absolute	5054.1	Carl Roth
Ethylcinnamate (ECi)	112372	Sigma-Aldrich
Fetal calf serum (FCS)	F2442	Sigma-Aldrich
Gibco™ Penicillin-streptomycin (10,000 U/mL)	11528876	ThermoFisher Scientific™
Glycine	G8898	ThermoFisher Scientific™
Heparin sodium salt from porcine intestinal mucosa	H3149-100KU	Merck
Hydrogenperoxide (H2O2) 30 %	CP26.1	Roth
Leupeptin	103476-89-7	Sigma-Aldrich

MACS BSA stock solution	130-091-376	Miltenyi Biotec
MES SDS running buffer 20x	NP0002	Invitrogen
Methanol	8388.1	Carl Roth
Mowiol 4-88	713.1	Carl Roth
NuPAGE 4-12 % Bis-Tris gel, 1mm x 17well	NP0329BOX	Novex™
Osmoium tetroxide	O5500	Merck
Paraformaldehyde (PFA)	30525-89-4	Merck
PCR buffer without $MgCl_2$, 10x concentrated	11699105001	Merck
Potassium chloride (KCl)	P9327	Sigma-Aldrich
Pre-Separation filters 30 µm	130-041-407	Miltenyi Biotec
Red Alert™ 10x western blot Stain	71078	Merck
Rotiphorese® Gel 40 (29:1 acrylamid/bisacrylamid)	A515.1	Carl Roth
Skim milk powder	70166	Merck
Sodium azide (NaN3)	014314.22	Invitrogen
Sodium chloride (NaCl)	3957.1	Carl Roth
Sodium citrate tribasic dihydrate	S4641	Sigma-Aldrich
Sodium dodecylsulfate (SDS)	5136.2	Carl Roth
Sucrose	S0389	Sigma-Aldrich
TEMED	T9281	Sigma-Aldrich
Tissue-Tek® O.C.T. Compound	4583	Sakura
TriPure Isolation Reagent	11667165001	Sigma-Aldrich
Tris	4855.1	Carl Roth
Triton X-100	648463	Sigma-Aldrich
Tween® 20	9127.2	Carl Roth
WesternBright Sirius chemiluminescence substrate	K-12043-D20	Advansta

3.1.2 Inhibitors, enzymes, recombinant proteins and kits

Chemical	Catalogue Number	Company
2x Taq Master Mix (Dye Plus)	P112-03	Vazyme
Blue S´Green qPCR 2x Mix	331416	Biozym
DC Protein Assay Kit 1	5000111	Biorad
Intracellular fixation and permeabilization buffer set	88-8824-00	ThermoFisher Scientific™

Liberase DH Research Grade	5401127001	Roche
Murine regenerating islet-derived protein 3β (REG3β)	AF5110	R&D Systems
pHrodo™ BioParticles™ conjugates for phagocytosis and phagocytosis kit	P35361	ThermoFisher Scientific™
PrimeScript RT Reagent Kit with gDNA eraser	RR047B	Takara Bio
RNeasy® Micro Kit	74004	Qiagen
SMART-Seq HT Kit		Takara Bio

3.1.3 Primary antibodies

Antibody	Catalogue number	Company	Application	Concentration
Goat anti-PROX-1	AF2727	R&D Systems	IHC, WB	1-100/1-500
Goat anti-CCL19	DY008	R&D Systems	WB	1-500
Goat anti-LYVE-1	AF2125	R&D Systems	IHC, WM, WB	1-300/1-100/1-500
Goat anti-CCL21	AF457	R&D Systems	IHC, WM, WB	1-100/1-200/1-500
Goat anti-VEGFR3	AF743	R&D Systems	WM, WB	1-100/1-500
Mouse anti-SMA-Cy3	C6198	Sigma-Aldrich	WM	1-100
Rabbit anti-CCL19	BS-2454R	Bioss	IHC	1-300
Rabbit anti-LYVE-1	11034	AngioBio	IHC, WM	1-300/1-100
Rabbit anti-Pan Actin	4968	Cell Signaling	WB	1-3000
Rabbit anti-VEGF-C	Ab9546	Abcam	WM, WB	1-100/1-1000
Rabbit anti-VEGF-D	26915-1-AP	ProteinTech	IHC	1-500
Rat anti-BrdU	NB500-169	Novus Biologicals	IHC	1-300
Rat anti-CD11b	101201	Biolegend	IHC	1-100
Rat anti-CD11b AF647	101220	Biolegend	In vivo labeling	10ug
Rat anti-CD45	103101	Biolegend	IHC, WM	1-100
Rat anti-CD68	MCA-1957	Biorad	IHC	1-300
Rat anti-F4/80	123101	Biolegend	IHC, WM	1-100
Rat anti-Ly6G	127601	Biolegend	IHC	1-100
Sheep anti-BrdU	NB500-235	Novus Biologicals	IHC	1-500

3.1.4 Conjugated antibodies for flow cytometry

Antibody	Catalogue number	Company	Clone
Armenian hamster anti-CD3e-PerCP-Cyanine5.5 monoclonal antibody	100327	Biolegend	145-2C11
Armenian hamster anti-CD11c-FITC monoclonal antibody	11-0114-82	eBioscience	N418
Armenian hamster anti-CD103-eFluor450 monoclonal antibody	48-1031-82	eBioscience	2E7
Mouse anti-CD64-PerCP-Cy5.5 monoclonal antibody	139308	Biolegend	X54-5/7.1
Mouse anti-CD64-APC monoclonal antibody	139306	Biolegend	X54-5/7.1
Mouse anti-NK1.1-PE-Cy7 monoclonal antibody	108713	Biolegend	PK136
Mouse anti-BrdU-PE monoclonal antibody	364116	Biolegend	3D4
Mouse anti-VEGF-C-APC monoclonal antibody	NBP2-74845AF647	Novus Biologicals	OTI4A1
Mouse anti-Troponin I type 3-Alexa Fluor488 monoclonal antibody	NB110-2546AF488	Novus Biologicals	19C7cc
Rabbit anti-VEGF-C-AlexaFluor647 polyclonal antibody	ITT4872-647	Gbiosciences	---
Rat anti-CD45R/B220-PE-Cy7 monoclonal antibody	103222	Biolegend	RA3-6B2
Rat anti-CD45–PE-Cy5.5 monoclonal antibody	103109	Biolegend	30-F11
Rat anti-CD45-FITC monoclonal antibody	103107	Biolegend	30-F11
Rat anti-CD45-V421 monoclonal antibody	103133	Biolegend	30-F11
Rat anti-CD11b-APC monoclonal antibody	101211	Biolegend	M1/70
Rat anti-CD11b-PE monoclonal antibody	101207	Biolegend	M1/70

Rat anti-CD11b-PE-Cy5 monoclonal antibody	101209	Biolegend	M1/70
Rat anti-CD11b-APC-Cy7 monoclonal antibody	101225	Biolegend	M1/70
Rat anti-CD11b-PE-Cy7 monoclonal antibody	101216	Biolegend	M1/70
Rat anti-F4/80-PE monoclonal antibody	123109	Biolegend	BM8
Rat anti-F4/80-BV421 monoclonal antibody	123137	Biolegend	BM8
Rat anti-Ly6G-FITC monoclonal antibody	127606	Biolegend	1A8
Rat anti-Ly6G-BV421 monoclonal antibody	127627	Biolegend	1A8
Rat anti-CD115-APC monoclonal antibody	135510	Biolegend	AFS98
Rat anti-CD115-BV421 monoclonal antibody	135513	Biolegend	AFS98
Rat anti-Ly6C-PE monoclonal antibody	128007	Biolegend	HK1.4
Rat anti-CD4-APC-Cy7 monoclonal antibody	100413	Biolegend	GK1.5
Rat anti-CD8a-PE-Cy5 monoclonal antibody	100709	Biolegend	53-6.7
Rat anti-CD90.2-PE-Cy7 monoclonal antibody	140310	Biolegend	53-2.1
Rat anti-CD117-PE monoclonal antibody	105807	Biolegend	2B8
Rat anti-CXCR2-PerCP-Cy5.5 monoclonal antibody	149307	Biolegend	SA044G4
Rat anti-CXCR4-BV421 monoclonal antibody	146511	Biolegend	L276F12
Rat anti-CD54-PE-Cy7 monoclonal antibody	116122	Biolegend	YN1/1.7.4
Rat anti-CD49d-PE monoclonal antibody	103607	Biolegend	R1-2
Rat anti-CD170 (SiglecF)-FITC monoclonal antibody	155503	Biolegend	S17007L
Rat anti-Ly6G-PE-efluor610 monoclonal antibody	61-9668-82	eBioscience	1A8

Rat anti-MHC class II-APC-eFluor780 monoclonal antibody	56-5321-82	eBioscience	M5/114.15.2
Rat anti-MHC class II-APC-Cy7 monoclonal antibody	107628	eBioscience	M5/114.15.2
Rat anti-CD19-PE-eFluor610 monoclonal antibody	61-0193-82	eBioscience	eBio1D3
Rat anti-IgM-eFluor450 monoclonal antibody	48-5790-82	eBioscience	Il/41
Rat anti-Ly6G/Ly6C (Gr-1)-APC monoclonal antibody	17-5931-82	eBioscience	RB6-8C5
Rat anti-CD64-AlexaFluor700 monoclonal antibody	FAB2071N	RnD Systems	290322

3.1.5 Secondary antibodies

Antibody	Catalogue number	Company	Application	Concentration
Donkey anti-rat AF488	A21208	Invitrogen	IHC	1-500
Donkey anti-goat AF594	A21468	Invitrogen	IHC	1-500
Donkey anti-goat AF647	A21447	Invitrogen	WM	1-400
Donkey anti-goat AF750	AB175744	Abcam	WM	1-400
Donkey anti-goat AF750	SAB46004	Sigma-Aldrich	IHC	1-500
Donkey anti-rabbit AF594	A21207	Invitrogen	IHC	1-500
Donkey anti-rabbit AF647	A31573	Invitrogen	IHC, WM	1-400/1-400
Donkey anti-rabbit AF790	A11374	Invitrogen	IHC, WM	1-500
Donkey anti-rat AF594	A21209	Invitrogen	IHC, WM	1-500/1-400
Donkey anti-rat AF647	A21208	Invitrogen	IHC	1-500
Donkey anti-sheep AF488	A11015	Invitrogen	IHC	1-500
Goat anti-rabbit HRP	HAF008	R&D Systems	WB	1-1000
Rabbit anti-goat HRP	HAF017	R&D Systems	WB	1-1000

3.1.6 Laboratory equipment

Equipment	Catalogue number	Company
10 cm Petri dishes	633180	Greiner Bio-One®
6-well Cellstar® cell culture plates	657160	Greiner Bio-One®
BD LSRFortessa™ cell analyzer	-	BD Bioscience
Casting chamber	NC2010	Hoefer
Cell scrapers 25 cm	83.3950	Sarstedt®
Centrifuge tubes	21008-918	Beckmann Coulter
ChemiDoc™ MP System	12003154	Bio-Rad®
DS-Qi2 Mono Digital microscope camera	-	Nikon
EasySep™ magnet	19762A	StemCell Technologies
FACS Aria III cell sorter	-	BD Bioscience
HERAcell™ 150 CO_2 incubator	50116047	ThermoFisher Scientific™
Heraeus™ Fresco™ 21 microcentrifuge	75002555	ThermoFisher Scientific™
Heraeus™ Multifuge™ X3R TX-1000	X3/X3R	ThermoFisher Scientific™
Hidex Sense microplate reader	425-301	Hidex
K8 monochrome digital camera	-	Leica Biosystems
LabChip Gx Touch 24	-	Perkin Elmer
Leica TCS SP8 confocal microscope	DMi8	Leica Microsystems
LSR Fortessa	-	BD Bioscience
MVX10 zoom body	-	Olympus
NanoDrop 2000c UV-Vis spectrophotometer	2000c	ThermoFisher Scientific™
Neubauer cell counting chamber	1100000	Optik Labor®
NextSeq2000 instrument	-	Illumina
Ni-E ECLIPSE widefield microscope	-	Nikon
Pre-Separation filters 30 µm	130-101-812	Miltenyi Biotec
Reichert Ultracut E ultramicrotome	CM1958	Leica Biosystems
SlideExpress 2 slideloader	-	Märzhäuser
Sonopuls® ultrasonic homogenizer	HD 2070	Bandelin®
SOLA light engine	-	Lumencor
StepOne™ Real-Time PCR System	-	ThermoFisher Scientific™
Surgical disposable scalpels	5518067	B.Braun®

Thunder Imager Live Cell & 3D assay	-	Leica Biosystems
UltraMicroscope II	D33617	LaVision BioTec
XCell II™ Blot Modules	EI9051	Novex™
XCell SureLock™ Mini-Cells	EI0001	Novex™
Zyla 4.2 PLUS sCMOS camera	-	Andor

3.1.7 Media and solutions

Immunohistochemistry in frozen sections	
Fixation solution	3 % PFA in PBS, pH 7,4
Permeabilization solution	0.01 % Triton X-100 in PBS, pH 7,4
Mowiol mounting medium	2.4 g Mowiol
	6 g Glycerol
	6 ml H_2O
	12 ml of 0.2 M Tris-Cl
	pH 8.5
Sodium citrate buffer for antigen retrieval	10mM Sodium citrate tribasic dehydrate, in H20, pH 6,0
Flow cytometry sample preparation	
Fixation solution	Ebioscience™ (catalogue number: 00-8222-49)
Permeabilization buffer	Ebioscience™ (catalogue number: 00-8333-56)
PEB	0,5 % BSA, 2 mM EDTA in PBS, pH 7,2
DNA isolation	
TENS buffer	60 ml 1M Tris-HCl, pH 8,0
	240 ml 0,5 M EDTA, pH 8,0
	24 ml 5M NaCl
	60 ml 20 % SDS
	final volume made to 1 L with distilled water

Whole-mount staining of hearts	
Block and permeabilize	1 % BSA
	0,1 % Triton X-100
	0,02 % NaN_3
	in PBS, pH 7,4
Ptx.2	1 % BSA
	0,2 % Triton X-100
	in PBS, pH 7,4
Permeabilization solution	2,3 % Glycine
	20 % DMSO
	0,02 % NaN_3
	in Ptx.2
Blocking solution	6 % FCS
	10 % DMSO
	0,02 % NaN3
	in Ptx.2
PtWH	0,2 % Tween
	0,1 % Heparin
	0,02 % NaN_3
	in PBS, pH 7,4
Antibody solution	5 % DMSO
	3 % FCS
	in PtWH, pH 7,4

Electrophoresis and blotting	
Extraction buffer (EP), proteins	0.1 M Tris-HCl, pH 8,8
	0.01 M EDTA
	0.04 M DTT
	10 % SDS
	pH 8.0
5x Laemmli buffer (LB)	1 M Tris-HCl (pH 6,8)
	10 % SDS
	50 % Glycerol
	dissolved in distilled water
Protease inhibitor mix	500 µg/ml Benzamidin
	2 µg/ml Aprotinin
	2 µg/ml Leupeptin
	2 mM PMSF
	1 mM Sodium vanadate
	20 mM Sodium fluoride
10x TBS buffer (5 liters)	400 g NaCl
	120.5 g Tris
	pH 7.6
	final volume made to 2 L with distilled water
1x TBS-T (5 liters)	250 ml 20x TBS buffer
	5 ml Tween 20
	final volume made to 5 L with distilled water
1X MES SDS running buffer (5L)	250ml 20xMES SDS running buffer
	final volume made up with distilled water
Blocking solution (Western blot)	5 % skim milk powder in TBS-T
20X Transfer buffer (2L)	163.2 g Bicine
	209.3 g Bis-Tris
	12 g EDTA
	final volume made to 2 L with distilled water
1x Transfer buffer (5L)	250 ml 20 x Transfer buffer
	1000 ml Methanol
	final volume made to 5 L with distilled water

3.1.8 Softwares

Softwares	Company
BD FACSDiva v6 software	BD Bioscience
Biorender.com	BioRender
DESeq2 version 1.30.0	Bioconductor
FIJI	Open source
GraphPad Prism 10.0	GraphAd Software, Inc.
Ilastik	Open Source
Image Lab	Bio-Rad®
Imaris	Bitplane
Imaris file converter	Bitplane
ImSpector	LaVision BioTec
Inkscape	Open Source
LAS X	Leica
LAS X Life Science	Leica
NIS-AR v.5.3	Nikon
Trimmomatic 0.39	Illumina

3.1.9 Genotyping primers

Primer	Sequence
Reg3b Forward	GTCCTCCATGTTGAAGAGAAC
Reg3b Reverse	ATTCCCATCCACCTCCATTG
LacZ Forward	GTTGCAGTGCACGGCAGATACACTTGCTGA
LacZ Reverse	GCCACTGGTGTGGGCCATAATTCAATTCGC

3.1.10 RT-qPCR primers

Primer	Sequence
Csf3 Forward	GCAGCCCAGATCACCCAGAAT
Csf3 Reverse	TGCAGGGCCATTAGCTTCAT
Cxcl12 Forward	GCACTTTCACTCTCGGTCCA
Cxcl12 Reverse	TCAGATGCTTGACGTTGGCT
Gdf15 Forward	TGCTGTCACTTGGAGACTGTG

Gdf15 Reverse	CAGGCGTGCTTTGATCTGC
Il6 Forward	TGCAAGAGACTTCCATCCAGT
Il6 Reverse	TTGTGAAGTAGGGAAGGCCG
Kitl Forward	TTATGTTACCCCCTGTTGCAG
Kitl Reverse	CTGCCCTTGTAAGACTTGACTG

3.1.11 Mice

For this study, 8-14 weeks male adult mice were used. Analogue to previous studies of my working group (Detzer, 2020; Lörchner et al., 2018), all animal experimentations were performed in accordance to the German animal welfare law and European Union ethical guidelines. Experiments were evaluated and approved by the local governmental animal protection authority (Regierungspräsidium Darmstadt). Mice were sacrificed using a CO_2 chamber and subsequent cervical dislocation.

3.1.11.1 Wild-type mice

Wild-type (WT) mice with a C57BL/6J background were bred in-house and served as control for all experiments, as described.

3.1.11.2 Mice deficient of regenerating islet-derived protein 3β (*Reg3b*$^{-/-}$)

Mice with a global genetic deletion of *Reg3b* (Reg3b/;B6;129-Reg2tm1Lchr/H) were generated by Lieu and collaborators (2006) and kindly provided by S. Hunt, University College of London. For the knockout, a region between exon 2 and exon 5 was replaced by a LacZ sequence and a *Neo* cassette. *Reg3b*$^{-/-}$ mice are phenotypically indistinguishable from WT mice. The gene knockout has no effects during development or fertility.

3.2 Methods

3.2.1 Experimental myocardial infarction in adult mice

Experimental myocardial infarction was performed by Roxanne Harzenetter, according to previous published studies from my group (Lörchner, Pöling et al., 2015; Lörchner, et al., 2018). Therefore, adult male mice aged 10 - 14 weeks were subjected to

permanent surgical ligation of the left anterior descending (LAD) coronary artery. Mice were injected subcutaneously with 0,1 mg/kg buprenorphine 30 min before surgery. The mouse trachea was cannulated with a 22 gauge blunt intravenous catheter and artificially ventilated using a rodent ventilator at 150 strokes per minute with a mixture of 80 % O_2 and 2 % isoflurane for anesthesia. Body temperature was maintained with the help of a heating pad. The fur was removed from the thoracic region and the thorax was opened under additional local intercostal anesthesia between the left 3rd and 4th ribs with subsequent pericardiotomy. The LAD artery was permanently ligated using a 7-0 silk suture in a single movement. Infarction was confirmed by paling of the left ventricle apex and detection of ST-T changes in the electrocardiogram. After suturing back the muscles and skin, animals were extubated and allowed to recover from surgery. A second dose of 0,1 mg/kg buprenorphine was subcutaneously injected 24 h after surgery, with further addition of metamizole (0,8 ml per 500 ml) to the drinking water during the first 5 days after surgery.

3.2.2 Intramyocardial injections

Intramyocardial injections were also performed by Roxanne Harzenetter, according to Lörchner et al. (2018). Two days after LAD ligation, the chest cavities of WT and *Reg3b*$^{-/-}$ mice were reopened for intramyocardial injections. 100 ng of recombinant mouse REG3β (diluted at 5 ng/µl) or equivalent volume of PBS were injected into three different locations along the border zone. The mice were allowed to recover for 5 more days and sacrificed on the 7th day since LAD ligation. Hearts were then perfused with PBS, fixed with 3 % PFA for 2 h at RT and harvested for whole-mount staining of cardiac lymphatics.

For immune cell tracing experiments, 20 µl of pHrodo red succinimidylester particles were injected into three different locations along the border zone, three days after LAD ligation. These pH-sensitive fluorogenic particles were then traced to distal organs (mediastinal lymph nodes, bone marrow and spleen).

3.2.3 5-Bromo-2'-deoxyuridine (BrdU) labeling of proliferating lymphatics

In order to label newly synthesized DNA, 0,8 mg/ml BrdU (Sigma-Aldrich) and 2 % sucrose were added to drinking water *ad libitum*. The BrdU-supplemented water was offered

to the mice directly after the surgery. Animals were sacrificed on day 4 or 7 and hearts were subsequently used for immunohistochemistry analysis.

3.2.4 5-Bromo-2'-deoxyuridine labeling of proliferating immune cells

In order to acutely label the newly synthesized DNA of immune cells in the bone marrow, mice received, 3 days after LAD ligation, an intraperitoneal injection of 250 µl of BrdU at 1 mg/ml (10mg/kg body weight). Animals were sacrificed 24 h after the injection, and hearts, mediastinal lymph nodes and tibias were collected, washed with PBS and subsequently used for flow cytometric analysis of cardiac and bone marrow neutrophils. Alternatively, for the analysis of proliferating tissue macrophages, BrdU was injected 4 days after LAD ligation, 2 h prior to sacrifice, as previously described (Dick et al., 2019).

3.2.5 Intraperitoneal injections of sVEGFR3-AAV

The AAV9 particles were purchased from the AAV Gene Transfer and Cell Therapy Core facility from Helsinki University, with the consent of Prof. Dr. Kari Alitalo. Mice received a single intraperitoneal injection of either AAV9-sVEGFR3 or AAV9-scramble 28 days prior to LAD ligation. Each animal was injected with $1x10^{11}$ viral particles diluted with PBS to 100 µl. 21 days after the AAV9 administration blood was collected from the submandibular area of the cheek and serum was isolated by centrifugation at high speed after clotting.

Blood serum was diluted 1:50 and processed according the methodology described in the western blot section (3.2.22). Serum samples were loaded onto 8 % Bis-Tris-acrylamide gels and separated by electrophoresis, prior to probing with goat anti-mouse VEGFR3 antibody. Using this strategy it was possible to identify animals, which were not overexpressing the vector, and exclude them from further analysis.

Animals overexpressing sVEGFR3 or scramble controls were then subjected to LAD ligation. After this, they started receiving 0,8 mg/ml BrdU in the drinking water, as previously described on section 3.2.3. Three days after LAD ligation, pHrodo was injected in the myocardium for tracing studies, as described on section 3.2.2. 6h after the dye injection, hearts were harvested for histology, whereas mediastinal lymph nodes and bone marrow were harvested for flow cytometric analysis.

3.2.6 Immunohistochemistry

3.2.6.1 Hearts, lymph nodes, spleen

Hearts were harvested and extensively washed in PBS in order to remove excess of blood. The excised hearts were fixed with 3 % PFA for 2 h at room temperature (RT) under rotations and transferred to 15 % sucrose solution for 2 h at RT; followed by overnight incubation in 30 % sucrose at 4 °C. The organs were embedded in Tissue-Tek® O.C.T.™ (first overnight at 4 °C to ensure O.C.T. penetration in the tissue, and then at -80 °C). Heart cryosections with a thickness of 10 µm were prepared from 6-8 different infarct regions, ranging from the apex to the level of the LAD knot. Slides containing cryosections were kept at -20 °C and washed with PBS prior to immunostaining.

Antigen retrieval was performed in order to recover BrdU epitopes. For that, 10 mM sodium citrate buffer pH 6,0 was freshly prepared and heated up to 99 °C. Slides were added to the boiling solution for 15 min, removed and left to cool down. After a PBS wash, slides were permeabilized for 10 min using 0,1 % Triton X-100, followed by another PBS wash. Unspecific binding was prevented by blocking the tissue with 3 % BSA solution for 1 h at RT. Primary antibodies were diluted in 1 % BSA solution and incubated overnight at 4 °C in the concentrations described in the materials section. After washing three times, respective secondary antibodies were added at a concentration of 1:400, for 1 h at RT, also in 1 % BSA solution. Unbound secondary antibody was washed away three times with PBS. When necessary, nuclei were counterstained using 4′,6-diamidin-2-phenylindol (DAPI) for 10 min at RT. Slides were washed two times with PBS, mounted in Mowiol and embedded with coverslips.

3.2.6.2 Bones

Femurs were collected from infarcted mice after intramyocardial injection of pHrodo. The associated skin, fat and skeletal muscle were thoroughly cleaned and the bones fixed using 4 % PFA for 2,5 h at 4 °C. Bones were decalcified using 0,5 M EDTA, pH 7,4 for 24 h at 4 °C, under constant rotations. After decalcification, bones were washed three times in PBS on a rocker and transferred to a 30 % sucrose solution. Prior to embedding in Tissue-Tek® O.C.T.™, the bones were incubated for 24 h in a solution containing 70 % O.C.T. and

30 % sucrose. Finally, embedded bones were longitudinally cut in 10 µm tick-sections using a cryotome.

For immunofluorescence stainings, bone sections were thawed, permeabilized using 0,2 % Triton X-100 in PBS and blocked using 3 % BSA. Primary antibodies were added to the sections overnight at 4 °C and the slides were washed extensively afterwards. Secondary antibodies were added for 1 h at RT, and washed prior to nuclear counterstaining with DAPI and mounting with Mowiol. All antibodies were diluted in a solution containing 1 % BSA and 0,03 % Triton X-100.

3.2.7 Imaging

Tile scan images were acquired using a Ni-E ECLIPSE widefield microscope equipped with a SlideExpress 2 slideloader, a SOLA light engine and a DS-Qi2 Mono Digital microscope camera. All acquisition parameters (light sources, illumination time, camera gain etc.) were set up with the software NIS-AR software v.5.3 and kept constant for the entire imaging experiment.

Image acquisition was automated using the NIS-AR JOBS module: overview images in the DAPI channel were acquired using a CFI Plan Achromat UW 2 x objective, allowing the selection of regions of interest in each slide. Within each region of interest, a focused plan was identified using the autofocus function on the DAPI channel. A 30 µm z-stack was acquired for all fluorescent channels (filters: DAPI-5060C, FITC-3540C, mCherry-B and Cy5-4040C). Slides were scanned as ND-acquisition using a CFI Plan Apochromat 10x Lambda objective. The resulting images were automatically processed in the NIS-AR software by an extended depth of focus (EDF) followed by a fluorescence stitching using the parameters “image registration” and “optimal path”.

Whenever a bigger magnification was necessary, the Leica Thunder Imager DMi8 was used together with a K8 monochrome digital microscope camera and the corresponding software LASX. DAPI was imaged using an excitation wavelength of 395 nm, a DFT51010 quad band filter cube and a 460 nm emission filter on an external filter wheel. Alexa Fluor 488 was imaged with an excitation wavelength of 475 nm, a DFT51010 quad band filter and a 535 nm external emission filter. Alexa Fluor 594 was imaged with an excitation wavelength of 575 nm, a CYR71010 quad band filter and a 642nm emission filter on an external wheel.

Alexa Fluor 647 was imaged with an excitation wavelength of 635 nm, DFT51010 quad band filter and a 642 nm emission filter on an external filter wheel. Both Alexa Fluor 750 and 790 were imaged with a 747 nm excitation wavelength and a CYR71010 100 % external emission filter.

Image analysis was performed using the software Fiji. In order to minimize biases during image analysis, quantifications were done using automated macros.

3.2.8 In vivo staining of cardiac leukocytes

10 µg of rat anti-mouse CD11b conjugated with Alexa Fluor 647 were injected retro-orbitally in anesthetized mice 14 days after LAD ligation. After 30 min, animals were sacrificed and the hearts were perfused with 20 ml of PBS. Hearts were then fixed for 2 h in 3 % PFA at RT under constant agitation and washed on PBS. After this, probes were dehydrated in an ascending ethanol/dH_20 series of: 30 %, 50 %, 70 %, 90 %, 100 % and 100 %, at 4^oC, allowing at least 4 h of incubation for each ethanol step. Aiming to minimize autofluorescence, samples were incubated for 1 h in 5 % DMSO diluted in methanol and subsequently bleached with 5 % hydrogen peroxide / 5 % DMSO diluted in methanol. After 4 h bleaching, samples were washed for 1 h in 100 % ethanol, brought to room temperature and cleared overnight using ethyl cinnamate. Cleared samples were then imaged using the La Vision Biotec Ultramicroscope II.

3.2.9 Whole-mount staining

3.2.9.1 Hearts

In order to tri-dimensionally visualize vessel coverage and the immune cell distribution, a 3-week whole-mount staining protocol was employed (**Fig. 6)**. For this, hearts were collected after perfusion with 30 ml PBS and fixation with PFA. For the whole-mount staining, hearts were permeabilized and blocked for 24 h using “Block and permeabilize” (see “Materials” section). A second permeabilization of 48 h was performed, followed by 48 h of blocking. Primary antibodies were diluted using the antibody solution and the hearts were stained for a total of 5 days at 4 °C. The excess of primary antibody was washed out 4 times in PTwH solution. Secondary antibodies were diluted in the same antibody solution and incubated for 4 days at 4 °C. After washing out unbound antibodies with PTwH, samples

were dehydrated in an ascending ethanol/dH_20 series of: 30 %, 50 %, 70 %, 90 %, 100 % and 100 %. Aiming to minimize autofluorescence, samples were bleached and cleared according to the description on 3.2.8. Cleared samples were then imaged using the La Vision Biotec Ultramicroscope II.

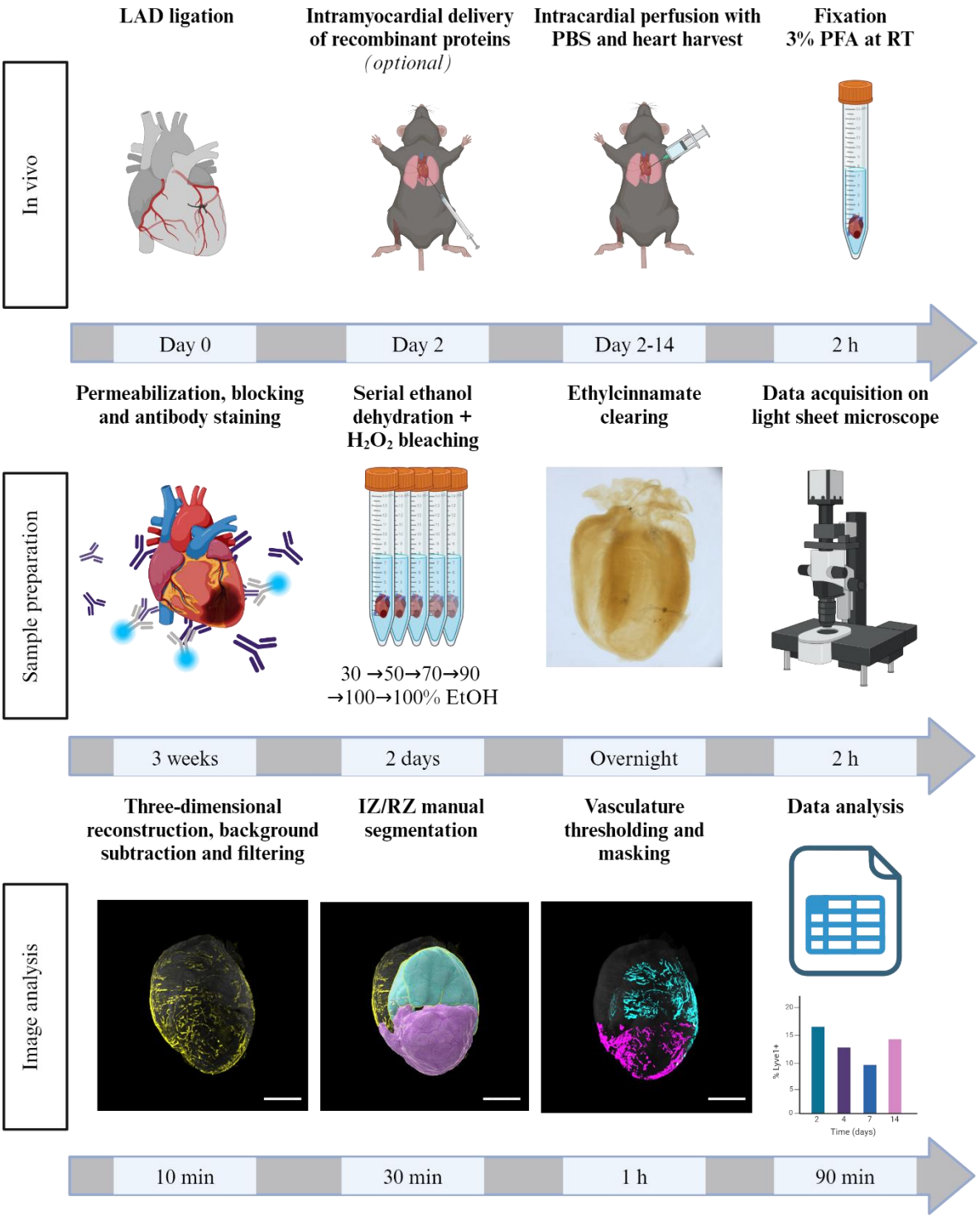

Figure 6. Methodological overview of cardiac whole-mount staining for three-dimensional lymphatic vessel reconstruction and analysis. Myocardial infarction was induced by ligation of the LAD coronary artery. When applicable, recombinant proteins were injected intramyocardially. Hearts were perfused using PBS and fixed in PFA. Whole-mount staining of vessels took a total of three weeks and comprised multiple steps and solutions, as

described in the method section. Dehydrated hearts were cleared using ethyl cinnamate, and imaged using the light sheet microscope, while immersed in the same solution. All Z stacks acquired were used to reconstruct the three-dimensional image. Images were preprocessed using Imaris background subtraction and filtering tools. The infarcted zone (IZ, magenta) and remote zone (RZ, cyan) were manually segmented using the differential autofluorescence deriving from cardiomyocytes. Finally, vasculature was thresholded and masked in- and outside each region. The percentage of lymphatic coverage was calculated as the volume of the vasculature divided by the volume of the IZ or RZ. Scale bar = 2mm. Illustration created with "BioRender.com".

3.2.10 Light sheet microscopy

Cleared samples were imaged on the La Vision Ultramicroscope II using the corresponding ImSpector software. The microscope consists of a MVX10 zoom body from Olympus with a 2 x objective. The microscope is equipped with a Zyla 4.2 PLUS sCMOS camera from Andor for image generation. 10 µm Z-steps and a total magnification of 1,26 x were used for image acquisition. Three-dimensional reconstruction was performed using the Imaris file converter. Images were processed using the Imaris software including background subtraction and median tools. The infarct zone (IZ) was delimited using the contour tool around the region with dim autofluorescent signal on the 488 channel. For segmenting of the remote zone (RZ), the first 300 planes (ventral → dorsal) from the non-infarcted left ventricle were contoured (**Fig. 7)**. The apex of non-infarcted hearts was contoured as the region downstream of the major trifurcation of the LAD artery. Lymphatic vessels were thresholded using the surface tool and made binary for volume quantification. Immune cells were thresholded using the Imaris spots function.

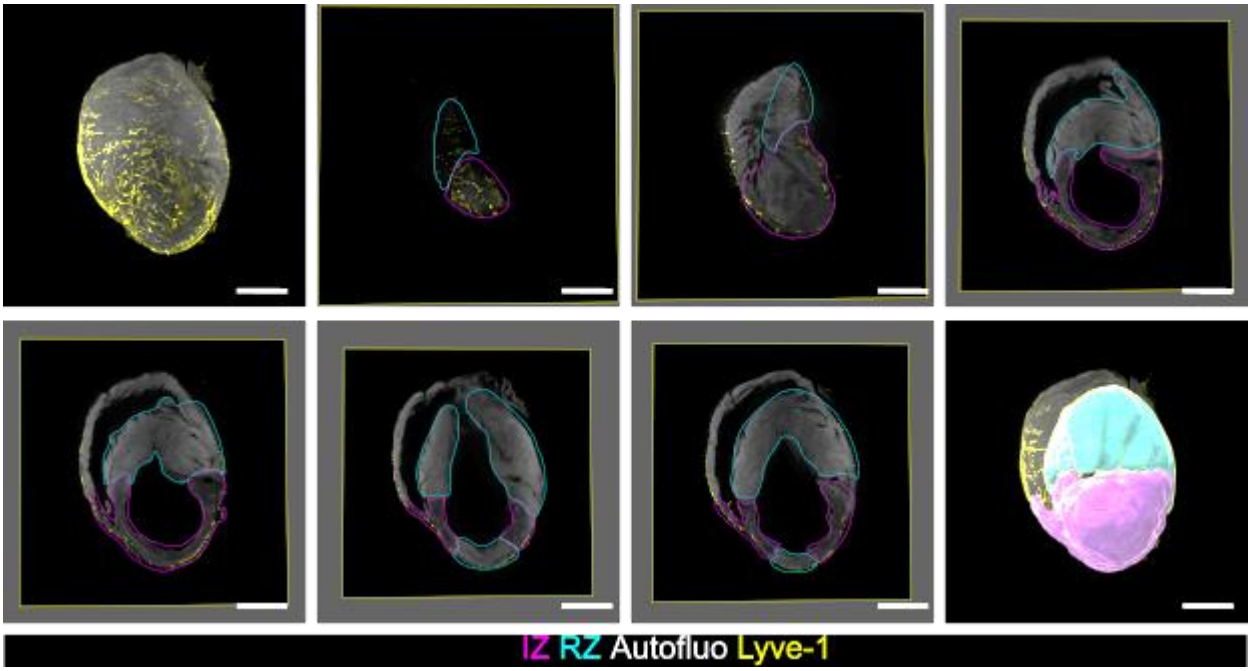

Figure 7. Segmentation strategy for the infarcted zone (IZ) and the remote zone (RZ). The infarcted zone (magenta) was segmented based on the weaker autofluorescence signal observed in the collagenous scar. The remote zone (cyan) was defined as the complementary volume of the left ventricle, characterized by the autofluorescence of living cardiomyocytes (including septum). Magnification = 1,26 x. Scale bar = 2 mm.

3.2.11 Cardiac leukocyte isolation from the infarcted heart

Infarcted hearts were harvested at different time points after LAD ligation. Excess of blood was removed from the ventricles and the left ventricle was manually dissected from the rest of the heart. The heart tissue was roughly minced using scissors and then enzymatically digested using 3 ml of 0,1 mg/ml liberase for 30 min at 37 °C. After enzymatic digestion, the supernatant containing cells was transferred to cold PEB buffer and kept on ice. The remaining non-digested tissue was subjected to a second round of enzymatic digestion. The combined cell suspension was centrifuged at 300 x g for 10 min at 4 °C and the pellet used for flow cytometric preparation. The pellet was resuspended in 3 ml of PEB and filtered using a 30 µm cell strainer. In order to remove the excess of extracellular matrix debris, the filtered cell suspension was centrifuged and the pellet was resuspended in a mixture of 3,1 ml of cold PEB buffer and 0,9 ml of debris removal solution from Miltenyi Biotec. After resuspension, 2 ml of PBS were slowly added to the side of the tube and the

content centrifuged at 3.000 x g for 10 min at 4 °C. The centrifugation led to the formation of a triphasic gradient, which contained cells in the lower phase, debris in the interphase and a supernatant. The supernatant and debris were carefully aspirated, the cell pellet was washed in 10 ml of cold PBS, and further centrifuged at 1.000 x g for 10 min at 4 °C. Finally, the single cell suspension was resuspended in PEB buffer and used for antibody staining.

3.2.12 Cardiac leukocyte isolation from mediastinal lymph nodes, spleen and bone marrow

Mediastinal lymph nodes and spleens were removed from infarcted mice, mashed in PEB buffer and filtered through a cell strainer of 30 µm pore size. The single cell suspensions were centrifuged at 300 x g for 10 min at 4 °C. Red blood cells in the spleen were lysed by adding 1 ml of ice-cold hypotonic water for 15 seconds. The cells were subsequently washed in 4 ml of PEB buffer, centrifuged at 300 x g for 10 min at 4 °C and resuspended in PEB buffer.

For isolation of bone marrow cells, the skin and skeletal muscle associated with the tibia bone were removed. After this, the extremities of the bone were flushed with 2 ml of PEB buffer. The recovered cell suspension was centrifuged at 300 x g for 10 min at 4 °C and the cell pellet was resuspended in PEB buffer.

3.2.13 Flow cytometry sample preparation

Single cell suspensions obtained from heart, lymph node, spleen and bone marrow were counted using a hemocytometer and adjusted to 1 x 10^6 cells per 100 µl of PEB buffer, according to manufacturer's instructions. Conjugated antibodies against surface epitopes were added for 20 min on ice and protected from light. Next, the cell suspension was washed using PEB buffer and centrifuged at 300 x g for 10 min at 4 °C. Whenever intracellular epitopes were targeted, the cells were fixed on ice using 100 µl of fixative buffer for 20 min. After this, cells were washed using 750 µl of saponin-containing permeabilization buffer and centrifuged at 300 x g for 10 min at 4 °C. 100 µl of permeabilization buffer containing the antibodies against intracellular epitopes were then added for another 20 min, on ice. Unbound antibodies were washed using the permeabilization buffer and the cell suspension was centrifuged at 300 x g for 10 min at 4 °C. Finally, the cell pellet was resuspended in 600 µl of PEB buffer and used for flow cytometric analysis.

3.2.14 Fluorescence-activated cell sorting (FACS) analysis and sorting

Antibody-stained leukocytes were analyzed on LSR Fortessa™ . First, cell population was discriminated from debris by plotting the forward scatter (FSC) against the light sideward scatter (SSC). Cell doublets were excluded by plotting forward scatter-height (FSC-H) against forward scatter-area (FSC-A).

The FACS strategy was adapted from Lörchner and collaborators (2018). $CD45^{hi}$ leukocytes were subdivided between myeloid ($CD11b^{hi}$) or non-myeloid leukocytes ($CD11b^{lo}$). Based on this initial stratification, neutrophils were defined as $CD45^{hi}$ $CD11b^{hi}$ $(F4/80\ CD64)^{lo}$ $Ly6G^{hi}$, cardiac tissue macrophages as $CD45^{hi}$ $CD11b^{hi}$ $Ly6G^{lo}$ $(F4/80\ CD64)^{hi}$, monocytes as $CD45^{hi}$ $CD11b^{hi}$ $Ly6G^{lo}$ $(F4/80\ CD64)^{lo}$ $CD115^{hi}$ and myeloid dendritic cells as $CD45^{hi}$ $CD11b^{hi}$ $Ly6G^{lo}$ $(F4/80\ CD64)^{lo}$ $(CD11c\ MHCII\ CD103)^{hi}$. Non-myeloid B lymphocytes were defined as $CD45^{hi}$ $CD11b^{lo}$ $(CD19\ IgM)^{hi}$, $CD4^{+}$ T lymphocytes as $CD45^{hi}$ $CD11b^{lo}$ $(CD19\ IgM)^{lo}$ $CD3^{hi}$ $CD4^{hi}$ $CD8^{lo}$ and $CD8^{+}$ T lymphocytes as $CD45^{hi}$ $CD11b^{lo}$ $(CD19\ IgM)^{lo}$ $CD3^{hi}$ $CD4^{lo}$ $CD8^{hi}$. $pHrodo^{+}$ leukocytes were gated based on the fluorescence shift from leukocytes derived from mice receiving an intramyocardial PBS injection.

For intracellular expression analysis of VEGF-C, VEGF-D in cardiac tissue macrophages and cardiac troponin I (cTnI) in $pHrodo^{+}$ leukocytes, cells were fixed and permeabilized using the intracellular fixation and permeabilization buffer set according to the manufacturer's protocol for staining of intracellular proteins. Both, fluorescence compensation and fluorescence minus one (FMO) controls were used to ensure correct compensation and gating. Data acquisition and analysis was carried out using BD FACS Diva v6 software. For calculation of cell numbers per mg of tissue, samples were normalized to heart weight.

Sorting of $pHrodo^{+}$ or $pHrodo^{-}$ neutrophils and macrophages extracted from the bone marrow was performed on the BD FACS Aria III cell sorter.

3.2.15 RNAseq of pHrodo-labeled leukocytes

3.2.15.1 RNA extraction

Total RNA was extracted using the RNeasy® Micro Kit, according to manufacturer's instructions. The cell pellet extracted from the bone marrow was homogenized using 350 µl of the provided homogenization buffer and centrifuged at 18.000 g for 3 min. The supernatant was mixed with the same volume of 70 % ethanol, and this mixture was transferred to an RNeasy MinElute spin column. The columns were again centrifuged at 18.000g for 15 min and the flow-through discarded. Genomic DNA was eliminated by adding DNAse I for 15 min at RT. After this, the DNAse was diluted and the column spinned at 8.000 g for 15 s. The flow-through was again discarded and the RNA washed in 80 % ethanol, followed by another round of centrifugation and flow-through elimination. The RNA in the columns was then eluted using a 14 µl of RNase-free water and 5 ng of total RNA was used for bulk RNAseq analysis.

3.2.15.2 Bulk RNA sequencing (RNAseq)

Bulk RNAseq was performed according to Lörchner et al. (2023) and Carpenter et al. (2023). The integrity of both RNA and library was verified using the LabChip Gx Touch 24 system. Approximately 5 ng of total RNA served as the starting material for cDNA preparation using the SMART-Seq HT Kit. Sequencing was conducted on the NextSeq2000 instrument using a P3 flowcell with a 1×72 bp single-end setup. Reads were processed with Trimmomatic version 0.39, which trimmed reads if their quality dropped below a mean Q-score of 15 within a 5-nucleotide window, retaining only those reads longer than 15 nucleotides (Bolger et al., 2014). The reads were mapped to the Ensembl mouse genome version mm10-101 using STAR 2.7.10a (Dobin et al., 2013). After alignment, duplicated, multi-mapped, ribosomal and mitochondrial reads were removed using Picard 2.27.4. Using featureCounts 2.0.4, reads overlapping exons could be distinguished from reads overlapping multiple genes (Y. Liao et al., 2014). The raw count matrix was normalized using DESeq2 version 1.36.0 (Love et al., 2014), which was also employed for creating contrasts. Genes were considered differentially expressed (DEG) if they had an average count > 5, an adjusted p-value < 0.05, and a log2 fold change between -0.585 and 0.585. The Ensembl annotation was enriched with UniProt data. All downstream analyses were based on the normalized gene

count matrix. Dimension reduction analyses (PCA) were performed on regularized log-transformed counts using the R package FactoMineR (Lê et al., 2008). DEGs were subjected to gene set overrepresentation analyses using KOBAS (Xie et al., 2011). Either up- or down-regulated genes were tested per contrast using two separate tests. Results showing a significant overrepresentation at False Discovery Rate (FDR) < 0.05 were taken into consideration.

3.2.16 RNA and protein extraction from bone marrow

Tibias and femurs of infarcted mice were harvested 4 days after LAD ligation and thoroughly cleaned from the surrounding muscle tissue. The right femur and right tibia were flushed with 2 ml PBS and cellular pellets were snap frozen in liquid nitrogen.

Pellets from the right femur were lysed using TriPure and processed according to manufacturer's instruction. The RNA concentration was confirmed using Nanodrop spectrophotometer and used for further cDNA preparation.

The cellular pellet from the right tibia was lysed in EP/5x LB buffer supplemented with 40 mM DTT and denatured under 99 ^{o}C for 1 min. Samples were then used for western blot analysis.

3.2.17 Reverse transcription

1 µg of total RNA was converted into cDNA using PrimeScript RT Reagent Kit with genomic DNA eraser, according to the manufacturer's instructions.

3.2.18 Real-time quantitative reverse transcription PCR (RT-qPCR)

For RT-qPCR analysis, 20 ng of cDNA template diluted at 5 ng/µl was mixed with 400 nM of reverse and forward primers, 5 µl of 2x S'Green supplemented with 1,75 µM ROX additive and ddH20 to complete for 10 µl of reaction. Only primer pairs with efficiency superior to 90 % and single-peak melting curves were used. RT-qPCR reactions were performed on a StepOne™ real-time PCR system and amplified according to the protocol described on **Table II**.

Table II: Reaction conditions for RT-qPCR

RT-qPCR		
95 °C	2 min	
95 °C	5 sec	x 40
60 °C	30 sec	
Melting curve according to instrument instructions		

3.2.19 Gravimetry

Infarcted hearts were harvested 4 days after LAD ligation, washed in PBS, and dissected into scar, free wall of left and right ventricle and septum. The tissues were dried on a gauze, weighed on a precision scale and collected into individual microcentrifuge tubes. The tubes were placed with open lids on a thermoblock set at 65 °C for 96 h, after which the dry tissues were weighed, again. The water content (%) was calculated as 1-(dry/wet tissue).

3.2.20 DNA isolation

Tissue derived from mouse ears was used for genotyping. For this purpose, the tissue was digested with 10 µl of proteinase K diluted in 500 µl of TENS buffer, at 1.150 rpm rotations for 2 h at 56 °C. After digestion, samples were centrifuged at 12.900 x g, for 5 min at RT. The supernatant mixed into a new tube containing 500 µl of isopropanol and again centrifuged at 12.900 x g for 10 min at RT. Supernatants were discarded and the DNA was precipitated with 700 µl of 80 % EtOH. Once more, the samples were centrifuged at 12.900 x g for 5 min, and the supernatant was discarded. The pellet containing DNA dried for 1 h, was resuspended with 300 µl of distilled water and further used for genotyping.

3.2.21 Polymerase chain reaction (PCR)

For PCR-based genotyping, 1 µl of isolated DNA was mixed with 8 µl of 2 x Taq polymerase master mix, 12 µl of DNAse-free water and 0,1 µl of primers. The identification of mutant genotype is based on two different PCR reactions: one for the WT *Reg3b* gene, and another for the inserted LacZ reporter construct, which interrupts the gene. The PCR results from *Reg3b*$^{-/-}$ animals show a band corresponding to the LacZ construct but not a band relative to the WT gene. Table III indicates the employed PCR protocols:

Table III: Genotyping protocol for the identification of *Reg3b*$^{-/-}$ animals

WT *Reg3b* gene			LacZ reporter construct		
93°C	3 min		93°C	3 min	
93°C	30 sec	x 36	93°C	30 sec	x 27
61°C	40 sec		61°C	30 sec	
72°C	60 sec		72°C	30 sec	
72°C	5 min		72°C	5 min	
12°C	∞		12°C	∞	

3.2.22 Western blot

In accordance with previous studies of my working group (Detzer, 2020; Lörchner et al., 2018), infarcted hearts were manually dissected into infarcted zone and non-infarcted remote zone, briefly washed in PBS and snap frozen in liquid nitrogen. Frozen tissue was physically crushed until pulverized and lysed in extraction buffer containing protease inhibitors. The protein lysates were homogenized by sonication and centrifuged at 18.000 x g for 15 min. The supernatant was separated from the pelleted insoluble material and used for protein quantification, using the DC protein assay kit. Protein volumes were adjusted to a concentration of 1,2 µg/µl and mixed with bromophenol blue and DTT to a final concentration of 40 mM. Samples were boiled at 99 ºC for 1 min and cooled down. Serum-derived proteins were neither quantified nor sonicated, but diluted 1:50 with EP/5x LB buffers at a ratio 3:2 ratio and treated with DTT prior to boiling. After a centrifugation at 18.000 x g for 15 min at RT, 12 µg of protein was loaded on 10 % Bis-Tris acrylamide gels. SDS-PAGE was performed at 75 V for 15 min followed by 165 V for 90 min. After electrophoresis, proteins were transferred to a nitrocellulose membrane at 30 V for 2 h. Membranes were stained with RedAlert™ and scanned for digital documentation. Epitopes were blocked using 5 % skimmed milk in TBS-T for 1 h at RT and antibodies of interest were incubated overnight in 3 % skimmed milk in TBS-T at 4ºC. Unbound antibody was recovered and membranes were washed extensively with TBS-T. Afterwards, the membranes were incubated with secondary antibodies conjugated to horseradish peroxidase (HRP) for 1 h at RT. Washed membranes were incubated with WesternBright Sirius chemiluminescence substrate and visualized under the ChemiDoc™ MP system. Mean volume pixel density of protein bands were quantified using the Image Lab software.

3.2.23 Statistical analysis

Statistical analysis and graphs were elaborated with Graphpad prism 10.0. A Shapiro-Wilk normality test was performed for groups with a sample size ≥ 6. Whenever the distribution was normal and two groups were being compared, a two-tailed unpaired Student's t-test was used. If the distribution was not normal or n < 6, a non-parametric two-tailed Mann-Whitney U test was used. Comparisons between three or more groups and a single independent variable were performed using a one-way ANOVA followed by a Bonferroni's post-hoc correction, or the non-parametric Kruskal-Wallis test, if the distribution was not normal. Finally, whenever two independent groups were compared over time or if two regions of the heart were taken into consideration, a two-way ANOVA was performed. Depending on the nature of multiple comparisons performed, either Tukey's or Šidák's post-hoc tests were applied. A p-value of < 0,05 was considered statistically significant.

4 RESULTS

4.1 The role of REG3β in controlling immune cell dynamics in infarcted heart

According to previous work from my group, increased expression of REG3β at sites of cardiac injury was found to be instrumental to cardiac healing, as *Reg3b*-deficient mice (*Reg3b*$^{-/-}$) were characterized by an imbalanced immune response and higher incidence of sudden death upon myocardial infarction (Lörchner, Pöling et al., 2015; Lörchner, et al., 2018).

To better understand how REG3β influences immune-inflammatory responses during cardiac repair, the kinetics of cardiac leukocyte composition in infarcted hearts of WT and *Reg3b*$^{-/-}$ mice was compared by flow cytometry, using hearts at basal state, as well as 2, 4, 7 and 14 days after LAD ligation **(Fig. 8**).

Analysis of the total leukocyte composition revealed that WT and *Reg3b*$^{-/-}$ hearts had similar amounts of leukocytes in comparison to WT before MI induction – when a pronounced infiltration of cardiac leukocytes took place (**Fig. 8A**). In only two days, the leukocyte population in WT increased 100 times, peaking at day 4, with 150 times more leukocytes in comparison to the basal state. According to the literature, the inflammatory response changes from the inflammatory phase to the proliferative phase during the course of the first week (Frangogiannis, 2012, 2014). Indeed, cardiac leukocyte counts slowly decreased, reaching much lower levels after 14 days, albeit still elevated in comparison to the basal state.

Although at the basal state infarcted mice with a germline deletion of *Reg3b* had similar numbers of leukocytes as in WT animals, *Reg3b*$^{-/-}$ hearts showed ~ 40 % less infiltration of leukocytes 2 days after MI (**Fig. 8A,B**). However, the cardiac leukocyte population in *Reg3b*$^{-/-}$ mice reached WT levels by day 4. Surprisingly, 7 days after MI, *Reg3b*$^{-/-}$ hearts showed 90 % more leukocytes in comparison to WT, reaching 120 % by 14 days (**Fig. 8B**). The delayed but overshooting accumulation of leukocytes in *Reg3b*$^{-/-}$ hearts suggest the existence of compensatory mechanisms, which eventually increase leukocyte numbers beyond regular limits.

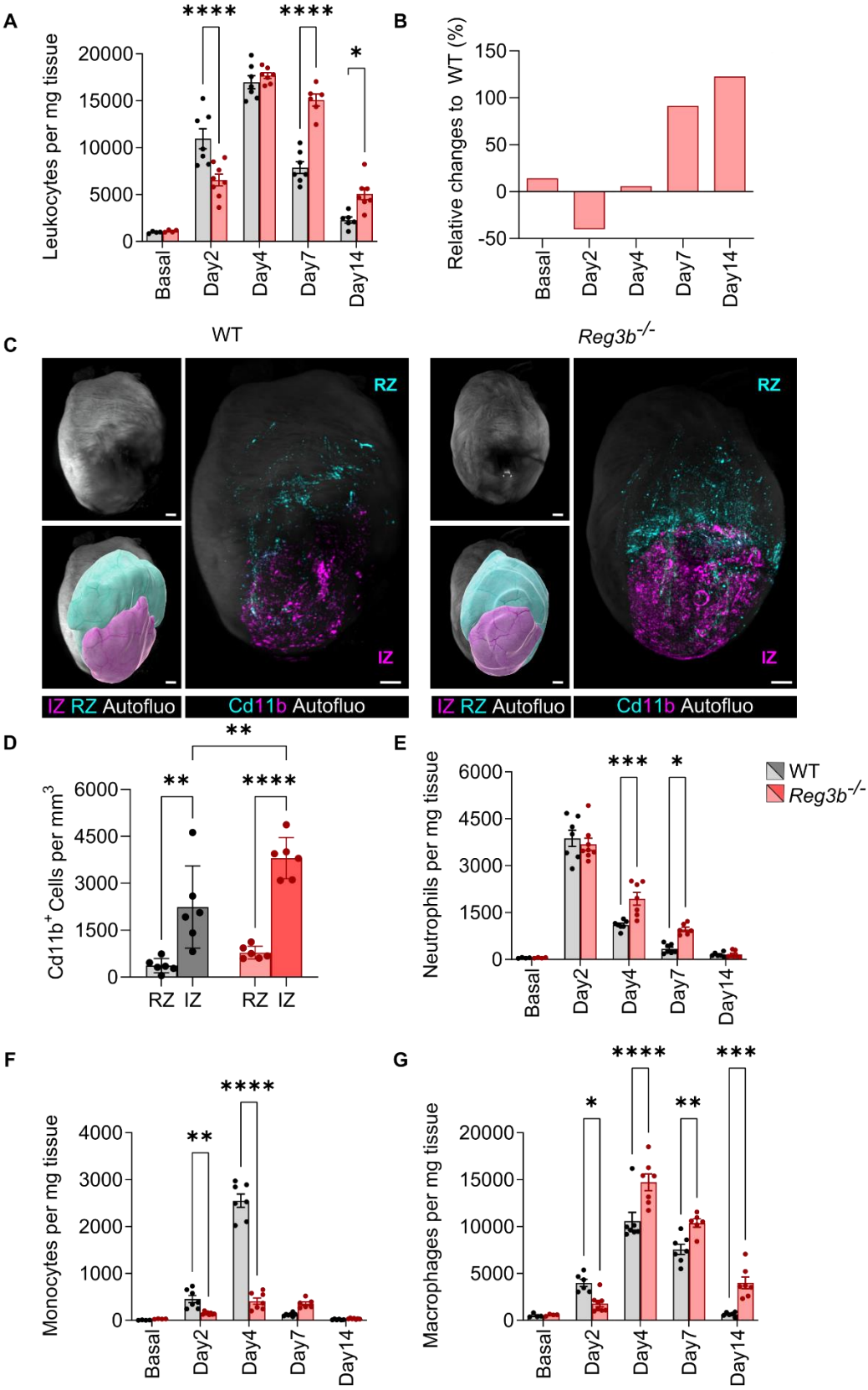
A
Leukocytes per mg tissue
20000
15000
10000
5000
0
****
****
*
Basal
Day2
Day4
Day7
Day14
B
Relative changes to WT (%)
150
100
50
0
-50
Basal
Day2
Day4
Day7
Day14
C
WT
Reg3b-/-
RZ
IZ
IZ RZ Autofluo
Cd11b Autofluo
D
Cd11b+Cells per mm3
6000
4500
3000
1500
0
**
**
****
RZ IZ RZ IZ
E
Neutrophils per mg tissue
6000
4500
3000
1500
0
***
*
WT
Reg3b-/-
Basal
Day2
Day4
Day7
Day14
F
Monocytes per mg tissue
4000
3000
2000
1000
0
**
****
Basal
Day2
Day4
Day7
Day14
G
Macrophages per mg tissue
20000
15000
10000
5000
0
*
****
**
***
Basal
Day2
Day4
Day7
Day14

Figure 8. Genetic deletion of *Reg3b* results in an unresolved immune response after myocardial infarction. (A) Kinetics of leukocyte composition per mg of tissue in WT and *Reg3b*$^{-/-}$ hearts. **(B)** Relative changes throughout time in comparison to basal leukocyte composition in WT animals. **(C)** Representative light-sheet microscopy of CD11b^{+} leukocytes (cyan and magenta) in infarcted heart. Autofluorescence is depicted in gray. Infarct zone (IZ, magenta) and Remote zones (RZ, cyan) were respectively delimited by the low and high autofluorescence signal derived from MI-induced cardiomyocyte death. Myeloid leukocytes inside the IZ and RZ are respectively colored in magenta and cyan. 1,26 x magnification. Scale bar = 0,5mm. **(D)** Quantification of CD11b^{+} leukocytes per mm^{3} in IZ and RZ. Kinetics of **(E)** neutrophils, **(F)** monocytes and **(G)** macrophages per mg of infarcted heart tissue in WT and *Reg3b*$^{-/-}$ hearts. Data are shown as mean ± SEM. **(A,E-G)** N = 4 (basal), 6 (day 14) or 7 (days 2,4,7); **(D)** N = 6. Statistical analysis **(A,E-G)**: Two-way ANOVA followed by Šidák multiple comparisons test. **(D)** Two-way ANOVA followed by Tukey's multiple comparison post-test. *p ≤ 0,05 ;** p ≤ 0,01 ; *** p ≤ 0,001 ; **** p ≤ 0,0001.

In order to visualize potential spatial changes in the distribution of leukocytes in infarcted hearts of *Reg3b*$^{-/-}$ mice in comparison to WT, the murine left anterior descending (LAD) coronary artery was ligated and, 14 days after MI, CD11b^{+} myeloid leukocytes were labeled in vivo with fluorescent antibodies. By employing light sheet microscopy, it was possible to image hearts in three dimensions, spatially delimiting the infarcted (IZ) and remote zones (RZ) based on their different autofluorescence signals **(Fig. 8C**).

Due to MI-induced inflammatory processes, the overall numbers of CD11b^{+} myeloid leukocytes were approximately five times higher in the IZ than in the RZ of both WT and *Reg3b*$^{-/-}$ hearts (**Fig. 8D**). In addition to that, *Reg3b*$^{-/-}$ hearts had ~ 70 % more CD11b^{+} myeloid leukocytes in the IZ than WT infarcted mice 14 days after myocardial infarction.

A complementary flow cytometric analysis unveiled the dynamics of major innate immune cell populations (neutrophils, macrophages, monocytes, dendritic cells), as well as populations from the adaptive arm of the immune cell system (B lymphocytes and T lymphocytes, the latter further stratified into CD4^{+} T and CD8^{+} T lymphocytes).

In accordance with the literature (Daseke et al., 2021; Ma, 2021), neutrophils strongly increased in the first 48 h since MI onset, although they were almost absent under basal conditions (**Fig. 8E**). Despite being considered “first responders” to cardiac tissue injury, the presence of neutrophils in this tissue is short-lived (Puhl & Steffens, 2019). Hence, the amount of neutrophils rapidly decreased from day 4 onwards, again reaching very low counts by the end of 2 weeks. In line with previous findings (Lörchner, Pöling et al., 2015), ~ 75 % more neutrophils were present in *Reg3b*$^{-/-}$ than in WT hearts at day 4 post-MI. By day 7 post

MI, *Reg3b*$^{-/-}$ hearts still had three times more neutrophils, whereas neutrophil counts in WT mice were approaching basal levels.

Along with neutrophils, macrophages and monocytes were highly abundant in the infarcted heart during the acute inflammatory process (**Fig. 8F,G**). Recruitment of monocytes and macrophages also started acutely after MI onset, and both populations peaked in the infarcted WT hearts 4 days after MI. Similar to previously published results (Lörchner, Pöling et al., 2015; Lörchner et al., 2018), *Reg3b*$^{-/-}$ infarcted hearts had ~ 30 % of the WT monocyte population 2 days after LAD ligation and ~ 50 % of the WT macrophage population (**Fig. 8F**). 4 days after MI, the total number of macrophages in *Reg3b*$^{-/-}$ was ~ 50 % higher than WT, although *Reg3b*$^{-/-}$ continued to have less monocytes than WT mice. In fact, the presence of macrophages in *Reg3b*$^{-/-}$ infarcted hearts remained significantly higher at 7 and 14 days after LAD ligation, even when the presence of macrophages had already reached similar levels to basal state in WT hearts (**Fig. 8G**).

Dendritic cells and lymphocytes were less abundant than neutrophils, monocytes and macrophages within the infarcted heart during the acute inflammatory phase (**Suppl. Fig. 1A-D**). Similar to neutrophils, monocytes and macrophages, the populations of dendritic cells, B and T lymphocytes also peaked at day 4. Interestingly, infarcted *Reg3b*$^{-/-}$ mice also had reduced levels of dendritic cells, B lymphocytes and $CD4^+$ T lymphocytes (but not of $CD8^+$ T lymphocytes) at days 2 and 4 post-MI (**Suppl. Fig. 1A-D**).

Overall, the kinetic analysis of the leukocyte composition landscape revealed an imbalanced immune cell composition in *Reg3b*$^{-/-}$ hearts, with a delayed initiation of inflammation followed by a prolonged inflammatory state, which extended into the reparative phase of myocardial healing. Altogether, these observations suggest a poorly controlled resolution of inflammation in infarcted *Reg3b*$^{-/-}$ mice.

The duration of immune cell permanence in the infarcted heart is governed by inhibition of immune cell recruitment, apoptosis, efferocytosis and lymphatic emigration (Ortega-Gómez et al., 2013), suggesting that REG3β might be an important regulator of (at least some of) these processes. Based on this, I hypothesized that REG3β may affect lymphangiogenesis and thereby control immune cell emigration, potentially adding another regulatory layer for controlling immune cell dynamics in the infarcted heart.

4.2 Loss of *Reg3b* enables increases lymphatic vessel proliferation in infarcted hearts

Classical histological staining of thin sections has pioneered detection of lymphatic vessels, but does not reveal the whole complexity of the lymphatic network. More recently, whole-mount staining protocols combined with tissue clearing techniques allowed a three-dimensional visualization of these vessels (Brakenhielm & Alitalo, 2019). In this study, I largely employed whole-mount and histological staining of lymphatic endothelial cells to compare how they are assembled in different compartments of the heart, and to what extent they remodel after injury.

The hyaluronic acid receptor 1 (LYVE-1) is expressed by lymphatic endothelial vessels and pre-collectors and is traditionally employed as a pan-lymphatic marker for whole-mount staining of the heart (Henri et al., 2016; Heron et al., 2022; Houssari et al., 2020; Tatin et al., 2017). As shown in **Fig. 9A**, this protocol allowed the identification of lymphatic vessels in atria (**Fig. 9B**), septum (**Fig. 9C**), valves (**Fig. 9D**) and both ventricles (**Fig. 9C**), particularly in the epicardium. Because a subpopulation of macrophages also expressed LYVE-1 (Bizou et al., 2021) (**Fig. 9A,** indicated by arrows on the apex), small and particular dot-like LYVE-1^{+} structures had to be filtered out for quantification.

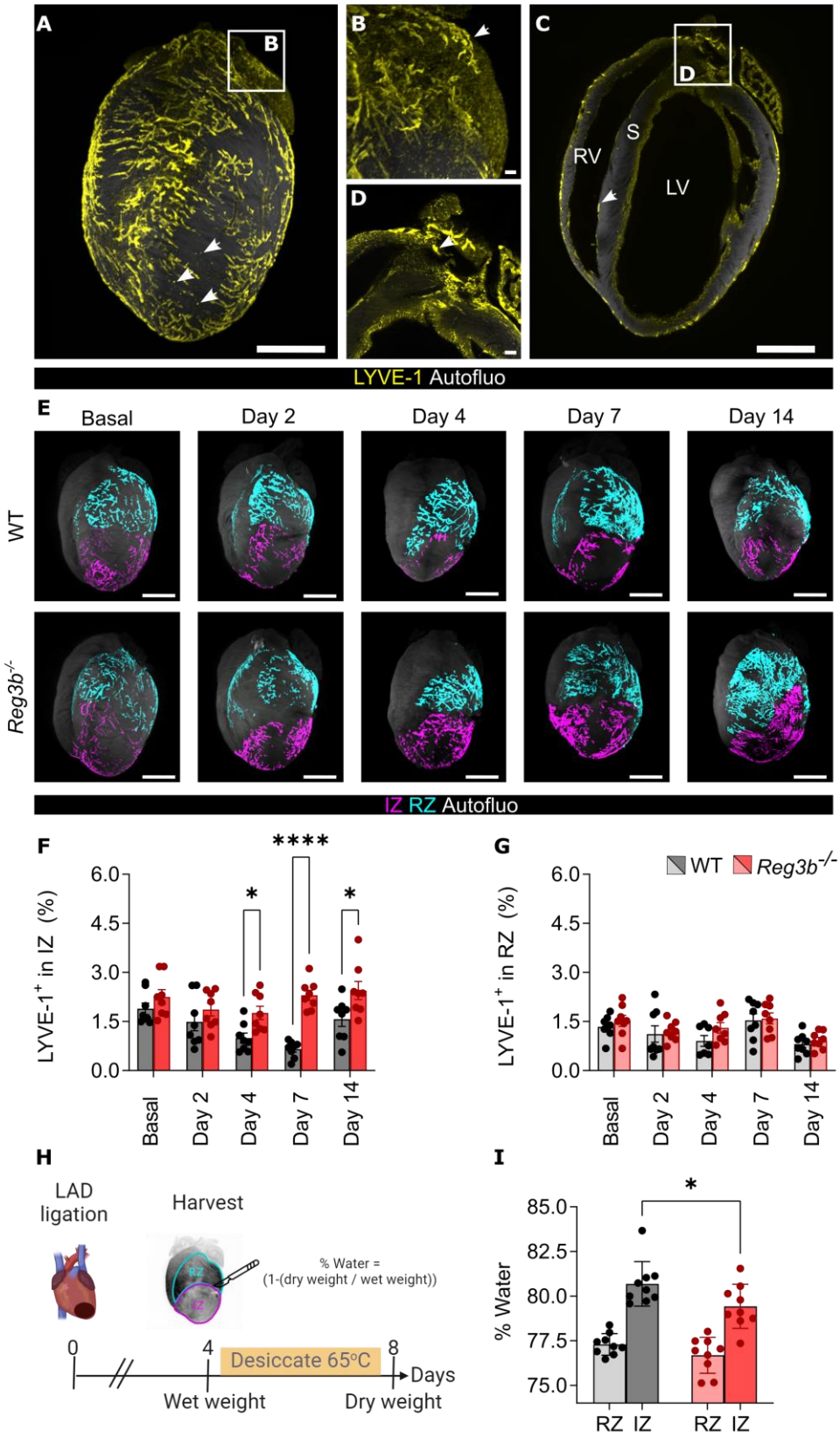
A
B
C
D
RV
S
LV
LYVE-1 Autofluo
E
Basal
Day 2
Day 4
Day 7
Day 14
WT
Reg3b-/-
IZ RZ Autofluo
F
LYVE-1+ in IZ (%)
6.0
4.5
3.0
1.5
0.0
****
*
*
Basal
Day 2
Day 4
Day 7
Day 14
G
WT
Reg3b-/-
LYVE-1+ in RZ (%)
H
LAD ligation
Harvest
% Water = (1-(dry weight / wet weight))
0
4
8
Desiccate 65°C
Days
Wet weight
Dry weight
I
% Water
85.0
82.5
80.0
77.5
75.0
*
RZ IZ RZ IZ

Figure 9: Cardiac lymphangiogenesis is increased in infarcted hearts of *Reg3b*$^{-/-}$ mice. **(A)** LYVE-1^{+} whole-mount staining of lymphatic vessels. These vessels were mostly present in the ventricular epicardium, as well as in **(B)** atria. **(C)** Optical longitudinal optical section showing LYVE-1^{+} vessels on septum and **(D)** tricuspid valve, as indicated by arrows. Scale bar = 2 mm (overviews) and 200µm (insets). RV, right ventricle, LV, left ventricle, S, septum. **(E)** Representative light sheet microscopy images LYVE-1^{+} lymphatic network in the infarcted zone (IZ, magenta) and remote zone (RZ, cyan) 0, 2, 4, 7 and 14 days after LAD ligation in WT and *Reg3b*$^{-/-}$ mice. 1,26 x magnification. Scale bar = 2 mm. **(F)** Quantification of IZ and **(G)** RZ covered with LYVE-1^{+} lymphatics. **(H)** Gravimetry experimental outline: 4 days after LAD ligation, infarcted hearts were collected and dissected between IZ and RZ. Tissues were weighed and desiccated over 4 days, after which they were again weighed, to calculate the water content. Illustration created with "BioRender.com". **(I)** Percentage of water in IZ and RZ 7 days after MI induction. Data are shown as mean ± SEM. (**E-G**) N = 8; (**I**) N = 9. Statistical analysis: **(F,G,I)** Two-way ANOVA followed by Šidák multiple comparisons test. *p ≤ 0,05 ;** p ≤ 0,01 ; *** p ≤ 0,001 ; **** p ≤ 0,0001.

Similar to the analysis of CD11b^{+} myeloid leukocytes in **Fig. 8**, and aiming to identify potential spatial differences in lymphatic distribution after injury, the left ventricle was divided in two different fractions: a hypoxic IZ of lower autofluorescence intensity and a non-hypoxic – but to some degree still inflamed –, more autofluorescent, RZ. Accordingly, the percentage of vessel coverage was analyzed separately between these two compartments, and vessels were digitally colored on either in magenta (IZ) or in cyan (RZ) (**Fig. 9E**).

In the basal state, WT and *Reg3b*$^{-/-}$ animals had comparable lymphatic coverage in both the apex and the base of the heart (**Fig. 9E-G**). Due to the hypoxic environment in the IZ, it was possible to observe a time-dependent death of lymphatic vessels during the first week after MI (**Fig. 9E,F**). In WT hearts, lymphatic vessel death was already evident at day 2 and progressed during the first week. Consequently, lymphatic coverage in WT IZ was reduced by ~ 50 % and ~ 70 % of the basal level 4 and 7 days after MI, respectively (**Fig. 9F**). Surprisingly, loss of lymphatic vessels in *Reg3b*$^{-/-}$ hearts was less intense, reaching a maximum of 35 % reduction at 4 days after LAD ligation in comparison to the basal level. In addition to that, lymphatic coverage in *Reg3b*$^{-/-}$ hearts almost recovered already one week after MI, nearly reaching basal levels. Therefore, in comparison to WT, lymphatic coverage in *Reg3b*$^{-/-}$ hearts was more elevated 4, 7 and 14 days after LAD ligation. This difference was most pronounced on day 7, with ~ 3,5 times higher coverage in *Reg3b*$^{-/-}$ hearts (**Fig. 9F**). No differences between in WT and *Reg3b*$^{-/-}$ hearts were seen in the RZ, where neither loss of lymphatics nor increased proliferation of lymph vessel cells was evident (**Fig. 9G**). The increased formation of lymphatic vessels in *Reg3b*$^{-/-}$ hearts after MI was unexpected, since

the elevated accumulation of leukocytes in *Reg3b*$^{-/-}$ hearts initially suggested potentially reduced drainage via lymphatic vessels. The results indicated that the system is more complex and involves more components than anticipated.

Next, the functionality of newly formed lymphatic vessels in *Reg3b*$^{-/-}$ hearts was investigated. One way to test the functionality of lymphatics in an inflamed organ is to measure their capability of resolving edema, avoiding increase in the interstitial pressure (Brakenhielm et al., 2020; Brakenhielm & Alitalo, 2019; Laine & Allen, 1991). Edema resolution can be quantified by calculating the water content in a tissue by weighing it before and after desiccation, using the formula: $\left[1 - \left(\frac{dry\ weight}{wet\ weight}\right)\right] * 100$ (**Fig. 9H**). Using this method, the cardiac water content 4 days after LAD ligation revealed a slight (-2,2 %) but significant reduction in the water content in *Reg3b*$^{-/-}$ compared to WT infarcted hearts (**Fig. 9I**).

In order to determine whether the increased lymphatic coverage in *Reg3b*$^{-/-}$ hearts results from enhanced de novo proliferation, BrdU was added to the water of infarcted mice for 7 days after MI. Since BrdU is a thymidine analogue, it is incorporated into newly synthesized DNA, allowing monitoring of proliferation in a given time window (**Fig. 10A**). BrdU^{+} nuclei of newly assembled lymphatic vessels in the infarcted area were identified by the presence of LYVE-1 and the lymphatic transcription factor Prospero Homeobox 1 (PROX-1) (**Fig. 10B**, indicated by arrows). Quantification of histological sections revealed that *Reg3b*$^{-/-}$ hearts not only had ~ 70 % more LYVE-1^{+} PROX-1^{+} nuclei, but also ~ 66 % more proliferating lymphatic nuclei (LYVE-1^{+} PROX-1^{+} BrdU^{+}) in comparison to WT hearts (**Fig. 10C**). Altogether, this finding indicates that the increased lymphatic cell proliferation is a reason for the improved recovery of the lymphatic coverage in *Reg3b*$^{-/-}$ hearts.

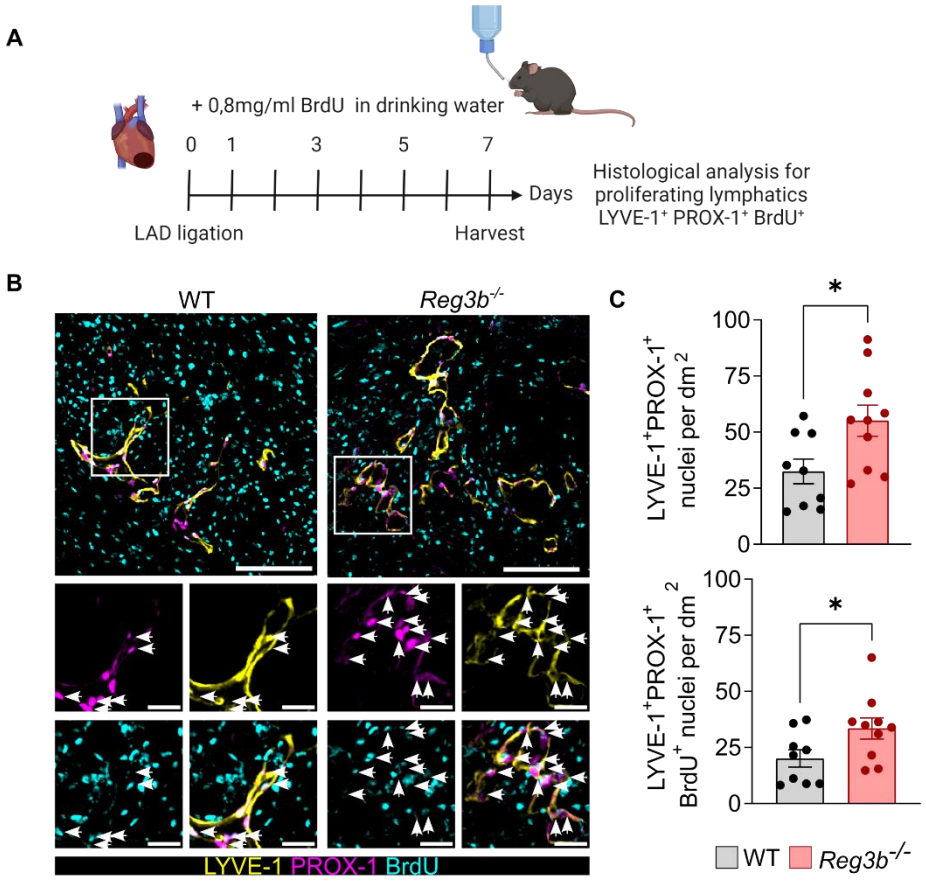

Figure 10. Lymphatic vessels in *Reg3b*$^{-/-}$ hearts proliferate more than WT. (A) After LAD ligation, mice received bromodeoxyuridine (BrdU) in drinking water for 7 days, after which their hearts were harvested for histological analysis. Illustration created with "BioRender.com". **(B)** Widefield microscopy of proliferating lymphatics (LYVE-1$^+$ PROX-1$^+$ BrdU$^+$) in WT and *Reg3b*$^{-/-}$ histological heart sections. LYVE-1$^+$ PROX-1$^+$ BrdU$^+$ are indicated with arrows. 10x magnification. Scale bar = 100 µm (overview) and 25 µm (insets). **(C)** Quantification of LYVE-1$^+$ PROX-1$^+$ lymphatic nuclei per dm^2 (upper) and proliferating LYVE-1$^+$ PROX-1$^+$ BrdU$^+$ proliferating lymphatic nuclei per dm^2 (lower). Data are shown as mean ± SEM. For image quantification, 8 sections in different heights the heart were averaged, per animal. N = 9-10. Statistical tests: **(C)** two-tailed unpaired Student's t-test. *p < 0,05.

Mechanistically, I reasoned that REG3β serves an anti-lymphangiogenic function in infarcted hearts, since its depletion increased lymphangiogenesis. To further test this hypothesis, infarcted WT and *Reg3b*$^{-/-}$ mice were intramyocardially injected with recombinant murine REG3β or vehicle (PBS), two days after LAD ligation (**Fig. 11A**). I chose this time point to allow a hypoxic-driven acute lymphatic cell death, thereby

temporally separating the hypothesized anti-lymphangiogenic effect from any confounding anti-survival effect.

The response to REG3β or PBS injections varied between genotypes. Whereas lymphatic coverage in WT remained unaltered in both groups, a significant reduction in lymphatic vessel coverage in IZ and RZ of *Reg3b*$^{-/-}$ hearts receiving REG3β injections became apparent **(Fig. 11B)**. The magnitude of this decrease was 32 % in RZ and 40 % in IZ (**Fig. 11C-D**).

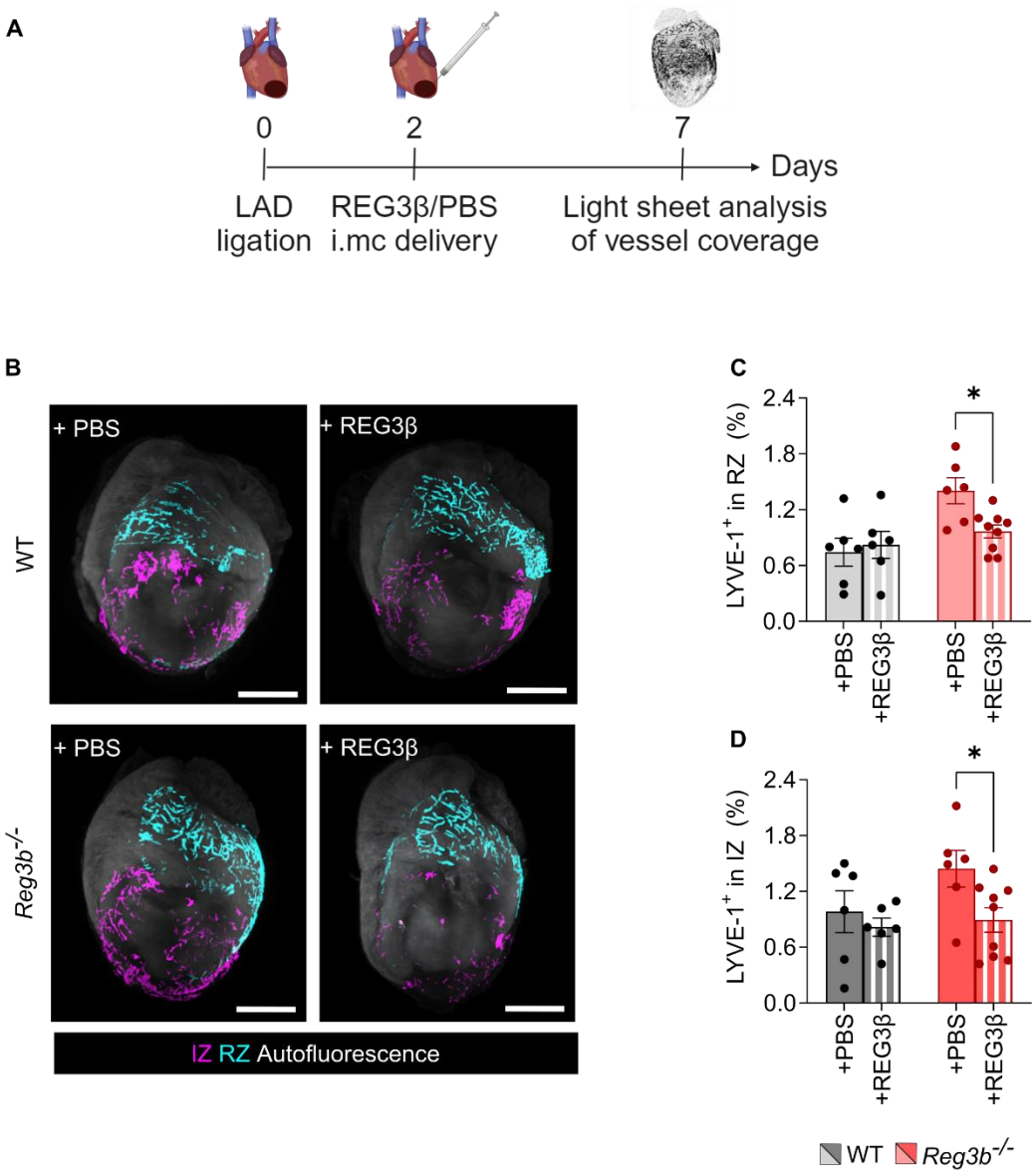

Figure 11. Intramyocardial injection of REG3β reduces lymphangiogenesis in infarcted hearts of *Reg3b*$^{-/-}$ but not WT mice. (A) Two days after LAD ligation, 100ng of REG3β or

PBS were injected into infarcted hearts of WT and *Reg3b*$^{-/-}$ mice. Hearts were harvested at day 7. Illustration created with "BioRender.com". **(B)** Representative light sheet microscopy of LYVE-1^{+} lymphatic network in infarcted zones (IZ, magenta) and remote zone (RZ, cyan) of WT and *Reg3b*$^{-/-}$ hearts injected with PBS or REG3β. 1,26 x magnification. Scale bar = 2mm **(C-D)** Quantification of IZ and RZ covered with LYVE-1^{+} lymphatics (percentage of tissue area). Data are shown as mean ± SEM. N = 6-9. Statistical analysis: **(C-D)** Two-way ANOVA followed by Šidák multiple comparisons test, *p ≤ 0, 05. i.mc: intramyocardial.

Altogether, an enhanced lymphatic proliferation took place after MI induction in *Reg3b*$^{-/-}$ hearts, which was prevented by local delivery of recombinant REG3β. Since vascular derived endothelial factors VEGF-C and -D are the most prominent regulators of lymphangiogenic responses **(Figs. 2,3)**, I next investigated their presence and sources in WT and *Reg3b*$^{-/-}$ hearts.

4.3 Macrophage-derived VEGF-C and VEGF-D promote lymphangiogenesis in *Reg3b*$^{-/-}$ hearts

According to the literature, cardiac dysfunction, such as myocardial infarction and pressure overload, leads to the increase of VEGF-C and VEGF-D expression (Chen et al., 2016; Glinton et al., 2022), which is paralleled by augmented expression of their cognate receptor, VEGFR3 (Klotz et al., 2015). In infarcted hearts, these factors are produced mostly by cardiomyocytes in the vicinity of the scar (Ishikawa et al., 2007) and by macrophages (Glinton et al., 2022).

In order to assess the expression levels of VEGF-C and VEGF-D in WT and *Reg3b*$^{-/-}$ hearts, protein lysates of RZ and IZ heart fractions were compared using western blot (**Fig. 12A**). Densitometry analysis of the western blot bands revealed a ~ 100 % increase of VEGF-C and VEGF-D expression in both RZ and IZ of *Reg3b*$^{-/-}$ hearts (**Fig. 12-B,C**).

Histological whole-mount staining of VEGF-C showed a punctuated staining pattern, which largely overlapped with CD68 staining for macrophages (**Fig. 12D**). Differently from VEGF-C, the distribution of VEGF-D in the infarcted tissue only partially overlapped with CD68^{+} macrophages, suggesting that there might be other cellular sources for this factor (**Fig. 12E**). Indeed, in addition to macrophages, cardiomyocytes in the border zone and endocardium distinctively expressed VEGF-D. Considering that *Reg3b*$^{-/-}$ hearts had ~ 50 % higher presence of macrophages in comparison to WT 4 days after MI onset (**Fig. 8G**), I focused on the expression of VEGF-C and VEGF-D by tissue macrophages.

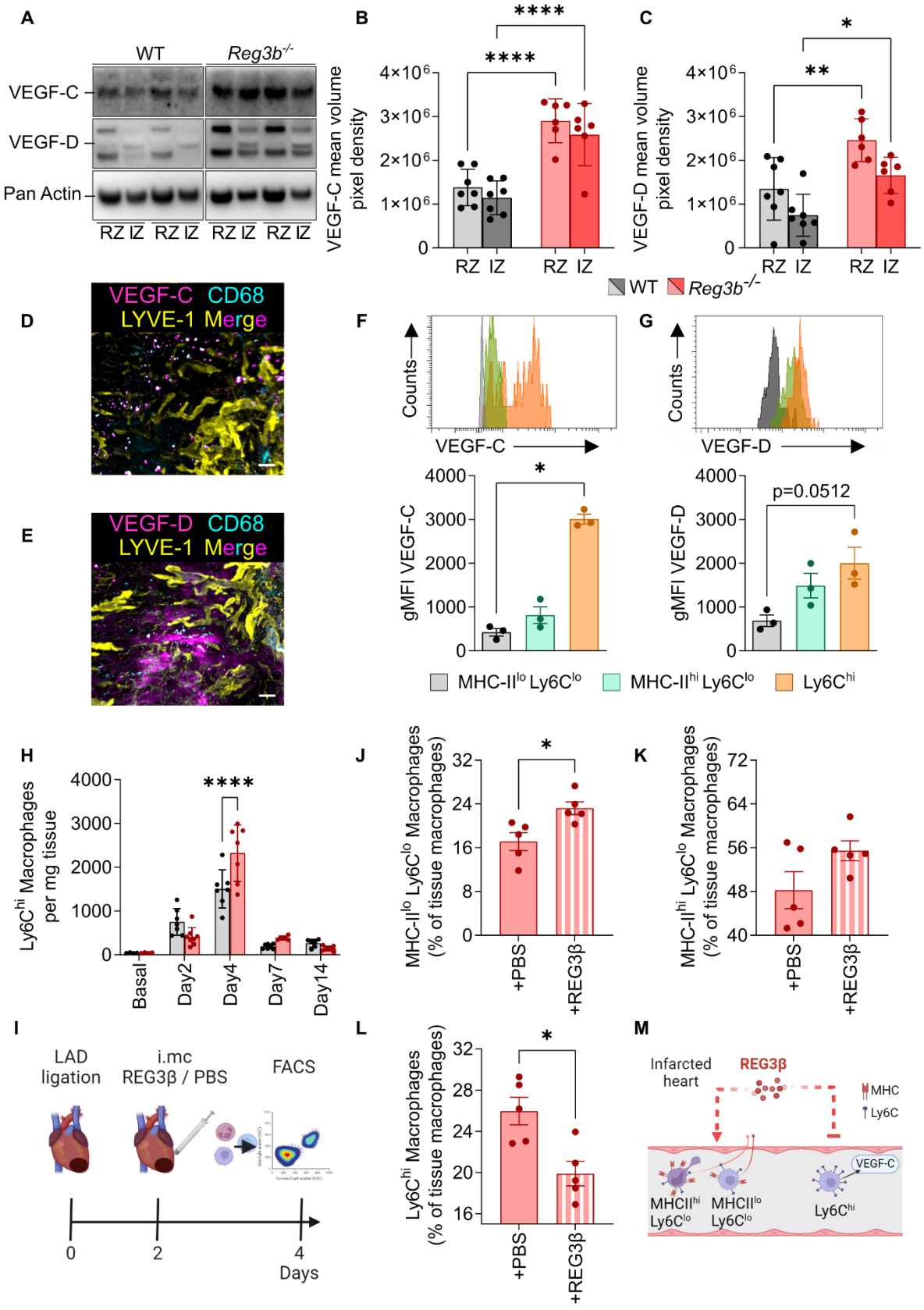
A
WT
Reg3b-/-
VEGF-C
VEGF-D
Pan Actin
RZ IZ RZ IZ RZ IZ RZ IZ
VEGF-C mean volume pixel density
B
****
****
4×10^6
3×10^6
2×10^6
1×10^6
0
RZ IZ RZ IZ
C
*
**
VEGF-D mean volume pixel density
WT Reg3b-/-
D
VEGF-C CD68
LYVE-1 Merge
E
VEGF-D CD68
LYVE-1 Merge
F
Counts
VEGF-C
gMFI VEGF-C
4000
3000
2000
1000
0
*
G
Counts
VEGF-D
gMFI VEGF-D
p=0.0512
MHC-II^lo Ly6C^lo
MHC-II^hi Ly6C^lo
Ly6C^hi
H
Ly6C^hi Macrophages per mg tissue
****
Basal
Day2
Day4
Day7
Day14
J
MHC-II^lo Ly6C^lo Macrophages (% of tissue macrophages)
32
24
16
8
0
*
+PBS
+REG3β
K
MHC-II^hi Ly6C^lo Macrophages (% of tissue macrophages)
72
64
56
48
40
+PBS
+REG3β
I
LAD ligation
i.mc REG3β / PBS
FACS
0
2
4
Days
L
Ly6C^hi Macrophages (% of tissue macrophages)
32
28
24
20
16
*
+PBS
+REG3β
M
Infarcted heart
REG3β
MHC
Ly6C
VEGF-C
MHCII^hi Ly6C^lo
MHCII^lo Ly6C^lo
Ly6C^hi

Figure 12. Ly6C^{hi} macrophages show elevated levels of VEGF-C and VEGF-D in infarcted hearts, driving cardiac lymphangiogenesis. **(A)** Representative western blots and **(B,C)** pixel density quantifications of VEGF-C and VEGF-D in fractionated infarcted heart lysates. **(D)** Light sheet microscopic images of VEGF-C, LYVE-1 and CD68^{+} macrophages in an infarcted heart. **(E)** Light sheet microscopic images of VEGF-D, LYVE-1 and CD68^{+} macrophages in an infarcted heart. 1,26 x magnification. Scale bar = 300 µm. **(F-G)** Upper: representative flow cytometric histogram distributions of VEGF-C and VEGF-D mean intensity fluorescence. Lower: quantification of VEGF-C and VEGF-D mean intensity fluorescence in macrophage subsets: MHCII^{lo} Ly6C^{lo} (gray); MHCII^{hi} Ly6C^{lo} (green) and Ly6C^{hi} (orange). **(H)** Kinetics of Ly6C^{hi} macrophage accumulation per mg of tissue in WT and *Reg3b*$^{-/-}$ hearts. **(I)** Two days after LAD ligation, 100ng of REG3β or PBS were injected into infarcted hearts of *Reg3b*$^{-/-}$ mice. Hearts were harvested on day 4. **(J)** Percentage of MHCII^{lo} Ly6C^{lo}; **(K)** MHCII^{hi} Ly6C^{lo} and **(L)** Ly6C^{hi} macrophages out of total macrophage population after intramyocardial injection of REG3β or PBS. **(M)** Schematic model: in accordance to Lörchner et al. (2018), pro-lymphangiogenic Ly6C^{hi} macrophage subset is not preferentially attracted upon REG3β injection in the heart. Illustration created with "BioRender.com". Data are shown as mean ± SEM. **(B,C)** N = 6-7; **(F,G)** N = 3; **(H)** N = 4-7; **(J-L)** N = 5. Statistical analysis: (**B,C,H**) Two-way ANOVA followed by Šidák multiple comparisons test; **(F,G)** One-way ANOVA followed by Dunn's multiple comparisons test; **(J-L)** Mann-Whitney U test. *p ≤ 0, 05, **p ≤ 0, 01; ***p ≤ 0, 001 ; ****p ≤ 0, 0001. i.mc: intramyocardial

Since phenotypic diversity of macrophages determines their function, the levels of VEGF-C and VEGF-D were determined in different population of macrophages, identified by molecular markers indicative of macrophage origin and function – the glycoprotein Ly6C and the molecular histocompatibility complex II (MHCII) (Epelman et al., 2014). In this respect, my group reported different biological functions of three different cardiac macrophage subsets and identified that Ly6C^{hi} macrophages carry pro-lymphangiogenic gene signature (Lörchner et al., 2018). A flow cytometric analysis of Ly6C^{hi}, MHCII^{hi} LyC^{lo}, MHCII^{lo} LyC^{lo} macrophages for VEGF-C and VEGF-D levels was performed (**Fig. 12F-G**). Mean fluorescence intensity (MFI) of VEGF-C in Ly6C^{hi} macrophages was ~ 6,5 x higher than in MHCII^{lo} LyC^{lo} macrophages, whereas, for VEGF-D, a ~ 3 x increase approached statistical significance. Besides, Ly6C^{hi} macrophage subset peaked in the tissue at day 4 post-MI and was ~ 54 % more abundant in *Reg3b*$^{-/-}$ than in WT hearts (**Fig. 12H)**.

In order to test whether different subsets of macrophages accumulate differently in response to local REG3β delivery, I performed a gain-of-function experiment. For this, recombinant REG3β was injected intramyocardially in *Reg3b*$^{-/-}$ infarcted mice, 2 days after LAD ligation **(Fig. 12I)**. REG3β delivery had distinct effects on each macrophage fraction: it increased the fraction of MHCII^{lo} LyC^{lo} macrophages by ~ 35 %, caused no significant

alterations in MHCII^{hi}/LyC^{lo} macrophages, and reduced Ly6C^{hi} macrophage accumulation by ~ 30 % **(Fig. 12J-L)**.

The effects of REG3β on the accumulation of each macrophage subset are summarized in **Fig. 12M.** Administration of recombinant REG3β favors the accumulation of Ly6C^{lo} macrophages to the detriment of VEGF-C-secreting Ly6C^{hi} subset, limiting lymphangiogenesis. Since *Reg3b*$^{-/-}$ infarcted mice differentially accumulate Ly6C^{hi} macrophages, enhanced lymphangiogenesis takes place. However, the enhanced formation of lymphatics does not mitigate cardiac inflammation. I next employed a fluorescent tracing approach for cardiac leukocytes to solve this paradox and uncover why *Reg3b*$^{-/-}$ infarcted hearts contain more leukocytes compared to WT hearts from day 4 onwards, despite the increased presence of lymphatic vessels.

4.4 Cardiac myeloid leukocytes emigrate systemically to distal organs

One of the key features of myeloid leukocytes is their ability to phagocytose – a functional characteristic, which can be harnessed for tracing myeloid leukocytes that leave the infarcted heart via the lymphatic vasculature. pHrodo particles are pH-sensitive fluorogenic probes which become increasingly fluorescent in lower pH (Jiang et al., 2023; Kapellos et al., 2016; Takahashi et al., 2017). These probes were injected intramyocardially after LAD ligation with the purpose of tracing leukocytes after phagocytosis (**Fig. 13A**).

The presence of cardiac troponin I in pHrodo^{+} myeloid leukocytes in distal organs (e.g. bone marrow) confirmed the cardiac origin of pHrodo particles (**Fig. 13B**). Flow cytometric analysis of CD11b^{+} myeloid leukocytes and histological sections revealed the presence of pHrodo not only in the heart, where these particles were injected, but also in mediastinal lymph nodes, closely associated to the heart, and in other organs associated with acute immune responses, namely the spleen and bone marrow (**Fig. 13C,D**).

A time-course pilot experiment defined the best time window to recover leukocytes in distal organs (**Fig. 13E-H**). Flow cytometric analysis of pHrodo^{+} myeloid leukocytes revealed a peak in distal organs within the first 6h after intramyocardial injection. Conversely, 24h after pHrodo delivery, at least half of pHrodo^{+} leukocytes in the heart had already either emigrated or been cleared, which was reflected by lower presence in distal

organs (**Fig. 13E-H**). Based on these results, I employed the 6 h time point for subsequent pHrodo tracing studies.

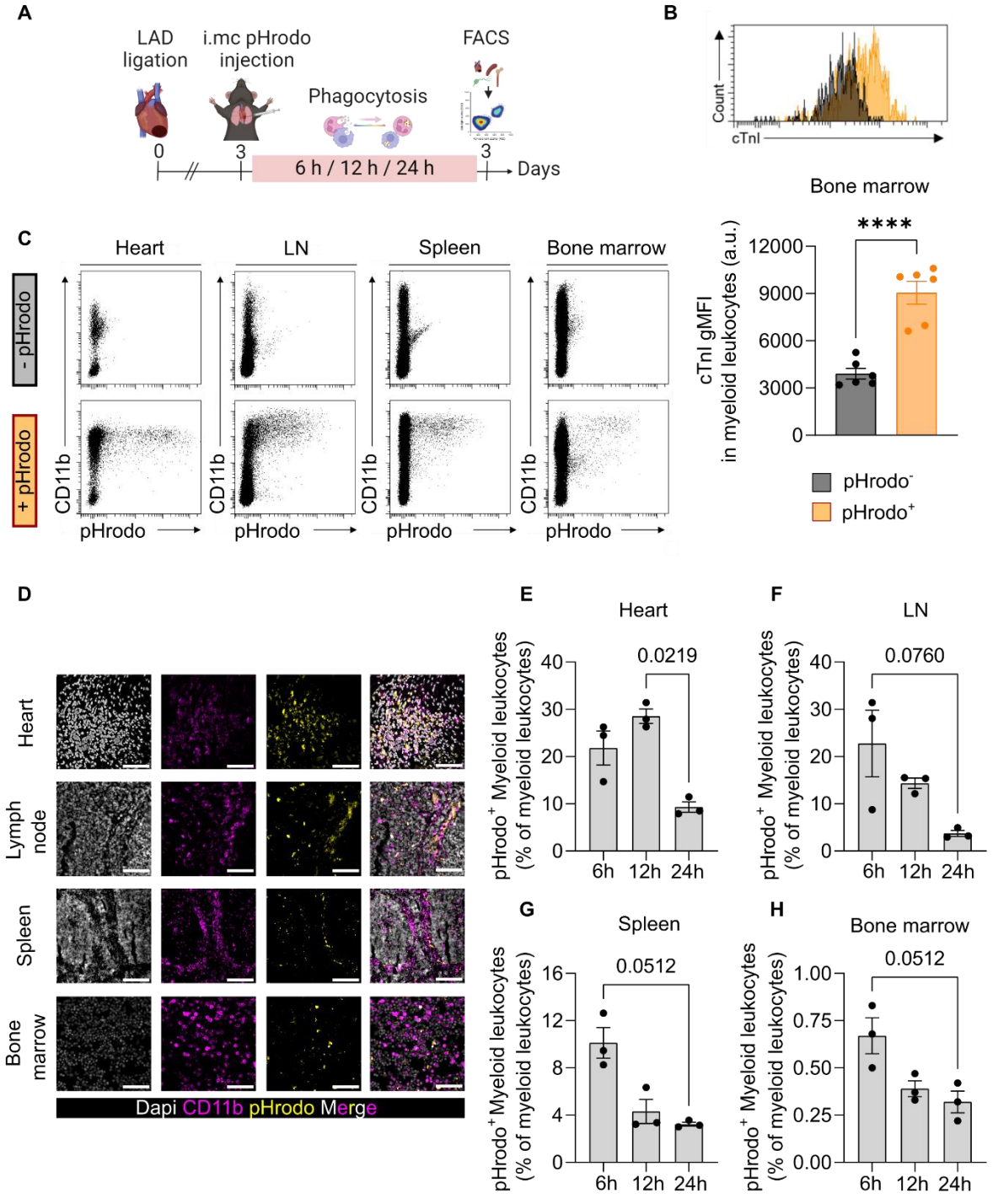

Figure 13. Cardiac leukocytes are detected in distal organs due to phagocytosis of the pHrodo dye. (A) Tracing strategy for pHrodo$^+$ leukocytes. pHrodo was injected intramyocardially 3 days after MI. The particles become fluorescent upon phagocytosis,

allowing tracing of phagocytosing cells to distal organs. A time-course pilot of 6h, 12h and 24h was performed to determine the best time point for recovery of pHrodo^{+} leukocytes in distal organs. Illustration created with "BioRender.com". **(B)** Representative flow cytometric histogram plots and quantification of cardiac troponin I (cTNI) gMFI in pHrodo^{+} and pHrodo^{-} leukocytes in the bone marrow. **(C)** Representative flow cytometric plots of pHrodo^{+} and pHrodo^{-} myeloid leukocytes in the heart, lymph node, spleen and bone marrow. **(D)** Widefield microscopic images of pHrodo^{+} CD11b^{+} myeloid leukocytes in the heart (20x magnification, scale bar = 100 µm), mediastinal lymph nodes (40x magnification, scale bar = 50 µm), spleen (10x magnification, scale bar = 200 µm) and bone marrow (40x magnification, scale bar = 50 µm). **(E-H)** Percentage of pHrodo^{+} myeloid leukocytes in the heart, lymph nodes, spleen and bone marrow after 6 h , 12 h and 24 h. Data are shown as mean ± SEM. **(B)** N = 6; **(E-H)** N = 3. Statistical analysis: **(B)** Two-tailed unpaired Student's t-test; **(E-H)** Kruskall Wallis test followed by Dunn's multiple comparison test. ****p ≤ 0,0001. i.mc: intramyocardial. LN: lymph nodes

The presence of pHrodo^{+} myeloid leukocytes was analyzed in lymph nodes, the spleen and bone marrow after LAD ligation by flow cytometry (**Fig. 14A**). In comparison to WT mice, more myeloid leukocytes were present in the lymph node and bone marrow of *Reg3b*$^{-/-}$ mice, but not in the spleen **(Fig. 14B)**. Furthermore, myeloid leukocytes were separated into neutrophils and macrophages, since these two subsets were differentially enriched 4 days post-MI in the hearts of *Reg3b*$^{-/-}$ mice. Neutrophils and macrophages migrated in a similar pattern to the parent myeloid leukocyte population **(Fig 14.C,D)**.

The presence of pHrodo^{+} myeloid leukocytes in mediastinal lymph nodes suggests the participation of lymphatics as conduits. In fact, almost all pHrodo^{+} immune cells recovered in the lymph nodes (and to large extent in the spleen and bone marrow) expressed CCR7, a relevant receptor for leukocyte migration into the lymphatic vasculature **(Fig. 14E)** (Aspelund et al., 2016; D. Kobayashi et al., 2017; Petrova & Young Koh, 2020; Rodríguez-Fernández & Criado-García, 2020).

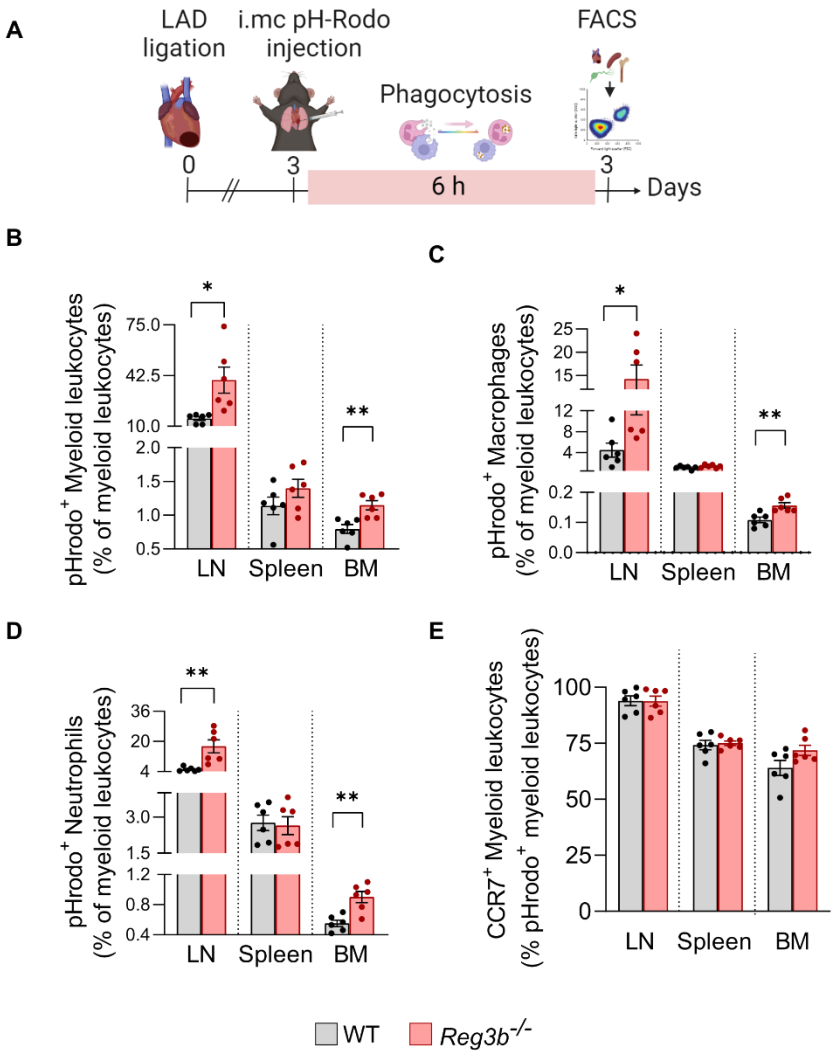

Figure 14. Genetic deletion of *Reg3b* results in increased emigration rates of neutrophils and macrophages from the infarcted heart towards mediastinal lymph nodes and bone marrow **(A)** Tracing strategy for pHrodo$^+$ leukocytes. pHrodo was injected intramyocardially 3 days after MI and became fluorescent upon phagocytosis, allowing tracing to distal organs, which was assessed by flow cytometry. Illustration created with "BioRender.com". **(B-D)** Percentage of pHrodo$^+$ myeloid leukocytes, macrophages and neutrophils in lymph nodes (LN), spleen and bone marrow (BM). **(E)** Percentage of CCR7$^+$ fraction of myeloid leukocytes among pHrodo$^+$ of myeloid leukocytes in lymph node, spleen and bone marrow. Data are shown as mean ± SEM. N = 6. Statistical analysis: Two-tailed unpaired Student's t-test. *p ≤ 0,05, **p ≤ 0,01.

In order to functionally link increased formation of lymphatics in *Reg3b*$^{-/-}$ hearts to higher emigration of leukocytes and VEGFR3 signaling, I performed a loss-of-function study by overexpressing the soluble form of VEGFR3 (sVEGFR3), a VEGF-C trap which

minimizes the availability of this ligand to activate native VEGFR3 (Antila et al., 2017; Karaman et al., 2013).

4.5 Attenuated lymph vessel formation by expression of sVEGFR3 lowers emigration of leukocyte from the infarcted heart

AAV9-sVEGFR3 or scramble constructs were injected intraperitoneally 4 weeks prior to LAD ligation into *Reg3b*$^{-/-}$ mice, allowing a slow and steady overexpression of sVEGFR3 (**Fig. 15A**). 3 weeks after injection, I harvested blood from the submandibular plexus to confirm the expression of the vector, using western blot analysis (**Fig. 15A,B**). This allowed me to identify and exclude non-responding animals from further analysis. Mice expressing sVEGFR3 underwent LAD ligation and intramyocardial injection of pHrodo, as previously described (**Fig. 13, Fig. 14**). Addition of BrdU to the drinking water after LAD ligation, allowed me to monitor potentially inhibition of de novo lymphangiogenesis.

sVEGFR3 successfully inhibited cardiac lymphangiogenesis upon MI (**Fig. 15C**), confirming previous results by Houssari et al. (2020). In comparison to scramble controls, mice overexpressing sVEGFR3 had almost 45 % lower LYVE-1^{+} lymphatic coverage and 40 % lower numbers of LYVE-1^{+} PROX-1^{+} nuclei in the infarcted tissue (**Fig. 15D,E**). The 57 % reduction in BrdU incorporation compared to the scramble group, indicated that this effect was due to lower proliferation of lymph endothelial cells in the sVEGFR3 group (**Fig. 15F**).

In addition, flow cytometric analysis of emigrating pHrodo^{+} myeloid leukocytes revealed a 30 % reduction of the emigration to lymph nodes (**Fig. 15G**) and a 50 % reduction of emigration to the bone marrow (**Fig. 15H**), corroborating the functional relevance of cardiac lymphatics in this process.

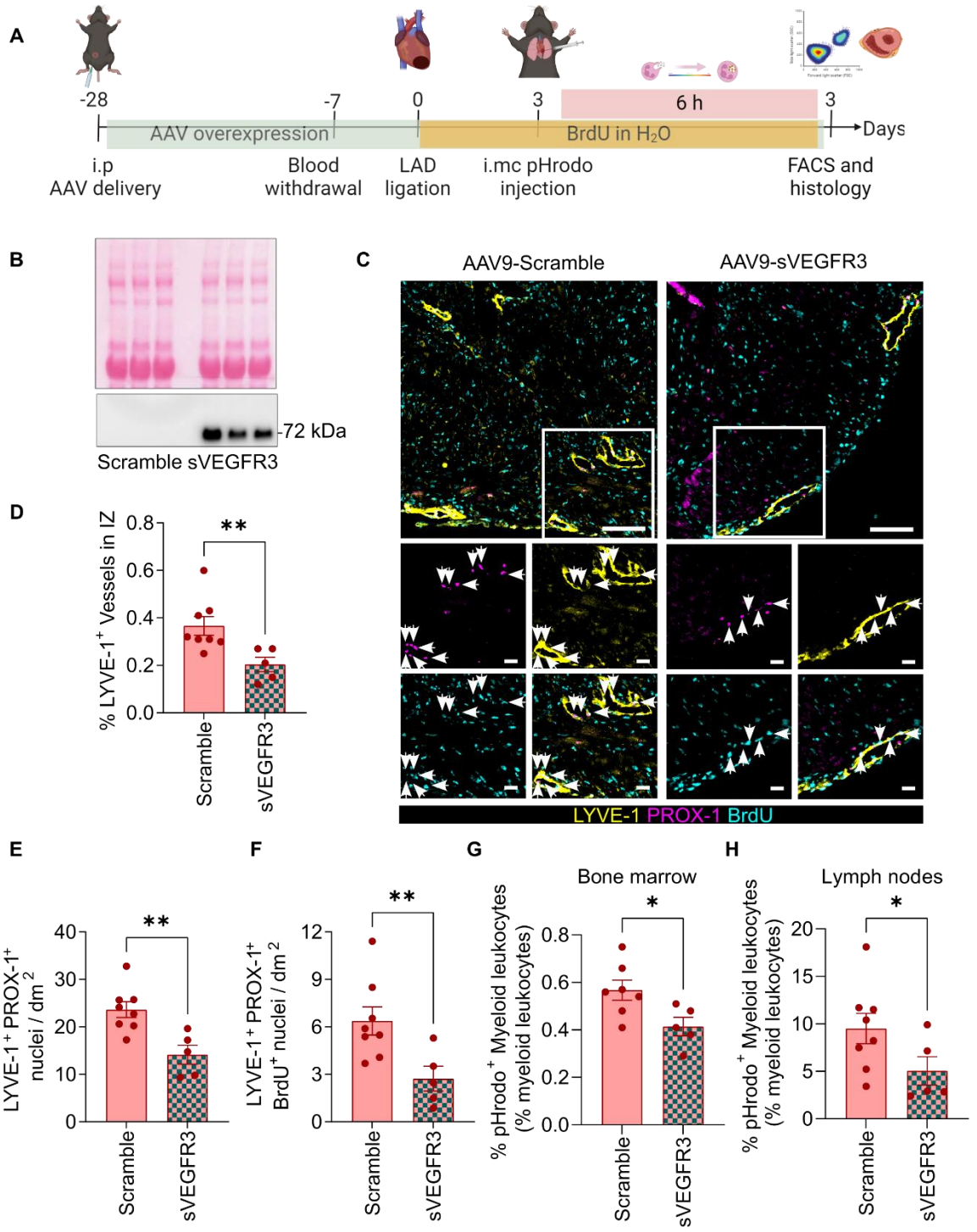

Figure 15. sVEGFR3 overexpression abrogates lymphangiogenesis and reduces leukocyte emigration to associated mediastinal lymph nodes, inhibiting homing to the bone marrow. (A) Experimental outline for inhibition of lymphangiogenesis via overexpression of soluble VEGFR3 (sVEGFR3). *Reg3b*$^{-/-}$ mice received a single intraperitoneal injection of AAV9-sVEGFR3 or AAV9-scramble 4 weeks prior to LAD ligation. Vector overexpression was monitored via WB and non-respondents were excluded

from further analysis. pHrodo intramyocardial injection was performed 3 days after LAD ligation, and BrdU was added to the drinking water to monitor de novo lymphangiogenesis. Illustration created with "BioRender.com". **(B)** Representative WB of murine serum 21 days post-AAV injection. **(C)** Representative widefield microscopic images of LYVE-1^+ PROX-1^+ $BrdU^+$ cardiac lymphatics in AAV9-sVEGFR3- and AAV9-scramble- treated mice 3 days after LAD ligation. Proliferating lymphatics (LYVE-1^+ PROX-1^+ $BrdU^+$) are indicated with arrows. 10x magnification. Scale bars = 100 µm (overview) and 25 µm (insets). **(D)** Percentage of LYVE-1^+ coverage in IZ. **(E)** Number of LYVE-1^+ PROX-1^+ lymphatic nuclei per dm^2 of IZ and of **(F)** proliferating LYVE-1^+ PROX-1^+ $BrdU^+$ lymphatic nuclei per dm^2 of IZ. **(G)** Percentage of $pHrodo^+$ myeloid leukocytes in the lymph node and **(H)** bone marrow. Data are shown as mean ± SEM. For image quantification, 8 sections in different heights the heart were averaged, per animal. **(D-H)** N = 5-8. Statistical analysis: Mann-Whitney U test. $*p \leq 0{,}05$, $**p \leq 0{,}01$. i.p: intraperitoneal. i.mc: intramyocardial

Altogether, this data demonstrate that the enhanced expansion of lymphatic vessels in the hearts of *Reg3b*$^{-/-}$ animals promotes emigration of leukocytes to distal organs upon MI. Similar to transendothelial migration in blood vessels, leukocytes migrate across the lymphatic endothelium in response to chemokine gradients (Farnsworth et al., 2019). I thus hypothesized that a differential chemoattraction of leukocytes to the lumen of lymphatic vessels may contribute to increased migration, and set out to investigate the expression of the best-documented chemokine-chemokine receptor pairs associated with lymphatic chemotaxis: CCL19/CCL21 and CCR7 (Beauvillain et al., 2011; Johnson & Jackson, 2010; Kilarski et al., 2013).

4.6 Increased expression of the chemokines CCL21 and CCL19 in *Reg3b*$^{-/-}$ hearts stimulate leukocyte emigration towards mediastinal lymph nodes

Both chemokines C-C motif ligands 21 and 19 (CCL21 and CCL19) act on the same leukocyte receptor, CCR7 – a G protein-coupled receptor which regulates the dynamics of the actin cytoskeleton and thus chemotaxis (Aspelund et al., 2016; D. Kobayashi et al., 2017; Petrova & Young Koh, 2020; Rodríguez-Fernández & Criado-García, 2020). Both chemokines were strongly expressed in the infarcted heart and in associated mediastinal lymph nodes, albeit by different cells (**Figs. 16, 17**).

CCL21 was detected in LYVE-1^+ lymphatic capillaries, showing a strong expression in inside the vessels, but also within the myocardium, with a typical gradient-like distribution (**Fig. 16A upper panel**). Additionally, LYVE-1^+ vessels in the mediastinal lymph nodes were also partially positive for CCL21, although its concentration was the highest in the

lymph node medulla, where it was expressed by fibroblastoid reticular cells (Petrova & Young Koh, 2020) (**Fig. 16A lower panel**).

To evaluate the expression levels of CCL21 in WT and *Reg3b*$^{-/-}$ hearts, protein lysates of RZ and IZ heart fractions were compared by western blot analysis (**Fig. 16B,D**). Densitometry analysis of the western blots revealed that CCL21 levels were the highest in the IZ in comparison to RZ, both 4 and 7 days after MI (**Fig. 16B,D**). Concentrations of CCL21 did not differ between genotypes 4 days after MI (**Fig. 16B,C**), but 7 days after MI, approximately ~ 100 % more CCL21 was present in the IZ of *Reg3b*$^{-/-}$ in comparison to WT (**Fig. 16D,E**). A similar result was obtained using whole-mount staining of CCL21 in infarcted hearts, where *Reg3b*$^{-/-}$ hearts had a 100 % increased CCL21 coverage of the IZ (**Fig. 16F,G**).

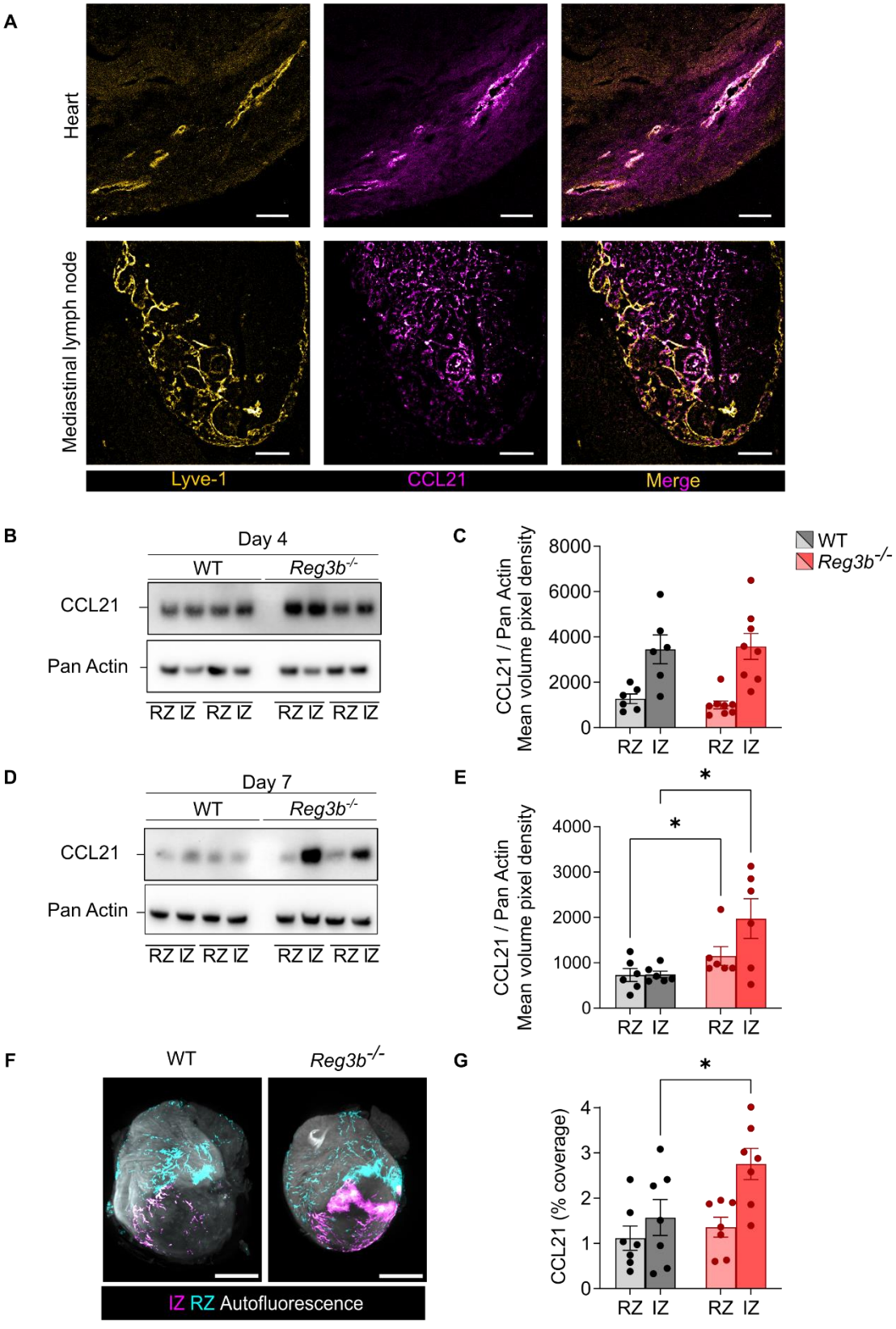
A
Heart
Mediastinal lymph node
Lyve-1
CCL21
Merge
B
Day 4
WT
Reg3b-/-
CCL21
Pan Actin
RZ IZ RZ IZ RZ IZ RZ IZ
C
WT
Reg3b-/-
CCL21 / Pan Actin
Mean volume pixel density
8000
6000
4000
2000
0
RZ IZ RZ IZ
D
Day 7
WT
Reg3b-/-
CCL21
Pan Actin
RZ IZ RZ IZ RZ IZ RZ IZ
E
CCL21 / Pan Actin
Mean volume pixel density
4000
3000
2000
1000
0
*
*
RZ IZ RZ IZ
F
WT
Reg3b-/-
IZ RZ Autofluorescence
G
CCL21 (% coverage)
4
3
2
1
0
*
RZ IZ RZ IZ

Figure 16. Lymphatic vessel-derived CCL21 chemokine is present at higher concentration in infarcted *Reg3b*$^{-/-}$ compared to WT hearts. (A) CCL21 and LYVE-1 co-localization in infarcted hearts (upper panel, confocal microscopy) and mediastinal lymph nodes (lower panel, widefield microscopy). Magnification = 10x (hearts) and 20x (lymph nodes). Scale bars = 100 µm. **(B,D)** Representative western blots and **(C,E)** quantification of CCL21 levels in RZ and IZ of heart lysates **(B,C)** 4 days and **(D,E)** 7 days after MI. **(F)** Representative light sheet microscopic image of CCL21 in RZ (cyan) and IZ (magenta) of infarcted hearts 7 days after LAD ligation. 1,26 x magnification. Scale bar = 2mm. **(G)** Quantification of CCL21 coverage in infarcted heart fractions (percentage of tissue volume). Data are shown as mean ± SEM. **(B-E)** N = 6; **(F-G)** N = 7. Statistical analysis: **(C,E,G)** Two-way ANOVA followed by Šidák multiple comparisons test. *$p \leq 0{,}05$.

Histological staining of CCL19 in the infarcted heart revealed strong signals in cardiomyocytes as well as in $CD45^+$ leukocytes (**Fig. 17A** upper panel). Mediastinal lymph nodes also showed strong CCL19 levels, the staining did not correlate well with $LYVE\text{-}1^+$ staining and had a rather punctuate-pattern (**Fig. 17A** lower panel), which can be attributed to leukocytes and marginal reticular cells (Petrova & Young Koh, 2020; Yan et al., 2019).

Whereas CCL21 was strongly present in the IZ, western blot analysis of CCL19 in cell lysates from infarcted hearts demonstrated overall stronger concentrations in the RZ (**Fig. 17B-D**). *Reg3b*$^{-/-}$ hearts had a ~ 100 % increased intensity of CCL19 levels in the RZ of in comparison to WT 4 days after LAD ligation (**Fig. 17B,C**). However, 7 days after MI these differences had already disappeared (**Fig. 17D,E**).

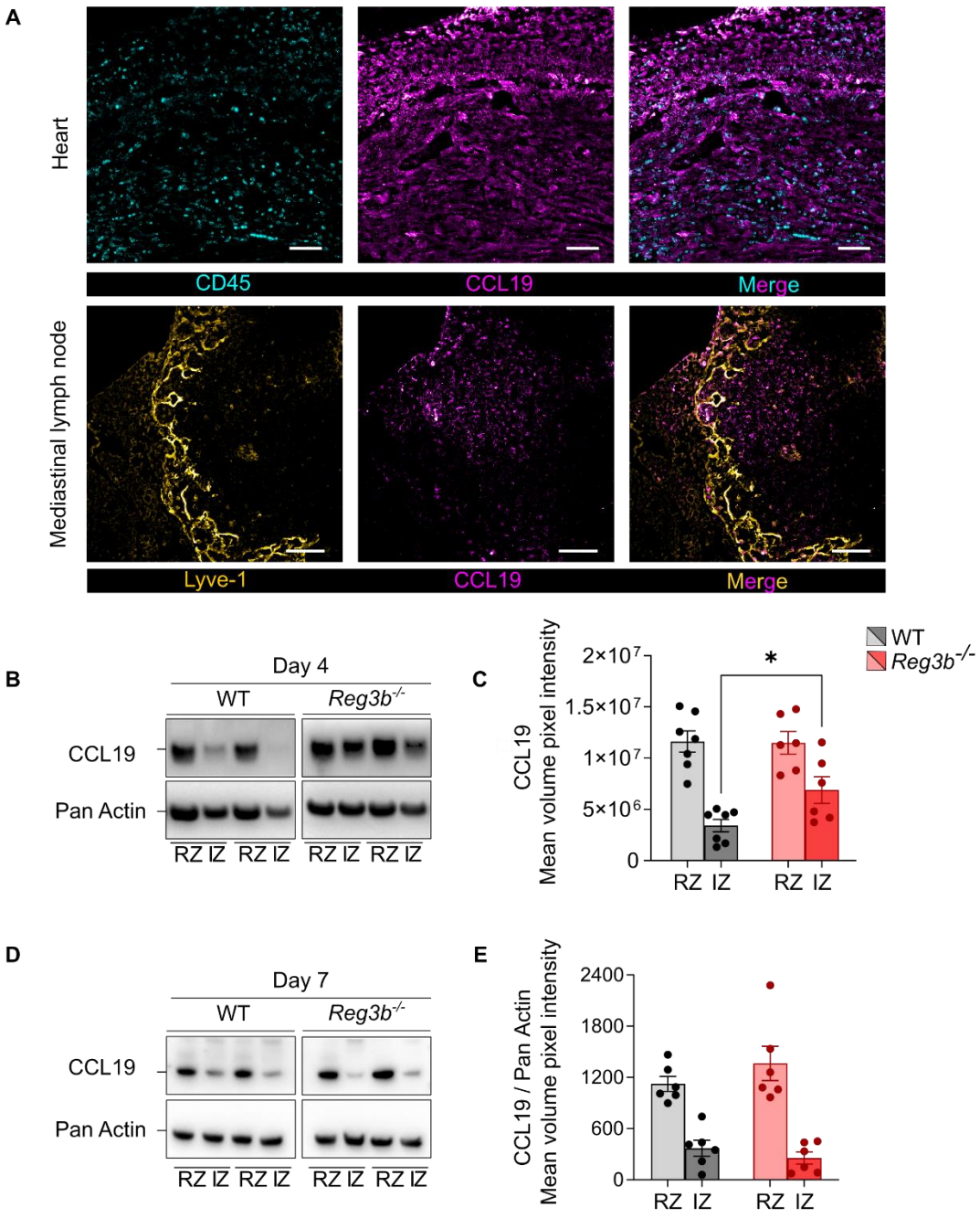

Figure 17. CCL19 chemokine levels are higher in the remote zones of infarcted *Reg3b*$^{-/-}$ than WT hearts. (A) CCL19 and CD45 co-presence in infarcted hearts (upper panel) and mediastinal lymph nodes (CCL19 and LYVE-1; lower panel). Magnification = 10x (hearts) and 20x (lymph nodes). Scale bar = 100 µm. **(B,D)** Representative western blots and **(C,E)** quantification of CCL19 levels in RZ and IZ of heart lysates **(B,C)** 4 days and **(D,E)** 7 days after MI. Data are shown as mean ± SEM. N = 6-7. Statistical analysis: **(C,E)** Two-way ANOVA followed by Šidák multiple comparisons test. *$p \leq 0{,}05$.

Taken together, analysis of the presence of CCL21 confirmed the increased lymphatic vessel coverage in hearts of *Reg3b*$^{-/-}$ animals after MI, and also revealed higher levels of CCL21 and CCL19 in mutant hearts. The higher levels of CCL21 and CCL19 may increase leukocyte emigration from the infarcted hearts of *Reg3b*$^{-/-}$ animals.

4.7 Emigrating cardiac leukocytes modify the bone marrow niche

In the last decades, scientists showed that the infarcted heart connects to distinct peripheral organs via cellular and acellular communication (Jahng et al., 2016). A few research groups explored the transport of cardiac-derived leukocytes towards the bone marrow. According to the current view, inflammasome-primed neutrophils produce IL-1β, and deliver this factor to the bone marrow, stimulating granulopoiesis (Sager et al., 2015; Sreejit et al., 2020, 2022). Other potential signaling modalities mediated by cardiac-derived leukocytes, connecting the infarcted heart and the bone marrow have not been explored.

To unravel which biological processes might be modulated in the bone marrow by emigrating cardiac leukocytes, I analyzed pHrodo^{+}-traced leukocytes that traveled from the infarcted murine heart to the bone marrow (**Fig. 18A**). Using FACS sorting, pHrodo^{+} and pHrodo^{-} macrophage and neutrophils fractions in the bone marrow were sorted and sequenced by bulk RNAseq. Principal component analysis showed 4 transcriptionally distinct groups, indicating not only a clear separation between macrophages and neutrophils, but also revealing a different RNA expression profile of heart-derived compared to bone marrow-resident leukocytes (**Fig. 18B**).

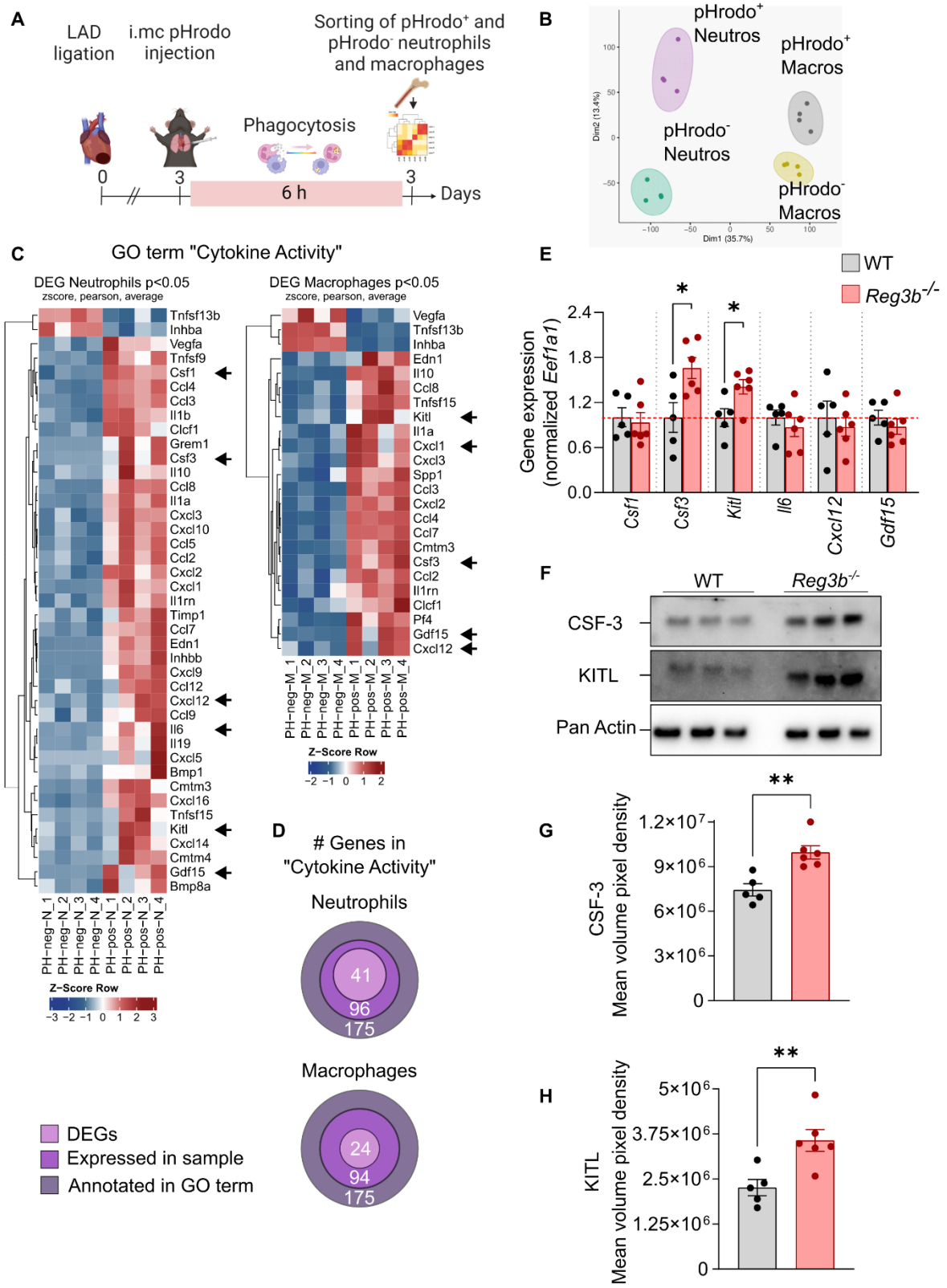

Figure 18. pHrodo$^+$ leukocytes in the bone marrow carry a pro-hematopoietic gene signature. (A) pHrodo$^+$ and pHrodo$^-$ macrophages and neutrophils were sorted from the bone marrow 6h after intramyocardial pHrodo injection in infarcted WT mice. Illustration created

with "BioRender.com". **(B)** Principal component analysis of pHrodo$^+$ and pHrodo$^-$ neutrophils and macrophage. **(C)** Heatmap of DEGs in "Cytokine activity" GO term in pHrodo$^+$ and pHrodo$^-$ neutrophils and macrophages. **(D)** Number of genes annotated for "Cytokine Activity" GO term, number of genes expressed and number of DEGs in each immune cell population. **(E)** Relative gene expression of *Csf1*, *Csf3*, *Kitl*, *Il6*, *Cxcl12* and *Gdf15* in bone marrows of WT and *Reg3b*$^{-/-}$ mice 4 days after LAD ligation. Gene expression was normalized to the endogenous gene *Eef1a1*. **(F**) Representative western blots and **(E,G,H)** corresponding pixel density quantifications of CSF-3 and KITL. Data are shown as mean ± SEM. **(E,G,H)** N = 5-6. Statistical analysis: Mann-Whitney U test. *p ≤ 0,05, **p ≤ 0,01. i.mc: intramyocardial. DEG: differentially expressed gene.

Since cytokines are key soluble intercellular messengers regulating interorgan communication (Vélez et al., 2023), I evaluated the differential cytokine expression signature in pHrodo$^+$ macrophage and neutrophils in comparison to their bone marrow naïve counterparts (pHrodo$^-$). Using Kobas (KEGG Orthology Based Annotation System) for Geneset Overrepresentation Analysis (GSO) of the data, I identified the GO term "Cytokine Activity" (GO: 0005125), which was upregulated in heart-derived neutrophils ($p < 0,00008$) as well as in macrophages ($p < 0,01591$). The corresponding heatmap in **Fig. 18C** shows the differentially expressed genes (DEGs) of each pHrodo$^+$ subset of neutrophils and macrophages. Out of 175 genes annotated on this pathway, 96 are expressed in neutrophils and 94 in macrophages. Interestingly, 41 out of 96 genes annotated to the GO term "Cytokine Activity" were differentially expressed between heart-derived and bone marrow-resident neutrophils. Likewise, 24 out of 94 genes annotated to the GO term "Cytokine Activity" were differentially expressed in heart-derived and bone marrow-resident macrophages **(Fig. 18D)**.

I then validated the expression of selected cytokines, associated with hematopoietic stem cell maintenance and differentiation (described in the following). For this, I harvested the bone marrow content of WT and *Reg3b*$^{-/-}$ 4 days after LAD ligation, and performed RT-qPCR gene expression analysis (**Fig. 18E)**.

Colony stimulating factors are a family of homodimeric cytokines, which include the monocyte colony-stimulating factor (M-CSF, encoded by *Csf1*), differentially expressed in pHrodo$^+$ neutrophils, and the granulocyte colony-stimulating factor (G-CSF, alias CSF-3, encoded by *Csf3*), upregulated in both pHrodo$^+$ neutrophils and macrophages (**Fig. 18E**). Whereas M-CSF is the primary growth factor driving proliferation of monocytes and their differentiation towards macrophages, CSF-3 binds to the cognate receptor on granulocytic precursors, stimulating their proliferation (Dutta & Nahrendorf, 2015; Mehta & Corey,

2021). Analysis of *Csf1* and *Csf3* gene expression in the bone marrows of infarcted WT and *Reg3b*$^{-/-}$ mice showed unaltered *Csf1* gene expression but a ~ 66 % increase in *Csf3* expression in *Reg3b*$^{-/-}$ mice (**Fig. 18E)**.

The stem cell factor (SCF, encoded by *Kitl*) acts on the KIT receptor to regulate hematopoietic stem cell maintenance and differentiation (Miao et al., 2020; Xu et al., 2018). It was possible to observe a ~ 40 % increase of *Kitl* expression in *Reg3b*$^{-/-}$ mice (**Fig. 18E**). In addition to that, Interleukin-6 (IL-6), a multifunctional cytokine that binds to a receptor of cognate name and acts both as an effector cytokine in inflammation as a stimulator of emergency myelopoiesis was analyzed (Chiba et al., 2018; Tie et al., 2019). Bone marrow expression of *Il6* gene was similar between WT and *Reg3b*$^{-/-}$ infarcted mice (**Fig. 18E**). Similarly, no differences were found for C-X-C motif ligand 12 (*Cxcl12*, alias *Sdf-1*), a key regulator of hematopoietic stem cell quiescence, which acts as a retention factor for immune cell progenitors within the bone marrow (Mitroulis et al., 2020) (**Fig. 18E**). Also, the expression of *Gdf15*, a cytokine that regulates differentiation of the erythrocyte lineage (Ranjbaran et al., 2020; Tanno et al., 2010), was not significantly altered (**Fig. 18E**).

Differential gene expression of CSF-3 and KITL was also confirmed at the protein level, using western blot analysis (**Fig. 18F**). CSF-3 and KITL levels were increased in the bone marrow of *Reg3b*$^{-/-}$ infarcted mice by 33 % and 58 %, respectively (**Fig. 18G-H**).

The upregulation of these growth factors in the bone marrow of *Reg3b*$^{-/-}$ mice suggests enhanced myelopoiesis after MI. Indeed, the biological process myeloid leukocyte differentiation (GO term: 0002573) is enriched in pHrodo^{+} neutrophils and macrophages, prompting me to investigate enhanced myelopoiesis in infarcted *Reg3b*$^{-/-}$ mice.

4.8 Emergency granulopoiesis is increased in *Reg3b*$^{-/-}$ mice and more neutrophils are sent to the infarcted heart

In order to test whether cardiac-derived leukocytes promote enhanced granulopoiesis in the bone marrows of *Reg3b*$^{-/-}$ mice and thus contribute to increased neutrophilia in the infarcted heart, infarcted mice received an intraperitoneal injection of BrdU 4 days after MI. Their bone marrows and hearts were then analyzed by flow cytometry (**Fig. 19A)**.

Neutrophils in the bone marrow incorporated ~ 30 % more BrdU into newly synthesized DNA (**Fig. 19B**). Accordingly, I also assessed the pool of neutrophil precursors

(preNeutros) in the bone marrow, as described by Evrard et al. (2018). I detected a 20 % reduction in preNeutros in the bone marrow of *Reg3b*$^{-/-}$ mice, which is in agreement with the 25 % increase in differentiated bone marrow neutrophils (**Fig. 19C-D**).

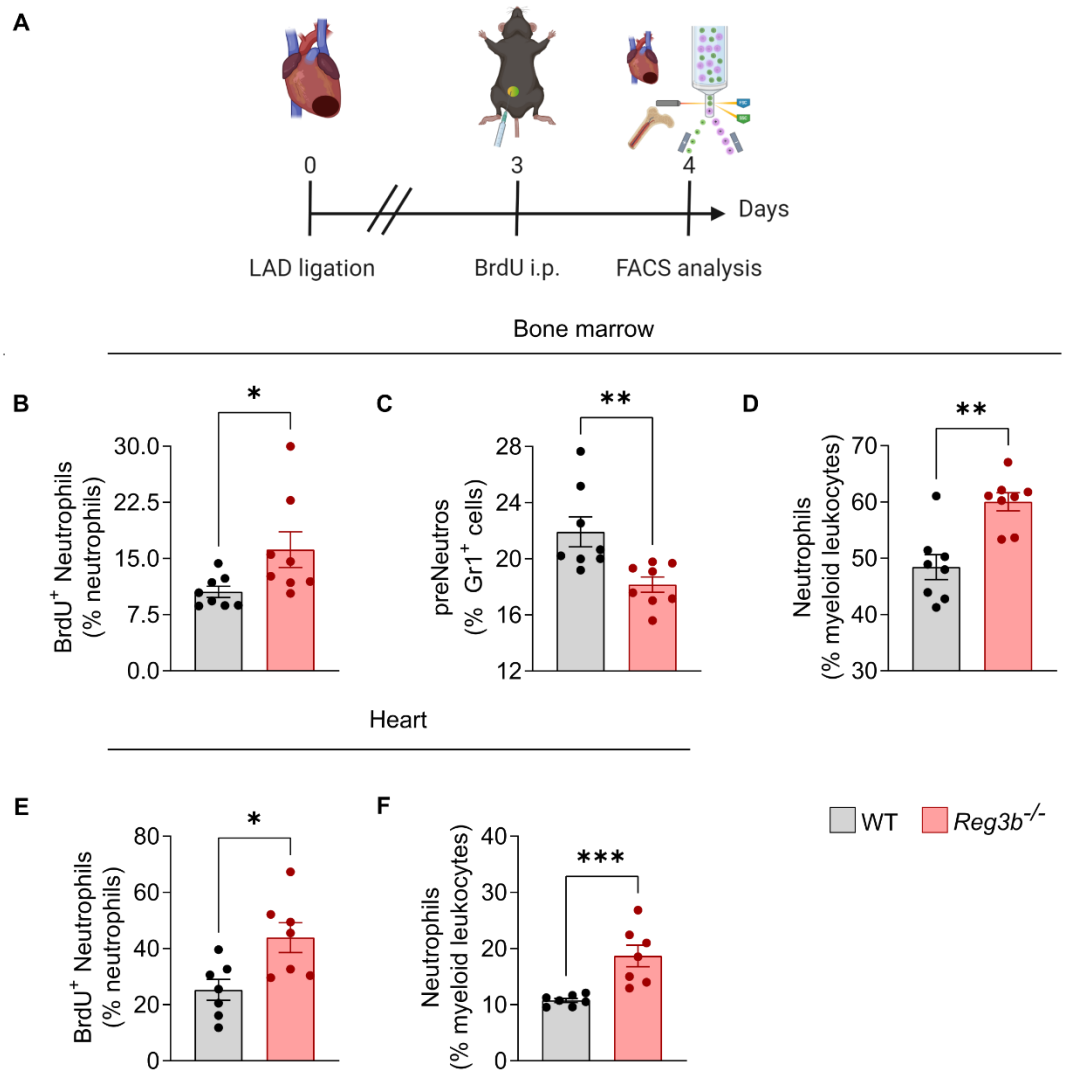

Figure 19. Neutrophils are more proliferative in *Reg3b*$^{-/-}$ than in WT mice. (A) BrdU was injected intraperitoneally 3 days after LAD ligation/one day prior to harvesting of heart and bone marrow for flow cytometric analysis. Illustration created with "BioRender.com". **(B)** Percentage of proliferating (BrdU^{+}) neutrophils among neutrophils in bone marrow **(C)** Percentage of preNeutros in the bone marrow. preNeutros were defined as GR1^{+} cells. **(D)** Percentage of neutrophils among myeloid leukocytes in the bone marrow. **(E)** Percentage of proliferating (BrdU^{+}) neutrophils in the infarcted heart out of total neutrophils **(F)** Percentage of neutrophils among myeloid leukocytes in the infarcted heart. Data are shown as mean ± SEM. **(B,C,D)** N = 8; **(E,F)** N = 7. Statistical analysis: **(B-F)** Mann-Whitney U Test. *p ≤ 0,05, **p ≤ 0,01.

These findings indicated augmented granulopoiesis due to genetic deletion of *Reg3b*, which has a direct impact on the heart, where ~ 75 % more $BrdU^+$ neutrophils were found (**Fig. 19E**). Altogether, the enhanced proliferation rate of neutrophils in the bone marrow of infarcted *Reg3b*$^{-/-}$ mice directly correlated with the 80 % increase in the presence of cardiac neutrophils (**Fig. 19F**).

4.9 Increased proliferation of cardiac tissue macrophages, but not of monocytes account for the increased and prolonged presence of macrophages in infarcted hearts

Experimental myocardial infarction in *Reg3b*$^{-/-}$ mice led to massive but delayed accumulation of macrophages (**Fig. 8G**). Whereas de novo production of neutrophil (granulopoiesis) exclusively takes place in the bone marrow, macrophages can derive from different sources. Basically, macrophages may differentiate from monocytes, released from the bone marrow, from monocytes present in the spleen or locally proliferate in distal tissues (Davies et al., 2013; Swirski et al., 2009). To understand the mechanisms leading to increased presence of macrophages in *Reg3b*$^{-/-}$ infarcted mice and to understand the contribution of local macrophages to this process, BrdU incorporation in monocytes and macrophages was evaluated (**Fig. 20A**).

Proliferation of monocytes was ~ 25 % reduced in the bone marrow of *Reg3b*$^{-/-}$ compared to WT mice (**Fig. 20B**), excluding this organ as the main source of increased macrophage presence in infarcted *Reg3b*$^{-/-}$ mice. Instead, flow cytometric analysis of $BrdU^+$ cardiac macrophages revealed that both 4 and 14 days after LAD ligation, macrophages of *Reg3b*$^{-/-}$ mice incorporated ~ 65 % more BrdU into newly synthesized DNA (**Fig. 20C**). Furthermore, histological staining of infarcted hearts 4 days after LAD ligation showed a higher accumulation of freshly produced macrophages, which expressed the nuclear proliferation marker Ki67 (**Fig. 20D**).

I then hypothesized that the increased presence of freshly produced macrophages in the infarcted heart is due to proliferation of local macrophages rather than reflecting increased production of monocytes in the bone marrow. To test this, I compared the proliferation ratios of TIM-4^+ $CCR2^-$ resident macrophages of fetal origin and of monocyte-derived $CCR2^+$ macrophages (Dick et al., 2019; Sansonetti et al., 2020).

Resident macrophages represent up to 10 % of the total cardiac macrophage population during acute stages of inflammation after MI, whereas the bulk is derived from monocytes infiltrating from the bone marrow (Dick et al., 2019). The data revealed a 50 % lower proliferation rate of resident macrophages in infarcted *Reg3b*$^{-/-}$ compared to WT hearts, either at day 4 or 14 (**Fig. 20E**). In contrast, monocyte-derived macrophages showed ~ 12 % higher proliferation rate in *Reg3b*$^{-/-}$ compared to WT hearts at day 4 and ~ 13,6 % more at day 14 (**Fig. 20F**). Therefore I concluded that increased proliferation rates of monocyte-derived macrophages substantially contributes to the higher presence of macrophages in *Reg3b*$^{-/-}$ infarcted hearts.

I then asked whether proliferation of tissue macrophage is the sole cause for the augmented presence of macrophages in infarcted *Reg3b*$^{-/-}$ hearts, or whether a prolonged permanence/survival in the tissue also contributes to this phenotype. Indeed, the viability of macrophages was ~ 13 % higher in *Reg3b*$^{-/-}$ than in WT hearts due to reduced apoptosis, as indicated per Annexin V flow cytometric staining (**Fig. 20G,H**). In contrast, neither necrosis nor late apoptotic rates were significantly altered between both genotypes (**Fig. 20I,J**). Along these lines, cardiac tissue macrophages showed ~ 23 % higher expression of triggering receptor 1 (TREM-1) in *Reg3b*$^{-/-}$ hearts and ~ 29 % increased expression of triggering receptor 2 (TREM-2), which have been shown to promote macrophage survival at sites of local inflammation (Z. Yuan et al., 2014) (**Fig. 20K,L**).

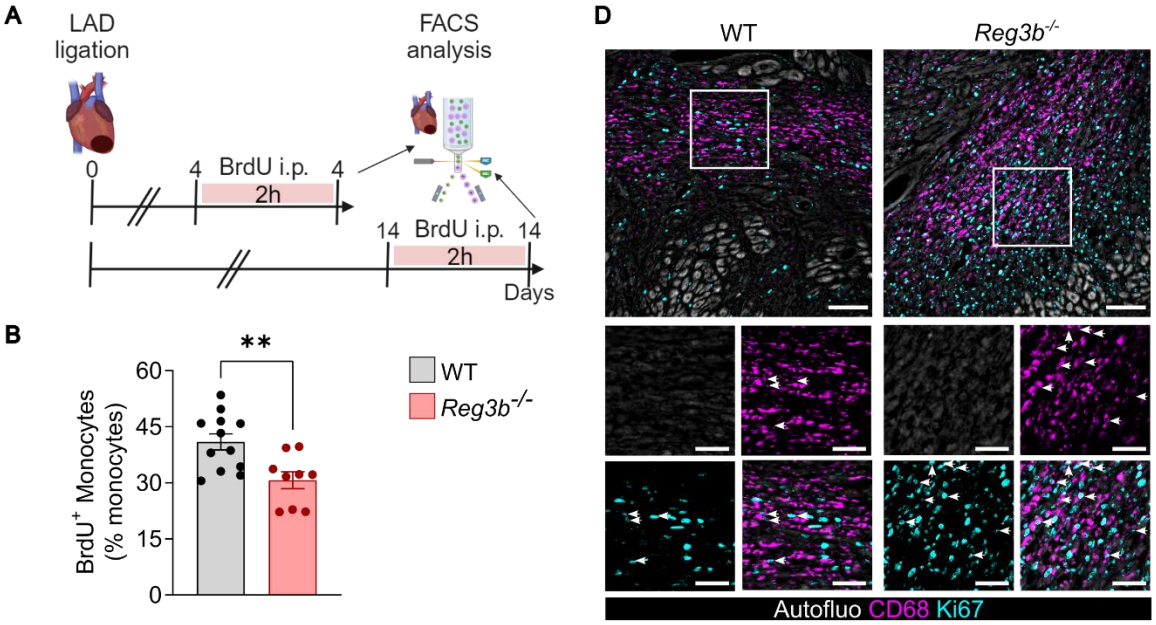
A
LAD ligation
FACS analysis
0
4
BrdU i.p.
2h
4
14
BrdU i.p.
2h
14
Days
B
WT
Reg3b-/-
BrdU+ Monocytes (% monocytes)
D
WT
Reg3b-/-
Autofluo CD68 Ki67

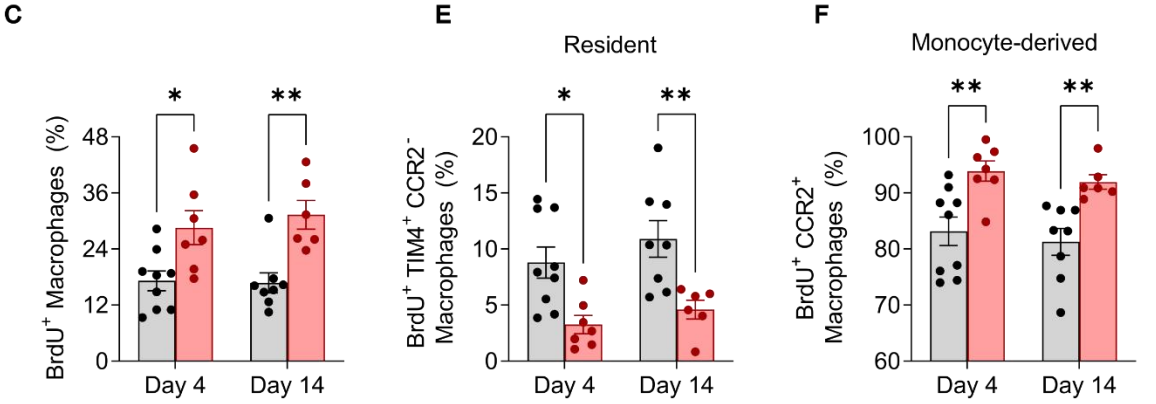
C
BrdU+ Macrophages (%)
Day 4
Day 14
E
Resident
BrdU+ TIM4+ CCR2- Macrophages (%)
F
Monocyte-derived
BrdU+ CCR2+ Macrophages (%)

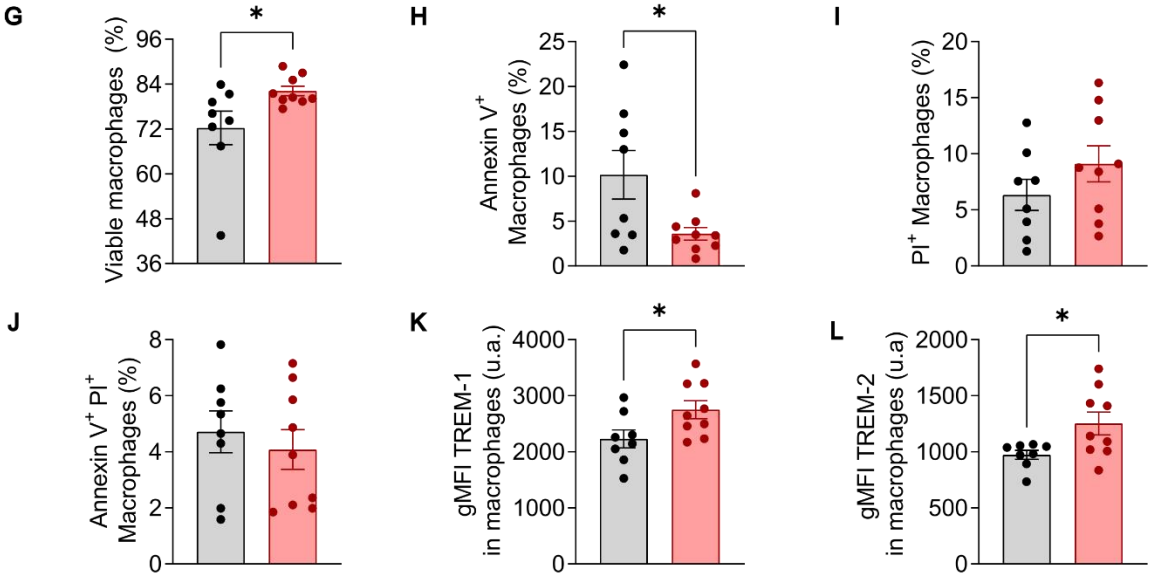
G
Viable macrophages (%)
H
Annexin V+ Macrophages (%)
I
PI+ Macrophages (%)
J
Annexin V+ PI+ Macrophages (%)
K
gMFI TREM-1 in macrophages (u.a.)
L
gMFI TREM-2 in macrophages (u.a)

Figure 20. Increased macrophage proliferation and survival in *Reg3b*$^{-/-}$ infarcted hearts. **(A)** Infarcted mice were injected with BrdU intraperitoneally 4 and 14 days after LAD ligation, 2h prior to organ harvest. Illustration created with "BioRender.com". **(B)** Representative widefield microscopic images of Ki67^{+}CD68^{+} proliferating macrophages in WT and *Reg3b*$^{-/-}$ hearts 4 days after MI. 20x magnification. Scale bars = 100 µm (overview) and 50 µm (insets). Flow cytometric quantification of **(C).** Percentage of BrdU^{+} macrophages (out of total macrophages). **(D)** Percentage of BrdU^{+} TIM4^{+} CCR2^{-} resident macrophages (out of total macrophages). **(E)** Percentage of BrdU^{+} CCR2^{+} monocyte-derived macrophages (out of total macrophages). **(F)** Percentage of viable macrophages (out of total macrophages) **(G)** Percentage of early apoptotic Annexin V^{+} macrophages (out of total macrophages). **(H)** Percentage of necrotic propidium iodide (PI)$^{+}$ (out of total macrophages). **(I)** Percentage of late apoptotic Annexin V^{+} PI^{+} macrophages (out of total macrophages). **(J)** TREM-1 and **(K)** TREM-2 global mean fluorescence intensity in macrophages. Data are shown as mean ± SEM. **(B)** N = 9-12; **(C-F)** N = 6-9; **(G-L)** N = 8-9. Statistical analysis: **(C-F)** Two-way ANOVA followed by Šidák multiple comparisons test **(B,G-L)** Two-tailed unpaired Student's t-test. *$p \leq 0{,}05$, ** $p \leq 0{,}01$. i.p: intraperitoneal

Based on these data, I concluded that higher numbers of cardiac-derived leukocytes stimulate granulopoiesis but not monocytopoiesis in the bone marrow of *Reg3b*$^{-/-}$ mice upon MI, leading to increased numbers of neutrophils in the infarcted heart. Conversely, the increased accumulation of cardiac tissue macrophages in *Reg3b*$^{-/-}$ mice at sites of injury primarily results from local proliferation of monocyte-derived macrophages and reduced apoptotic.

Taken together, the c-type lectin REG3β regulates the dynamics of inflammation in infarcted hearts by a novel mechanism. By curbing the accumulation of pro-lymphangiogenic macrophages, REG3β slows lymphangiogenesis, thereby limiting the drainage of cardiac-derived leukocytes and their homing to the bone marrow, where they deliver biochemical cues to further amplify cardiac inflammation.

5 DISCUSSION

5.1 Biphasic accumulation of leukocytes in infarcted *Reg3b*$^{-/-}$ mice

A rapid initiation of inflammation is important to remove dead cardiomyocytes and to enable formation of a replacement scar. Accordingly, a timely chemoattraction of neutrophils and macrophages – the most abundant innate immune cell players – to the heart is essential to establish an efficient response to myocardial injury (Ma, 2021; Moskalik et al., 2022; Sager et al., 2016; Silvestre-Roig et al., 2020). The immune cell composition changes dramatically throughout different phases of inflammation, which is the result of a harmonized interplay between cytokines, chemokines and different immune cells (Frangogiannis, 2018). In order to avoid unspecific degradation of healthy tissue, proinflammatory leukocytes must leave the infarcted heart in a coordinated manner, and be replaced by other leukocytes, which coordinate pro-reparative processes (Prabhu & Frangogiannis, 2016; Weil & Neelamegham, 2019). The highly complex nature of cardiac healing has prompted many researchers to search for novel players that regulate the dynamics of inflammation.

Previously, my group has published several studies on the acute effects of REG3β on the leukocyte response in the infarcted heart (Detzer, 2020; Lörchner, Pöling et al., 2015; Lörchner, et al., 2018; Lörchner, Widera, et al., 2018). In the present work, I have recapitulated the delayed acute infiltration of macrophages during the 2 first days after LAD ligation in *Reg3b*$^{-/-}$mice, which was caused by the absence of REG3β (Lörchner, Pöling et al., 2015; Lörchner et al., 2018). Furthermore, neutrophils persist for until one week after LAD ligation in *Reg3b*$^{-/-}$ mice, since REG3β directly induces death of neutrophils (Detzer, 2020). In contrast, neutrophils are rapidly depleted in in infarcted hearts of WT mice.

In this work, I have extended the analysis of different immune cell subtypes kinetics in *Reg3b*$^{-/-}$ mice, which now covers a broader window of time, encompassing not only the very acute inflammatory phase, but also the proliferative phase of cardiac healing (Forte et al., 2018; Weil & Neelamegham, 2019). Overall, *Reg3b*$^{-/-}$ mice show an intensified immune response during the first 2 weeks since onset of MI. The initial deficiency of macrophages, resulting from deletion of *Reg3b* becomes overcompensated already 4 days after MI, and persists until 2 weeks post-MI. Interestingly, the relative increase of macrophages in infarcted *Reg3b*$^{-/-}$ hearts was not caused by increased influx of bone marrow-derived monocytes (Mass et al., 2023), which remained less abundant compared to WT mice throughout the

investigated time period. Instead, I observed increased proliferation of monocyte-derived macrophages, which are among the most abundant immune cell type in the infarcted heart, explaining the global increase of myeloid cells in *Reg3b*$^{-/-}$ infarcted hearts.

In accordance with my group´s previous findings (Detzer, 2020), such immune misbalance resulted in a highly inflammatory environment. Leukocyte accumulation was strongest inside the IZ, where the tissue is more hypoxic and more cytokines are released. These findings prompted me to investigate whether other mechanisms underlie the chronically unresolved inflamed state in *Reg3b*$^{-/-}$ infarcted mice. Due to assumed role of lymphatics in promoting resolution of cardiac inflammation (Henri et al., 2016; Shimizu et al., 2018; Vieira et al., 2018), I hypothesized that the absence of REG3β may alter formation of lymphatic vessels in the infarcted heart.

5.2 Enhanced lymphangiogenesis in infarcted *Reg3b*$^{-/-}$ hearts does not correlate with improved resolution of inflammation

Previous reports suggested that lymphatic expansion upon MI happens most intensely in the border zone (BZ), the area adjacent to the infarct zone, where inflammatory processes and hypoxia are more moderate, but still sufficient to induce cytokine release and tissue remodeling (Klotz et al., 2015). Subsequent studies did often not discriminate between regions of the heart when analyzing lymphatic vessel proliferation (Henri et al., 2016; Keller et al., 2021; Vieira et al., 2018).

Because the definition of BZ has no consensus in the literature (Kung et al., 2018; Zhu et al., 2022), I opted to use the presence/absence of viable cardiomyocytes distal to the surgical knot as the sole parameter to distinguish between the IZ and the viable myocardium (here called RZ). Therefore, I have not taken into consideration the microenvironmental gradient which distinguishes a highly inflammatory IZ from very proximal areas of the left ventricle, where the effects of hypoxia are minimized (Rexius-Hall et al., 2022).

In this study, lymphatics inside of the scar died acutely, and the remaining vessels proliferated thereafter. Overall, there was an increased lymphangiogenic response of *Reg3b*$^{-/-}$ compared to WT mice inside the IZ but not in RZ. The more rapid recovery of lymphatic vessels in infarcted *Reg3b*$^{-/-}$ mice allowed better resolution of edema – which suggests that these newly formed vessels are functional.

Mechanistically, the most potent activator of lymphatic vessel proliferation is VEGF-C, although other non-VEGF ligands have been identified to play a relevant role in this process, including the infarcted heart (Harris et al., 2022; Tatin et al., 2017; Trincot et al., 2018). Analysis of protein extracts of infarcted hearts revealed that *Reg3b*$^{-/-}$ mice have overall higher levels of VEGF-C and VEGF-D expression. The cellular origin for VEGF-C in the infarcted heart – and in other inflammatory settings (Kataru et al., 2009) – is primarily macrophages, although cardiomyocytes have also been found to be a possible source of this factor (Ishikawa et al., 2007). Macrophages in the infarcted heart activate expression of *Vegfc* gene in response to efferocytosis of dead cardiomyocytes (Glinton et al., 2022) and therefore I decided to narrow my focus on them as a primary sources of pro-lymphangiogenic factors.

Consistent with the results of other studies (Jin et al., 2022; Martini et al., 2019), the current data showed that macrophages account for the majority of leukocytes in all phases of the inflammatory response in the infarcted heart. After initial defects in the chemoattraction of macrophages in infarcted *Reg3b*$^{-/-}$ mice, macrophages became more abundant in mutants compared to WT controls. Spatially, leukocyte accumulation was at least 5-fold greater in the IZ than in the RZ. Considering that enhanced lymphangiogenesis happened in the IZ as well, it is reasonable to believe that macrophages contribute to the enhanced lymphangiogenesis in *Reg3b*$^{-/-}$ mice by secreting VEGF-C.

It is naïve to assume that all types of macrophages equally promote lymphangiogenesis, since macrophages are heterogeneous with varying functions depending on their origin and subtype classification (Y. H. Li et al., 2022; Sansonetti et al., 2020). Previously, my group reported different biological functions of macrophages based on Ly6C and MHCII expression, and identified that Ly6C^{hi} macrophages carry a gene expression signature, which theoretically promotes lymph vessel development (Lörchner et al., 2018).

Local delivery of recombinant REG proteins to WT infarcted hearts stimulated the accumulation of MHCII^{lo}/LyC^{lo} macrophages and MHCII^{hi}/LyC^{lo} macrophages, while it suppressed Ly6C^{hi} chemoattraction (Lörchner, et al., 2018). Delivery of recombinant REG3β directly to the infarcted heart of to *Reg3b*$^{-/-}$ mice was sufficient in preventing the expansion of lymphatic vessel vasculature in the IZ and RZ by halting the accumulation of Ly6C^{hi} macrophages. In light of these observations, it is reasonable to conclude that the genetic

deletion of *Reg3b* enables lymphatic proliferation via the preferential accumulation of VEGF-C-secreting Ly6C^{hi} macrophages.

Although the data showed that monocyte-derived Ly6C^{hi} macrophages were the most relevant VEGF-C source, Glinton and collaborators (2022) have shown that resident CCR2^{-} TIM4^{+} macrophages secrete VEGF-C at comparatively higher levels than monocyte-derived CCR2^{+} macrophages. In spite of this discrepancy in respect to the origin of macrophages, I detected a strong VEGF-C expression in Ly6C^{lo} macrophages (of tissue origin), albeit lower than in Ly6C^{hi} counterparts.

Despite the fact that VEGF-C and VEGF-D drive to some extent blood vessel expansion, they have a relatively low affinity for VEGFR2 (Joukov et al., 1996, 1997). Therefore, I decided to exclude possible effects on formation of blood capillaries from this study. Another reason was that VEGFR2 mostly drives formation of new blood vessels during early developmental stages (vasculogenesis) (Hamada et al., 2000; Shalabi et al., 1995), and its contribution during revascularization of infarcted myocardium is still not completely clear (K. Kobayashi et al., 2017). Moreover, analysis of total angiogenesis-promoting VEGF-A in heart tissue lysates did not suggest any differences in the availability of this ligand in *Reg3b*$^{-/-}$ mice in comparison to WT (data not shown).

Although the available results indicate that REG3β indirectly limits cardiac lymphangiogenesis by changing the composition of macrophages, it is not possible to rule out completely that it directly halts lymphangiogenesis. I made several attempts to analyze the impact of REG3β on commercially available human dermal lymphatic endothelial cells. However, I encountered numerous technical problems, preventing acquisition of reliable results. Culture of these cells was very challenging; with each passage they became markedly less responsive and did not consistently proliferate when stimulated with positive controls (e.g. addition of VEGF-C) (data not shown). Therefore, this aspect remains to be investigated in a future study.

Altogether, I report that de novo proliferation of lymphatic vessels is the probable cause for accelerated recovery of the lymphatic coverage in the IZ of *Reg3b*$^{-/-}$ hearts. Furthermore, I provided evidence that VEGF-C-secreting macrophages stimulate this process. I did not observe accelerated resolution of inflammation in *Reg3b*$^{-/-}$ mice, despite enhanced lymphangiogenesis, although different studies emphasized the importance of

cardiac lymphatics in resolving inflammation (Henri et al., 2016; Shimizu et al., 2018; Vieira et al., 2018). Instead, I found a positive correlation between increased cardiac lymphatic vessel coverage and increased presence of immune cells. Such discrepancy was also described by Keller (2021), and, in my view, suggests that the newly assembled vessels were either unable to attract leukocytes or enabled overcompensation of inflammatory responses.

5.3 Leukocytes emigrate from the heart towards lymph nodes and bone marrow via afferent lymphatics

Newly assembled lymphatic capillaries secrete CCL21 in order to attract $CCR7^+$ leukocytes into their lumen (Hampton & Chtanova, 2019). Additionally, CCL19, produced by myeloid leukocytes, also attract $CCR7^+$ leukocytes towards lymphoid organs. Such chemokine gradients start in the lymphatic capillaries and are the strongest in the lymph node medulla, facilitating the extravasation of leukocytes (Petrova & Young Koh, 2020).

According to the data, CCL19 and CCL21 levels were higher in infarcted hearts of *Reg3b*$^{-/-}$ mice, and likely contributed to leukocyte emigration. In agreement with the enhanced presence of immune cell in *Reg3b*$^{-/-}$ mice, leukocyte-derived CCL19 was highly present 4 days after LAD ligation. In contrast, lymphatic-derived CCL21 was highly expressed in infarcted *Reg3b*$^{-/-}$ mice 7 days after LAD ligation, when cardiac lymphatic coverage on *Reg3b*$^{-/-}$ mice reaches a maximum. Thus, it is probable that CCL19 and CCL21 are relevant for leukocyte drainage in different time points.

It is important to recognize that most of the research on leukocyte migration into lymphatic vessels and lymph nodes has been done with dendritic cells (DCs) (especially, due to their prominent antigen-presenting capabilities) (Choo et al., 2017; Johnson & Jackson, 2010; Y. Xiong et al., 2017). Very few studies have investigated in detail how other $CCR7^+$ leukocytes, such as macrophages and neutrophils, migrate through the lymphatic system (Beauvillain et al., 2011; Xuan et al., 2015). Here, emigrating cardiac-derived leukocytes entering the lymph nodes and bone marrow (including macrophages and neutrophils) were mostly $CCR7^+$. Still, one should not neglect other chemokines which might attract leukocytes to lymphatics, such as CCL1, CCL2, CXCL1, CXCL5, CXCL12 (among others), as cited in Jackson (2019), but which were not covered by my work.

Other studies addressed the drainage of immune cells in the infarcted heart by lymphatic vessels towards mediastinal lymph nodes, using cardiomyocyte reporter mouse lines as tracers (Glinton et al., 2022; Vieira et al., 2018). Here – with the intent to limit the tracing studies to a time window when *Reg3b* had already modulated lymphatic vessel formation – an intramyocardial delivery of a fluorogenic probe (pHrodo) was employed. I assumed that these cells would get transported towards other distal organs, which were therefore also included in the tracing approach. Of note, blockage of lymphatic proliferation via overexpression of a VEGF-C trap (sVEGFR3) reduced the presence of cardiac-derived leukocytes in lymph nodes and bone marrow, emphasizing the functional relevance of cardiac lymphatics in enabling such interorgan circuit.

One open question left by this work is how cardiac-derived leukocytes in the mediastinal lymph nodes reach the bone marrow. Recently, lymphatic vessels in the bone were described, after a long lasting paradigm that this organ is devoid of lymphatics (Aspelund et al., 2016; Biswas et al., 2023). Despite this new finding, it is very unlikely that immune cells travel exclusively via lymphatics all the way to the bone marrow. First, most lymphatics described by Biswas and collaborators (2023) are present in cortical regions of the bone and penetrate very little into the bone marrow, which essentially prevents distribution throughout the whole bone. Second, the anatomy of the lymphatic system is intimately interconnected with blood circulation, in that efferent lymphatic collectors drain into the vena cava via the thoracic duct. Additionally, the lymph nodes themselves are highly vascularized, which could potentially enable immune cells to reach the blood circulation directly from there (Von Andrian & Mempel, 2003). Combined, this argues for the participation of the blood vasculature in the process of immune cell trafficking.

I did not take reverse migration of leukocytes from the tissue to blood vessels into consideration. This concept has been described in zebrafish embryos (Mathias et al., 2006, cited in Robertson et al., 2014) and in murine hepatic lesions (Wang et al., 2017) using live imaging techniques. However, due to technical limitations such approaches are not available for murine hearts. Although reverse migration may participate in trafficking of leukocytes, a major contribution in the infarcted heart seems unlikely.

5.4 Cardiac-derived leukocytes modify the bone marrow niche, promoting granulopoiesis but not monocytopoiesis

In the last decades, researchers have developed the concept of a "cardiovascular continuum", which not only encompasses the heart and blood vessels, but also peripheral organs such as the spleen, bone marrow and the nervous system (Libby et al., 2016). Landmark studies performed by the groups of Dr. Nahrendorf and Dr. Nagareddy have employed parabiosis and bone marrow transplantation to describe a crosstalk between infarcted heart and hematopoiesis (Sager et al., 2015; Sreejit et al., 2020, 2022). They elegantly showed that activated neutrophils produce S100A8/A9 in the infarcted heart, which primes the inflammasome of freshly incoming neutrophils (Sreejit et al., 2020, 2022). As a result, these neutrophils produce interleukin-1β (IL-1β), which stimulates granulopoiesis in the bone marrow in a paracrine manner (Sager et al., 2015; Sreejit et al., 2020, 2022).

My results indicate the presence of cardiac-derived leukocytes in the bone marrow after MI. The number of pHrodo^{+} leukocytes in the bone marrow is rather small (~ 1 % compared to the total myeloid leukocyte reservoir in this organ). In spite of that, these cardiac-derived leukocytes show a strong proinflammatory gene expression, including multiple cytokines, which set them apart from bone-marrow resident counterparts. This enables a systemic interorgan communication between the infarcted heart and the bone marrow niche. Considering that the number of cardiac-derived leukocytes is increased in the bone marrow of *Reg3b*$^{-/-}$ mice, I reason that the interorgan communication between heart and bone marrow is intensified after loss of *Reg3b*.

pHrodo^{+} leukocytes in the bone marrow showed distinct upregulation of leukocyte growth factors, including the cytokines CSF-3 and KITL. This finding suggests a differential myelopoietic response in *Reg3b*$^{-/-}$ mice with increased formation of neutrophils. Since neutrophils are short-lived in the tissue and are exclusively derived from proliferating precursors in the bone marrow (Overbeeke et al., 2022), the higher rate of neutrophil formation in the bone marrow is a prerequisite for enhanced immigration into the heart.

The differential expression of *Csf1* by pHrodo^{+} versus resident neutrophils prompted me to hypothesize that enhanced monocytopoiesis in *Reg3b*$^{-/-}$ mice might also explain the elevated presence of macrophages in their infarcted hearts. This assumption turned out to be wrong. I neither observed increased expression of *Csf1*, nor augmented proliferation of

monocytes in the bone marrow of *Reg3b*$^{-/-}$ mice – rather the opposite. In fact, the attenuated monocytopoiesis is in line with the deficient accumulation of monocytes in infarcted *Reg3b*$^{-/-}$ hearts, as shown by the initial kinetics analysis. A possible explanation for this surprising finding might be a negative feedback emanating from increased local proliferation of macrophages in the infarcted heart. The reduced proliferation of monocytes in the bone marrows of infarcted *Reg3b*$^{-/-}$ hearts suggests increased proliferation of macrophages in the heart as the main reason for the elevated presence of macrophages

Interestingly, the proliferating cardiac macrophage fraction in *Reg3b*$^{-/-}$ mice is CCR2^{+}, meaning they have a monocyte origin (Bajpai et al., 2019; Sager et al., 2016). However, this does not necessarily mean that CCR2^{+} macrophages have freshly extravasated into the infarcted heart tissue from the blood circulation. I reason that the strongly inflammatory environment in the infarcted heart recruited CCR2^{+} macrophages to enter the cell cycle. A second explanation for the abundant numbers of macrophages in *Reg3b*$^{-/-}$ infarcted hearts might be the acquisition of anti-apoptotic properties, which allow a long lasting presence in the tissue.

In respect to VEGF-C driven lymphangiogenesis, two different explanations should be considered. The enhanced proliferation of CCR2^{+} macrophages in infarcted *Reg3b*$^{-/-}$ hearts, particularly of the VEGF-C producing Ly6C^{hi} macrophages may stimulate cardiac lymphangiogenesis. Alternatively, Ly6C^{hi} macrophages may accumulate in infarcted *Reg3b*$^{-/-}$ hearts due to changes in the composition of locally available chemoattractants, thus enabling an expansion of cardiac lymphatics. Either way, emigrating cardiac-derived leukocytes foster differential granulopoiesis in the BM, leading to intensified infiltration of neutrophils in the heart.

In summary, REG3β controls the turnover of neutrophils in infarcted hearts by at least two independent mechanisms: First, REG3β-dependent cytotoxicity directly limits the activity of mature neutrophils in infarcted hearts (Detzer, 2020). Second, REG3β curbs a positive feedback on bone marrow granulopoiesis by indirectly restricting lymphatic vessel proliferation in the heart. In combination, these two processes prevent excessive accumulation of neutrophils in the damaged heart. Altogether, these data paint a complex picture, refuting a simplistic view that cardiac lymphangiogenesis directly enables resolution of inflammation.

6 CONCLUSION

In this work, I describe how REG3β restricts lymphatic-dependent leukocyte drainage from the infarcted tissue, leading to substantial consequences in other organs. Mechanistically, REG3β limits the accumulation of a subpopulation of VEGF-C-producing Ly6C^{hi} macrophages, thereby delaying initiation of lymphangiogenesis. As a result, fewer lymphatic vessels form, secreting less CCL21, and fewer leukocytes migrate into lymphatic vessels. Drainage via lymphatic vessels enabled transport of leukocytes to the bone marrow, reflecting heart-bone interorgan communication. Cardiac-derived leukocytes promote granulopoiesis in the bone marrow via CSF-3 and KITL, resulting in the release of more neutrophils, prolonging the inflammatory response in the infarcted heart (**Fig. 21**).

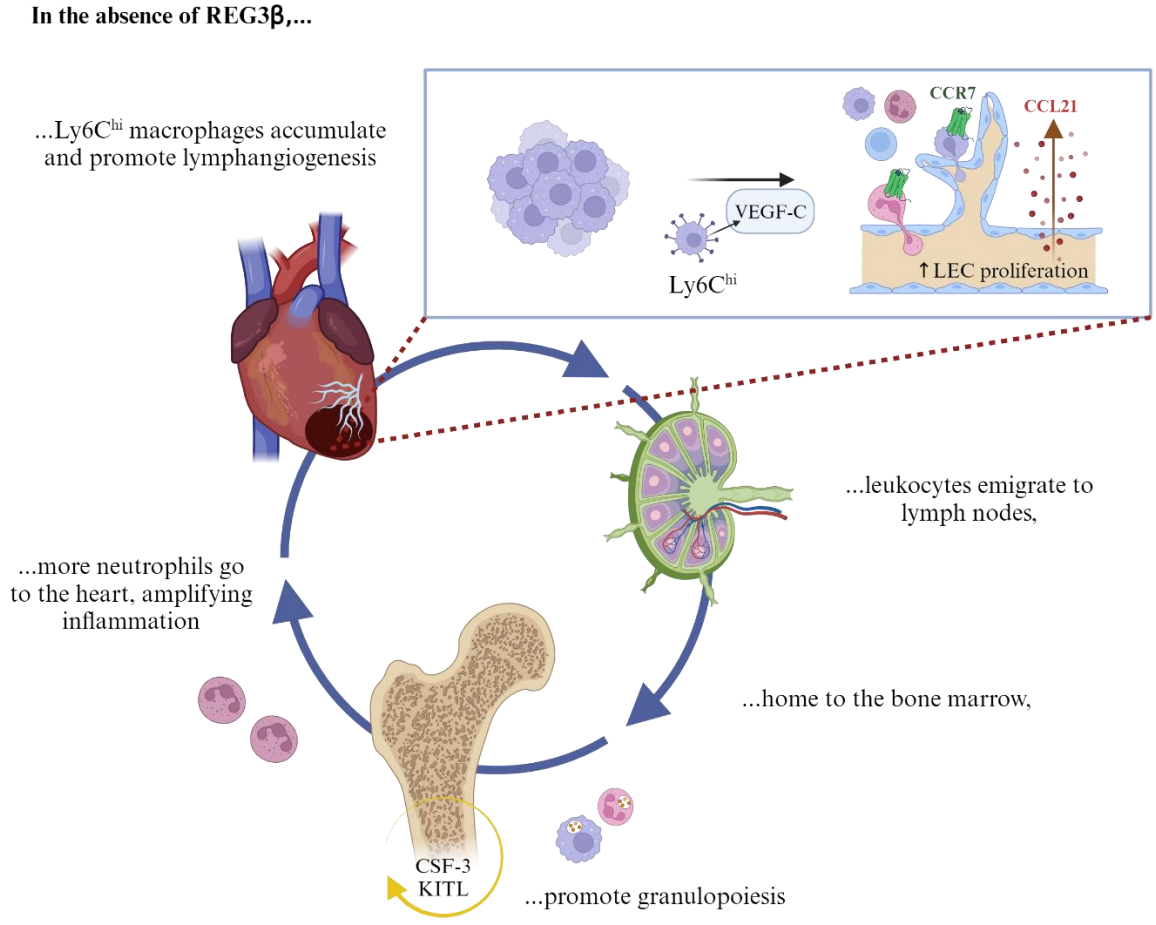

Figure 21. Graphic summary of interorgan communication loop between the infarcted heart and the bone marrow in *Reg3b*$^{-/-}$ mice. Macrophages accumulate in the infarcted heart, persisting until at least two weeks after MI induction. The overrepresented presence of VEGF-C-secreting Ly6C^{hi} macrophages in *Reg3b*$^{-/-}$ hearts enables lymphatic vessel proliferation. Although the newly formed lymphatics reduce edema, secrete CCL21 and

attract leukocytes towards mediastinal lymph nodes, they fail to promote resolution of inflammation. Cardiac leukocytes emigrate via lymphatics and home to the bone marrow, where they modify the local niche, promoting granulopoiesis. Consequently, freshly produced neutrophils are sent to the heart, further amplifying a vicious inflammatory response. Illustration created with “BioRender.com”.

Altogether, the anti-lymphangiogenic effect of REG3β in the heart indirectly curbs excessive granulopoiesis, avoiding an uncontrolled amplification of cardiac inflammation.

7 ABSTRACT

The initiation and resolution of immune-inflammatory processes through precise regulation of leukocyte accumulation from the blood and lymphatic drainage, respectively, are critical for efficient wound healing and tissue remodeling after myocardial infarction. Previous work from my group identified regenerating islet-derived protein 3 beta (REG3β) as a novel cardiomyocyte-derived secretory protein that restricts neutrophil accumulation in the injured myocardium. In the present work, I investigated the role of the cardiac lymphatic network in REG3β-mediated resolution of cardiac inflammation. Flow cytometry-based kinetic immune cell profiling in combination with light sheet fluorescence microscopy imaging of the lymphatic network of infarcted hearts revealed a persistent accumulation of innate immune cells and increased lymphatic vessel formation in REG3β-deficient (*Reg3b*$^{-/-}$) mice. The *Reg3b* mutants showed an accumulation of Ly6C^{hi} macrophages, which stimulated lymphangiogenesis by secretion of VEGF-C/-D. In addition, the levels of chemokines CCL19 and CCL21 were higher in the walls of the lymphatic vessels in the heart of infarcted *Reg3b*$^{-/-}$ mice. The enhanced expression of CCL19 and CCL21 correlated with an increased emigration of CCR7^{+} pHrodo dye-labelled cardiac neutrophil granulocytes and macrophages towards mediastinal lymph nodes and bone marrow. AAV9-mediated overexpression of sVEGFR3 blocked this process. RNAseq analysis of heart-derived leukocytes in the bone marrow showed that such leukocytes are able to promote granulopoiesis. Indeed, more neutrophil granulocytes were produced in the bone marrow of *Reg3b*$^{-/-}$ mice after myocardial infarction, which explains the continuous infiltration of newly formed BrdU^{+} neutrophils into infarcted *Reg3b*$^{-/-}$ hearts. Additionally, an increased proliferation of macrophages was found in the infarcted hearts of *Reg3b* mutants, which is probably the cause for the significantly increased amount of myeloid leukocytes during myocardial healing. Overall, my findings suggest an increased inflammatory circuit upon myocardial infarction in which REG3β restricts lymphatic drainage and homing of cardiac leukocytes to the bone marrow, thereby attenuating signals that stimulate the production of new immune cells and cause excessive cardiac inflammation.

8 ZUSAMMENFASSUNG

Der Beginn und die Beendigung von immun-entzündlichen Prozessen durch präzise Regulation der Ansammlung von Leukozyten aus dem Blut bzw. der Lymphdrainage sind von entscheidender Bedeutung für eine effiziente Wundheilung und den Gewebeumbau nach einem Herzinfarkt. Frühere Arbeiten meiner Gruppe identifizierten das Regenerating islet-derived protein 3 beta (REG3β) als ein neuartiges, von Kardiomyozyten stammendes sekretorisches Protein, welches die Akkumulation von neutrophilen Granulozyten im verletzten Myokard einschränkt. Ich habe in der vorliegenden Arbeit die Rolle des lymphatischen Netzwerks bei der REG3β-vermittelten Auflösung der kardialen Entzündung untersucht. Die durchflusszytometrie-basierte kinetische Immunzell-Profilierung in Kombination mit einer lichtscheibenfluoreszenzmikroskopischen Darstellung des lymphatischen Netzwerks von infarzierten Herzen enthüllte eine anhaltende Anhäufung angeborener Immunzellen und eine verstärkte Bildung von Lymphgefäßen in REG3β-defizienten (*Reg3b*$^{-/-}$) Mäusen. Die *Reg3b*-Mutanten zeigten eine Ansammlung von Ly6C^{hi}-Makrophagen, welche die Lymphangiogenese durch Sekretion von VEGF-C/-D stimulierten. Darüber hinaus waren die Level der Chemokine CCL19 und CCL21 in den Wänden der Lymphgefäße im Herzen von infarzierten *Reg3b*$^{-/-}$-Mäusen erhöht. Die vermehrte Expression von CCL19 und CCL21 korrelierte mit einer verstärkten Auswanderung von CCR7^{+}-pHrodo-Farbstoff-markierten kardialen neutrophilen Granulozyten und Makrophagen in mediastinale- Lymphknoten sowie ins Knochenmark. Eine viral vermittelte Überexpression von sVEGFR3 blockierte diesen Prozess. Die RNAseq-Analyse von aus dem Herzen stammenden Leukozyten im Knochenmark zeigte, dass solche Leukozyten in der Lage sind, die Granulopoese zu fördern. Tatsächlich wurden im Knochenmark von *Reg3b*$^{-/-}$-Mäusen nach Myokardinfarkt mehr neutrophile Granulozyten produziert, was die kontinuierliche Infiltration von neu entstandenen BrdU^{+}-Neutrophilen in infarzierte- *Reg3b*$^{-/-}$-Herzen erklärt. Zudem wurde eine vermehrte Proliferation von Makrophagen in den infarzierten Herzen der *Reg3b*-Mutanten gefunden, was wahrscheinlich die Ursache für die deutlich erhöhte Menge an myeloischen Leukozyten während der Myokardheilung ist. Meine Ergebnisse deuten insgesamt auf einen verstärkten Entzündungskreislauf nach einem Herzinfarkt hin, in dem REG3β die Lymphdrainage und die Ansiedlung von Herzleukozyten im Knochenmark

einschränkt, wodurch Signale gedämpft werden, welche die Produktion neuer Immunzellen anregen und eine übermäßige Herzentzündung bedingen.

9 LIST OF ABBREVIATIONS

Abbreviation	Meaning
3D	Three dimensional
AF	Alexa fluor
ANOVA	Analysis of variance
BM	Bone marrow
BPB	Bromophenol blue
BrdU	Bromodeoxyuridine/5-bromo-2'-deoxyuridine
BSA	Bovine serum albumin
BZ	Border zone
CCL1	Chemokine (C-C motif) ligand 1
CCL12	Chemokine (C-C motif) ligand 12
CCL19	Chemokine (C-C motif) ligand 19
CCL2	Chemokine (C-C motif) ligand 2
CCL21	Chemokine (C-C motif) ligand 21
CCR2	C-C chemokine receptor type 2
CCR7	C-C chemokine receptor type 7
CD11b	Cluster of differentiation 11B
CD31	Cluster of differentiation 31
CD45	Cluster of differentiation 45
CD54	Cluster of differentiation 54
CD68	Cluster of differentiation 68
CD8	Cluster of differentiation 8
CSF-3	Colony stimulating factor 3
cTnI	Cardiac troponin I
CXCL1	C-X-C motif) ligand 1
CXCL5	C-X-C motif) ligand 5
CXCL12	C-X-C motif) ligand 12
CXCR4	C-X-C chemokine receptor type 4
DAMPs	Danger associated molecular patterns
DAPI	4′,6-diamidino-2-phenylindole
DC	Dendritic cell
DMSO	Dimethyl sulfoxide
dNTP	Deoxynucleotide triphosphate
DTT	Dithiothreitol
EC	Endothelial cell
ECi	Ethyl cinnamate
EDTA	Ethylenediaminetetraacetic acid
EP	Extraction buffer
EXTL3	Exostosin-like glycosyltransferase 3

F4/80	Mucin-like hormone receptor 1
FACS	Fluorescence-activated cell sorting
FCS	Fetal calf serum
FDR	False discovery rate
FMO	Fluorescence minus one
G-CSF	Granulocyte-macrophage colony-stimulating factor
G-CSFR	Granulocyte-macrophage colony-stimulating factor receptor
GSO	Gene structure ontology
H202	Hydrogen peroxide
HEPES	4-(2-hydroxyethyl)-1-piperazineethanesulfonic acid
HRP	Horseradish peroxidase
i.mc	Intramyocardial
i.p	Intraperitoneal
I/R	Ischemia-reperfusion
IBD	Inflammatory bowel disease
ICAM1	Intercellular adhesion molecule
IL-1	Interleukin-1
IL-1b	Interleukin-1b
IL-6	Interleukin-6
IZ	Infarct zone
KCl	Potassium chloride
Ki67	Antigen kiel 67
LAD	Left anterior descending artery
LB	Laemmli buffer
LEC	Lymphatic endothelial cell
LN	Lymph node
$Ly6C^{hi}$	Lymphocyte antigen 6 complex high
$Ly6C^{lo}$	Lymphocyte antigen 6 complex low
Ly6G	Lymphocyte antigen 6 complex, locus G.
LYVE-1	Lymphatic vessel endothelial hyaluronic acid receptor
MFI	Mean Fluorescence Index
MHCII	Major histocompatibility complex II
MHCIIhi	Major histocompatibility complex II high
MHCIIlo	Major histocompatibility complex II low
MI	Myocardial infarction
MRI	Magnetic resonance imaging
NaCl	Sodium chloride
O.C.T.	Optimal cutting temperature
PAP	Pancreatitis-associated protein
PBS	Phosphate buffer saline
PFA	Paraformaldehyde

rec	recombinant
REG	Regenerating islet-derived protein
*Reg1/*REG1A	Regenerating islet-derived protein 1/1A
*Reg1/*REG1B	Regenerating islet-derived protein 1/1B
Reg2	Regenerating islet-derived protein 2
*Reg3a/*REG3A	Regenerating islet-derived protein 3 alpha/3A
Reg3b	Regenerating islet-derived protein 3 beta
Reg3d	Regenerating islet-derived protein 3 delta
*Reg3g/*REG3G	Regenerating islet-derived protein 3 gamma/3G
REG4	Regenerating islet-derived protein 4
ROS	Reactive oxygen species
RT	Room temperature
RZ	Remote zone
Sca-1	Stem cells antigen-1
SCF	Stem cell factor
SDS	Sodium dodecyl sulfate
SEM	Standard deviation of the mean
Siglec	Sialic acid binding immunoglobulin-type lectins
SMA	Smooth muscle actin
sVEGFR3	Soluble vascular endothelial receptor 3
TIM4	T-cell/transmembrane immunoglobulin and mucin domain containing 4
TREM1	Triggering receptor expressed on myeloid cells 1
TREM2	Triggering receptor expressed on myeloid cells 2
VEGF-A	Vascular endothelial factor A
VEGF-B	Vascular endothelial factor B
VEGF-C	Vascular endothelial factor C
VEGF-D	Vascular endothelial factor D
VEGFR1	Vascular endothelial growth factor receptor 1
VEGFR2	Vascular endothelial growth factor receptor 2
VEGFR3	Vascular endothelial growth factor receptor 3
WB	Western blot
WM	Whole-mount
WT	Wild-type

10 LIST OF FIGURES

11 LIST OF TABLES

12 REFERENCES

Achen, M. G., Jeltsch, M., Kukk, E., Makinen, T., Vitali, A., Wilks, A. F., Alitalo, K., & Stacker, S. A. (1998). Vascular endothelial growth factor D (VEGF-D) is a ligand for the tyrosine kinases VEGF receptor 2 (Flk1) and VEGF receptor 3 (Flt4). *PNAS*, *95*(1), 548–553. https://doi.org/https://doi.org/10.1073/pnas.95.2.548

Adamo, L., Rocha-Resende, C., Prabhu, S. D., & Mann, D. L. (2020). Reappraising the role of inflammation in heart failure. *Nature Reviews Cardiology*, *17*(5), 269–285. https://doi.org/10.1038/s41569-019-0315-x

Aida, K., Kobayashi, T., Takeshita, A., Jimbo, E., Nishida, Y., Yagihashi, S., Hosoi, M., Fukui, T., Sugawara, A., & Takasawa, S. (2018). Crucial role of Reg I from acinar-like cell cluster touching with islets (ATLANTIS) on mitogenesis of beta cells in EMC virus-induced diabetic mice. *Biochemical and Biophysical Resarch Communications*, *503*(6), 963–969. https://doi.org/10.1016/j.bbrc.2018.06.103

Alam, A., Blanc, I., Gueguen-Dorbes, G., Duclos, O., Bonnin, J., Barron, P., Laplace, M. C., Morin, G., Gaujarengues, F., Dol, F., Hérault, J. P., Schaeffer, P., Savi, P., & Bono, F. (2012). SAR131675, a potent and selective VEGFR-3-TK inhibitor with antilymphangiogenic, antitumoral, and antimetastatic activities. *Molecular Cancer Therapeutics*, *11*(8), 1637–1649. https://doi.org/10.1158/1535-7163.MCT-11-0866-T

Antila, S., Karaman, S., Nurmi, H., Airavaara, M., Voutilainen, M. H., Mathivet, T., Chilov, D., Li, Z., Koppinen, T., Park, J. H., Fang, S., Aspelund, A., Saarma, M., Eichmann, A., Thomas, J. L., & Alitalo, K. (2017). Development and plasticity of meningeal lymphatic vessels. *Journal of Experimental Medicine*, *214*(12), 3645–3667. https://doi.org/10.1084/jem.20170391

Anzai, A., Choi, J. L., He, S., Fenn, A. M., Nairz, M., Rattik, S., McAlpine, C. S., Mindur, J. E., Chan, C. T., Iwamoto, Y., Tricot, B., Wojtkiewicz, G. R., Weissleder, R., Libby, P., Nahrendorf, M., Stone, J. R., Becher, B., & Swirski, F. K. (2017). The infarcted myocardium solicits GM-CSF for the detrimental oversupply of inflammatory leukocytes. *Journal of Experimental Medicine*, *214*(11), 3293–3310. https://doi.org/10.1084/jem.20170689

Aspelund, A., Robciuc, M. R., Karaman, S., Makinen, T., & Alitalo, K. (2016). Lymphatic System in Cardiovascular Medicine. *Circulation Research*, *118*(3), 515–530. https://doi.org/10.1161/CIRCRESAHA.115.306544

Aspelund, A., Tammela, T., Antila, S., Nurmi, H., Leppänen, V. M., Zarkada, G., Stanczuk, L., Francois, M., Mäkinen, T., Saharinen, P., Immonen, I., & Alitalo, K. (2014). The Schlemm's canal is a VEGF-C/VEGFR-3-responsive lymphatic-like vessel. *Journal of*

Clinical Investigation, *124*(9), 3975–3986. https://doi.org/10.1172/JCI75395

Azevedo, P. S., Polegato, B. F., Minicucci, M. F., Paiva, S. A. R., & Zornoff, L. A. M. (2016). Cardiac Remodeling: Concepts, Clinical Impact, Pathophysiological Mechanisms and Pharmacologic Treatment. *Arquivos Brasileiros de Cardiologia*, *106*(1), 62–69. https://doi.org/10.5935/abc.20160005

Bajpai, G., Bredemeyer, A., Li, W., Zaitsev, K., Koenig, A. L., Lokshina, I. ;, Mohan, J. ;, Ivey, B. H., His-Min;, Weinheimer, C. ;, Kovacs, A., Epelman, S. ;, Artyomov, M. ;, Kreisel, D., & Lavine, K. J. (2019). Tissue Resident CCR2− and CCR2+ Cardiac Macrophages Differentially Orchestrate Monocyte Recruitment and Fate Specification Following Myocardial Injury. *Circulation Research*, *124*(2), 263–278. https://doi.org/10.1161/CIRCRESAHA.118.314028

Baldwin, M. E., Halford, M. M., Roufail, S., Williams, R. A., Hibbs, M. L., Grail, D., Kubo, H., Stacker, S. A., & Achen, M. G. (2005). Vascular Endothelial Growth Factor D Is Dispensable for Development of the Lymphatic System. *Molecular and Cellular Biology*, *25*(6), 2441–2449. https://doi.org/10.1128/MCB.25.6.2441-2449.2005

Ballesteros, I., Rubio-Ponce, A., Genua, M., Lusito, E., Kwok, I., Fernández-Calvo, G., Khoyratty, T. E., van Grinsven, E., González-Hernández, S., Nicolás-Ávila, J. Á., Vicanolo, T., Maccataio, A., Benguría, A., Li, J. L. Y., Adrover, J. M., Aroca-Crevillen, A., Quintana, J. A., Martín-Salamanca, S., Mayo, F., … Hidalgo, A. (2020). Co-option of Neutrophil Fates by Tissue Environments. *Cell*, *183*(5), 1282–1297. https://doi.org/10.1016/j.cell.2020.10.003

Beauvillain, C., Cunin, P., Doni, A., Scotet, M., Jaillon, S., Loiry, M. L., Magistrelli, G., Masternak, K., Chevailler, A., Delneste, Y., & Jeannin, P. (2011). CCR7 is involved in the migration of neutrophils to lymph nodes. *Blood*, *117*(4), 1196–1204. https://doi.org/10.1182/blood-2009-11-254490

Biswas, L., Chen, J., De Angelis, J., Zeng, F., Ramasamy, S. K., & Kusumbe Correspondence, A. P. (2023). Lymphatic vessels in bone support regeneration after injury. *Cell*, *186*, 382–397. https://doi.org/10.1016/j.cell.2022.12.031

Bizou, M., Itier, R., Majdoubi, M., Abbadi, D., Pichery, E., Dutaur, M., Marsal, D., Calise, D., Garmy-Susini, B., Douin-Echinard, V., Roncalli, J., Parini, A., & Pizzinat, N. (2021). Cardiac macrophage subsets differentially regulate lymphatic network remodeling during pressure overload. *Scientific Reports*, *11*(16801), 1–19. https://doi.org/10.1038/s41598-021-95723-y

Bolger, A. M., Lohse, M., & Usadel, B. (2014). Trimmomatic: A flexible trimmer for Illumina sequence data. *Bioinformatics*, *30*(15), 2114–2120.

https://doi.org/10.1093/bioinformatics/btu170

Brakenhielm, E., & Alitalo, K. (2019). Cardiac lymphatics in health and disease. *Nature Reviews Cardiology*, *16*(10), 56–68. https://doi.org/10.1038/s41569-018-0087-8

Brakenhielm, E., González, A., & Díez, J. (2020). Role of Cardiac Lymphatics in Myocardial Edema and Fibrosis: JACC Review Topic of the Week. In *Journal of the American College of Cardiology* (Vol. 76, Issue 6, pp. 735–744). Elsevier USA. https://doi.org/10.1016/j.jacc.2020.05.076

Carpenter, B. J., Lecacheur, M., Mangold, Y. N., & Cui, K. (2023). NAD + controls circadian rhythmicity during cardiac aging NAD + controls circadian rhythmicity during cardiac aging. *BioRxiv*, *N/A*(11), 1–17.

Casanova-Acebes, M., Pitaval, C., Weiss, L. A., sar Nombela-Arrieta, C., Chè vre, R., A-Gonzá lez, N., Kunisaki, Y., Zhang, D., van Rooijen, N., Silberstein, L. E., Weber, C., Nagasawa, T., Frenette, P. S., Castrillo, A., & Hidalgo, A. (2013). Rhythmic Modulation of the Hematopoietic Niche through Neutrophil Clearance. *Cell*, *153*(5), 1025–1035. https://doi.org/10.1016/j.cell.2013.04.040

Casanova-Acebes, M., Nicolás-Ávila, J. A., Yao Li, J. L., García-Silva, S., Balachander, A., Rubio-Ponce, A., Weiss, L. A., Adrover, J. M., Burrows, K., A-González, N., Ballesteros, I., Devi, S., Quintana, J. A., Crainiciuc, G., Leiva, M., Gunzer, M., Weber, C., Nagasawa, T., Soehnlein, O., … Hidalgo, A. (2018). Neutrophils instruct homeostatic and pathological states in naive tissues. *Journal of Experimental Medicine*, *215*(11), 2778–2795. https://doi.org/10.1084/jem.20181468

Chen, X., Lv, Y., Zhao, D., Zhang, L., Zheng, F., Yang, J.-Y., Li, X., Wang, L., Guo, L.-Y., Pan, Y., Yan, Y., Chen, S.-Y., Wang, J.-N., Tang, J.-M., & Wan, Y. (2016). Vascular endothelial growth factor-C protects heart from ischemia/reperfusion injury by inhibiting cardiomyocyte apoptosis. *Molecular and Cellular Biochemistry*, *413*(7), 9–23. https://doi.org/10.1007/s11010-015-2622-9

Chen, Z., Downing, S., & Tzanakakis, E. S. (2019). Four Decades After the Discovery of Regenerating Islet-Derived (Reg) Proteins: Current Understanding and Challenges. *Frontiers in Cell and Developmental Biology*, *7*(10), 1–16. https://doi.org/10.3389/fcell.2019.00235

Chiba, Y., Mizoguchi, I., Hasegawa, H., Ohashi, M., Orii, N., Nagai, T., Sugahara, M., Miyamoto, Y., Xu, M., Owaki, T., & Yoshimoto, T. (2018). Regulation of myelopoiesis by proinflammatory cytokines in infectious diseases. *Cellular and Molecular Life Sciences*, *75*(8), 1363–1376. https://doi.org/10.1007/s00018-017-2724-5

Choo, E. H., Lee, J. H., Park, E. H., Park, H. E., Jung, N. C., Kim, T. H., Koh, Y. S., Kim, E., Seung, K. B., Park, C., Hong, K. S., Kang, K., Song, J. Y., Seo, H. G., Lim, D. S., & Chang, K. (2017). Infarcted Myocardium-Primed Dendritic Cells Improve Remodeling and Cardiac Function after Myocardial Infarction by Modulating the Regulatory T Cell and Macrophage Polarization. *Circulation*, *135*(15), 1444–1457. https://doi.org/10.1161/CIRCULATIONAHA.116.023106

Cohn, J. N., Ferrari, R., & Sharpe, N. (2000). Cardiac remodeling-concepts and clinical implications: A consensus paper from an International Forum on Cardiac Remodeling. *Journal of the American College of Cardiology*, *35*(3), 569–582. https://doi.org/10.1016/S0735-1097(99)00630-0

Daseke, M. J., Chalise, U., Becirovic-Agic, M., Salomon, J. D., Cook, L. M., Case, A. J., & Lindsey, M. L. (2021). Neutrophil signaling during myocardial infarction wound repair. *Cellular Signalling*, *77*(1), 1–14. https://doi.org/10.1016/j.cellsig.2020.109816

Davies, L. C., Rosas, M., Jenkins, S. J., Liao, C. Te, Scurr, M. J., Brombacher, F., Fraser, D. J., Allen, J. E., Jones, S. A., & Taylor, P. R. (2013). Distinct bone marrow-derived and tissue-resident macrophage lineages proliferate at key stages during inflammation. *Nature Communications*, *4*(1886), 1–7. https://doi.org/10.1038/ncomms2877

De Caro, A., Lohse, J., & Sarles, H. (1979). Characterization of a protein isolated from pancreatic calculi of men suffering from chronic calcifying pancreatitis. *Biochemical and Biophysical Research Communications*, *87*(4), 1176–1182. https://doi.org/10.1016/S0006-291X(79)80031-5

Detzer, J. (2020). *Reg3beta restricts the spatiotemporal accumulation of neutrophil granulocytes within the ischemic heart*. Justus-Liebig-Universität Giessen.

Dick, S. A., Macklin, J. A., Nejat, S., Momen, A., Clemente-Casares, X., Althagafi, M. G., Chen, J., Kantores, C., Hosseinzadeh, S., Aronoff, L., Wong, A., Zaman, R., Barbu, I., Besla, R., Lavine, K. J., Razani, B., Ginhoux, F., Husain, M., Cybulsky, M. I., … Epelman, S. (2019). Self-renewing resident cardiac macrophages limit adverse remodeling following myocardial infarction. *Nature Immunology*, *20*(1), 29–39. https://doi.org/10.1038/s41590-018-0272-2

Dobin, A., Davis, C. A., Schlesinger, F., Drenkow, J., Zaleski, C., Jha, S., Batut, P., Chaisson, M., & Gingeras, T. R. (2013). STAR: Ultrafast universal RNA-seq aligner. *Bioinformatics*, *29*(1), 15–21. https://doi.org/10.1093/bioinformatics/bts635

Dutta, P., & Nahrendorf, M. (2015). Monocytes in Myocardial Infarction. *ATVB*, *35*(5), 1066–1070. https://doi.org/10.1161/ATVBAHA.114.304652

Dutta, P., Sager, H. B., Stengel, K. R., Naxerova, K., Courties, G., Saez, B., Silberstein, L., Heidt, T., Sebas, M., Sun, Y., Wojtkiewicz, G., Feruglio, P. F., King, K., Baker, J. N., Van Der Laan, A. M., Borodovsky, A., Fitzgerald, K., Hulsmans, M., Hoyer, F., … Nahrendorf, M. (2015). Myocardial infarction activates CCR2+ hematopoietic stem and progenitor cells. *Cell Stem Cell*, *16*(5), 477–487. https://doi.org/10.1016/j.stem.2015.04.008

Eash, K. J., Means, J. M., White, D. W., & Link, D. C. (2009). CXCR4 is a key regulator of neutrophil release from the bone marrow under basal and stress granulopoiesis conditions. *Blood*, *113*(19), 4711–4719. https://doi.org/10.1182/blood-2008- 09-177287

Epelman, S., Lavine, K. J., Beaudin, A. E., Sojka, D. K., Carrero, J. A., Calderon, B., Brija, T., Gautier, E. L., Ivanov, S., Satpathy, A. T., Schilling, J. D., Schwendener, R., Sergin, I., Razani, B., Forsberg, E. C., Yokoyama, W. M., Unanue, E. R., Colonna, M., Randolph, G. J., & Mann, D. L. (2014). *Embryonic and Adult-Derived Resident Cardiac Macrophages Are Maintained through Distinct Mechanisms at Steady State and during Inflammation*. https://doi.org/10.1016/j.immuni.2013.11.019

Evrard, M., Kwok, I. W. H., Chong, S. Z., Teng, K. W. W., Becht, E., Chen, J., Sieow, J. L., Penny, H. L., Ching, G. C., Devi, S., Adrover, J. M., Li, J. L. Y., Liong, K. H., Tan, L., Poon, Z., Foo, S., Chua, J. W., Su, I. H., Balabanian, K., … Ng, L. G. (2018). Developmental Analysis of Bone Marrow Neutrophils Reveals Populations Specialized in Expansion, Trafficking, and Effector Functions. *Immunity*, *48*(2), 364-379.e8. https://doi.org/10.1016/j.immuni.2018.02.002

Farnsworth, R. H., Karnezis, T., Maciburko, S. J., Mueller, S. N., & Stacker, S. A. (2019). The Interplay Between Lymphatic Vessels and Chemokines. *Frontiers in Immunology*, *10*(4), 1–14. https://doi.org/10.3389/fimmu.2019.00518

Ferrara, N., Houck, K., Jakeman, L., & Leung, D. W. (1992). Molecular and Biological Properties of the Vascular Endothelial Growth Factor Family of Proteins. *Endocrine Reviews*, *13*(1), 18–32. https://doi.org/10.1210/EDRV-13-1-18

Forte, E., Bastos Furtado, M., & Rosenthal, N. (2018). The interstitium in cardiac repair: role of the immune–stromal cell interplay. *Nature Reviews Cardiology*, *15*, 601–616. https://doi.org/10.1038/s41569-018-0077-x

Frangogiannis, N. G. (2012). Regulation of the inflammatory response in cardiac repair. *Circulation Research*, *110*(1), 159–173. https://doi.org/10.1161/CIRCRESAHA.111.243162

Frangogiannis, N. G. (2014). The inflammatory response in myocardial injury, repair, and

remodelling. *Nature Publishing Group*, *11*(5), 255–265. https://doi.org/10.1038/nrcardio.2014.28

Frangogiannis, N. G. (2018). Cell biological mechanisms in regulation of the post-infarction inflammatory response. *Current Opinion in Physiology*, *1*(10), 7–13. https://doi.org/10.1016/j.cophys.2017.09.001

Frantz, S., Hundertmark, M. J., Schulz-Menger, J., Bengel, F. M., & Bauersachs, J. (2022). Left ventricular remodelling post-myocardial infarction: pathophysiology, imaging, and novel therapies. *European Heart Journal*, *43*(27), 2549–2561. https://doi.org/10.1093/eurheartj/ehac223

Glinton, K. E., Ma, W., Lantz, C., Grigoryeva, L. S., DeBerge, M., Liu, X., Febbraio, M., Kahn, M., Oliver, G., & Thorp, E. B. (2022). Macrophage-produced VEGFC is induced by efferocytosis to ameliorate cardiac injury and inflammation. *Journal of Clinical Investigation*, *132*(9), 1–14. https://doi.org/10.1172/JCI140685

Haiko, P., Makinen, T., Keskitalo, S., Taipale, J., Karkkainen, M. J., Baldwin, M. E., Stacker, S. A., Achen, M. G., & Alitalo, K. (2008). Deletion of Vascular Endothelial Growth Factor C (VEGF-C) and VEGF-D Is Not Equivalent to VEGF Receptor 3 Deletion in Mouse Embryos. *Molecular and Cellular Biology*, *28*(15), 4843–4850. https://doi.org/10.1128/mcb.02214-07

Halade, G. V, & Lee, D. H. (2022). Inflammation and resolution signaling in cardiac repair and heart failure. *EBioMedicine*, *79*(5), 1–9. https://doi.org/10.1016/j

Hamada, K., Oike, Y., Takakura, N., Ito, Y., Jussila, L., Dumont, D. J., Alitalo, K., & Suda, T. (2000). VEGF-C signaling pathways through VEGFR-2 and VEGFR-3 in vasculoangiogenesis and hematopoiesis. *Blood*, *96*(12), 3793–3801.

Hampton, H. R., & Chtanova, T. (2019). Lymphatic migration of immune cells. *Frontiers in Immunology*, *10*(5), 1–10. https://doi.org/10.3389/fimmu.2019.01168

Harris, N. R., Bálint, L. Ó., Dy, D. M., Nielsen, N. R., Méendez, H. G., Aghajanian, A., & Caron, K. M. (2023). THE EBB AND FLOW OF CARDIAC LYMPHATICS: A TIDAL WAVE OF NEW DISCOVERIES. In *Physiological Reviews* (Vol. 103, Issue 1, pp. 391–432). American Physiological Society. https://doi.org/10.1152/physrev.00052.2021

Harris, N. R., Nielsen, N. R., Pawlak, J. B., Aghajanian, A., Rangarajan, K., Serafin, D. S., Farber, G., Dy, D. M., Nelson-Maney, N. P., Xu, W., Ratra, D., Hurr, S. H., Qian, L., Scallan, J. P., & Caron, K. M. (2022). VE-Cadherin Is Required for Cardiac Lymphatic Maintenance and Signaling. *Circulation Research*, *130*(1), 5–23.

https://doi.org/10.1161/CIRCRESAHA.121.318852

Hellenthal, K. E. M., Brabenec, L., & Wagner, N. M. (2022). Regulation and Dysregulation of Endothelial Permeability during Systemic Inflammation. *Cells*, *11*(12), 1–21. https://doi.org/10.3390/cells11121935

Henri, O., Pouehe, C., Houssari, M., Galas, L., Nicol, L., Edwards-Lévy, F., Henry, J. P., Dumesnil, A., Boukhalfa, I., Banquet, S., Schapman, D., Thuillez, C., Richard, V., Mulder, P., & Brakenhielm, E. (2016). Selective Stimulation of Cardiac Lymphangiogenesis Reduces Myocardial Edema and Fibrosis Leading to Improved Cardiac Function Following Myocardial Infarction. *Circulation*, *133*(15), 1484–1497. https://doi.org/10.1161/CIRCULATIONAHA.115.020143

Heron, C., Dumesnil, A., Houssari, M., Renet, S., Lebon, A., Godefroy, D., Schapman, D., Henri, O., Riou, G., Nicol, L., Henry, J., Pieronne-Deperrois, M., Ouvrard-Pascaud, A., Hägerling, R., Chiavelli, H., Michel, J., Mulder, P., Fraineau, S., Richard, V., … Brakenhielm, E. (2022). Regulation and impact of cardiac lymphangiogenesis in pressure-overload-induced heart failure. *Cardiovascular Research*, *00*(5), 1–14. https://doi.org/10.1101/2021.04.27.441616

Hou, W.-R., Xie, S.-N., Wang, H.-J., Su, Y.-Y., Lu, J.-L., Li, L.-L., Zhang, S.-S., & Xiang, M. (2011). Intramuscular delivery of a naked DNA plasmid encoding proinsulin and pancreatic regenerating III protein ameliorates type 1 diabetes mellitus. *Pharmacological Research*, *63*(12), 320–327. https://doi.org/10.1016/j.phrs.2010.12.009

Houssari, M., Dumesnil, A., Tardif, V., Kivelä, R., Pizzinat, N., Boukhalfa, I., Godefroy, D., Schapman, D., Hemanthakumar, K. A., Bizou, M., Henry, J. P., Renet, S., Riou, G., Rondeaux, J., Anouar, Y., Adriouch, S., Fraineau, S., Alitalo, K., Richard, V., … Brakenhielm, E. (2020). Lymphatic and Immune Cell Cross-Talk Regulates Cardiac Recovery after Experimental Myocardial Infarction. *Arteriosclerosis, Thrombosis, and Vascular Biology*, *40*(7), 1722–1737. https://doi.org/10.1161/ATVBAHA.120.314370

Hu, D., Li, L., Li, S., Wu, M., Ge, N., Cui, Y., Lian, Z., Song, J., & Chen, H. (2019). Lymphatic system identification, pathophysiology and therapy in the cardiovascular diseases. *Journal of Molecular and Cellular Cardiology*, *133*(6), 99–111. https://doi.org/10.1016/j.yjmcc.2019.06.002

Huang, L. H., Lavine, K. J., & Randolph, G. J. (2017). Cardiac Lymphatic Vessels, Transport, and Healing of the Infarcted Heart. *JACC: Basic to Translational Science*, *2*(4), 478–482. https://doi.org/10.1016/j.jacbts.2017.02.005

Ishikawa, Y., Akishima-Fukasawa, Y., Ito, K., Akasaka, Y., Tanaka, M., Shimokawa, R.,

Kimura-Matsumoto, M., Morita, H., Sato, S., Kamata, I., & Ishii, T. (2007). Lymphangiogenesis in myocardial remodelling after infarction. *Histopathology*, *51*(3), 345–353. https://doi.org/10.1111/j.1365-2559.2007.02785.x

Jackson, D. G. (2019). Leucocyte trafficking via the lymphatic vasculature-mechanisms and consequences. *Frontiers in Immunology*, *10*(3), 1–38. https://doi.org/10.3389/fimmu.2019.00471

Jahng, J. W. S., Song, E., & Sweeney, G. (2016). Crosstalk between the heart and peripheral organs in heart failure. *Experimental and Molecular Medicine*, *48*(3), 1–11. https://doi.org/10.1038/emm.2016.20

Jiang, S., He, Y., Brandt, J. H., Zhao, L., & Chen, J. (2023). Sensing Mechanism and Excited-State Dynamics of a Widely Used Intracellular Fluorescent pH Probe: pHrodo. *The Journal of Physical Chemistry Letters*, *14*(11), 10482–10488. https://doi.org/10.1021/acs.jpclett.3c02653

Jin, K., Gao, S., Yang, P., Guo, R., Li, D., Zhang, Y., Lu, X., Fan, G., & Fan, X. (2022). Single-Cell RNA Sequencing Reveals the Temporal Diversity and Dynamics of Cardiac Immunity after Myocardial Infarction. *Small Methods*, *6*(3), 1–15. https://doi.org/10.1002/smtd.202100752

Johnson, L. A., & Jackson, D. G. (2010). Inflammation-induced secretion of CCL21 in lymphatic endothelium is a key regulator of integrin-mediated dendritic cell transmigration. *International Immunology*, *22*(10), 839–849. https://doi.org/10.1093/intimm/dxq435

Joukov, V., Pajusola, K., Kaipainen, A., Chilov, D., Lahtinen, I., Kukk, E., Sakselal, O., Kalkkinen2, N., Alitaio3, K., Alitalo, K., & Eriksson, U. (1996). A novel vascular endothelial growth factor, VEGF-C, is a ligand for the Flt4 (VEGFR-3) and KDR (VEGFR-2) receptor tyrosine kinases. *The EMBO Journal*, *15*(2), 290–298. https://doi.org/https://doi.org/10.1002/j.1460-2075.1996.tb00359.x

Joukov, V., Sorsa, T., Kumar, V., Jeltsch, M., Claesson-Welsh, L., Cao, Y., Saksela, O., Kalkkinen, N., & Alitalo, K. (1997). Proteolytic processing regulates receptor specificity and activity of VEGF-C. *EMBO Journal*, *16*(13), 3898–3911. https://doi.org/10.1093/emboj/16.13.3898

Kain, V., & Halade, G. V. (2020). Role of Neutrophils in Ischemic Heart Failure. *Pharmacol. Ther.*, *205*(1), 1–22. https://doi.org/10.1016/j.pharmthera.2019.107424

Kapellos, T. S., Taylor, L., Lee, H., Cowley, S. A., James, W. S., Iqbal, A. J., & Greaves, D. R. (2016). A novel real time imaging platform to quantify macrophage phagocytosis.

Biochemical Pharmacology, *116*(7), 107–119. https://doi.org/10.1016/j.bcp.2016.07.011

Karaman, S., Nurmi, H., Antila, S., & Alitalo, K. (2013). Stimulation and Inhibition of Lymphangiogenesis Via Adeno-Associated Viral Gene Delivery. In *Lymphangiogenesis: Methods and Protocols* (Vol. 1846, pp. 1–32). https://doi.org/10.1016/B978-1-4160-3106-2.00019-2

Kataru, R. P., Jung, K., Jang, C., Yang, H., Schwendener, R. A., Baik, J. E., Han, S. H., Alitalo, K., & Koh, G. Y. (2009). Critical role of CD11b macrophages and VEGF in inflammatory lymphangiogenesis, antigen clearance, and inflammation resolution. *Blood*, *113*(22), 5650–5655. https://doi.org/10.1182/blood-2008-09-176776

Keller, T. C. S., Lim, L., Shewale, S. V., McDaid, K., Martí-Pàmies, Í., Tang, A. T., Wittig, C., Guerrero, A. A., Sterling, S., Leu, N. A., Scherrer-Crosbie, M., Gimotty, P. A., & Kahn, M. L. (2021). Genetic blockade of lymphangiogenesis does not impair cardiac function after myocardial infarction. *Journal of Clinical Investigation*, *131*(20), 1–10. https://doi.org/10.1172/jci147070

Khan, M. A., Hashim, M. J., Mustafa, H., Baniyas, M. Y., Al Suwaidi, S. K. B. M., AlKatheeri, R., Alblooshi, F. M. K., Almatrooshi, M. E. A. H., Alzaabi, M. E. H., Al Darmaki, R. S., & Lootah, S. N. A. H. (2020). Global Epidemiology of Ischemic Heart Disease: Results from the Global Burden of Disease Study. *Cureus*, *12*(7), 1–12. https://doi.org/10.7759/cureus.9349

Kilarski, W. W., Güç, E., Teo, J. C. M., Oliver, S. R., Lund, A. W., & Swartz, M. A. (2013). Intravital Immunofluorescence for Visualizing the Microcirculatory and Immune Microenvironments in the Mouse Ear Dermis. *PLoS ONE*, *8*(2), 1–6. https://doi.org/10.1371/journal.pone.0057135

Kirkin, V., Thiele, W., Baumann, P., Mazitschek, R., Rohde, K., Fellbrich, G., Weich, H., Waltenberger, J., Giannis, A., & Sleeman, J. P. (2004). MAZ51, an indolinone that inhibits endothelial cell and tumor cell growth in vitro, suppresses tumor growth in vivo. *International Journal of Cancer*, *112*(6), 986–993. https://doi.org/10.1002/ijc.20509

Klotz, L., Norman, S., Vieira, J. M., Masters, M., Rohling, M., Dubé, K. N., Bollini, S., Matsuzaki, F., Carr, C. A., & Riley, P. R. (2015). Cardiac lymphatics are heterogeneous in origin and respond to injury. *Nature*, *522*(7554), 62–67. https://doi.org/10.1038/nature14483

Kobayashi, D., Endo, M., Ochi, H., Hojo, H., Miyasaka, M., & Hayasaka, H. (2017). Regulation of CCR7-dependent cell migration through CCR7 homodimer formation. *Scientific Reports*, *7*(1), 1–14. https://doi.org/10.1038/s41598-017-09113-4

Kobayashi, K., Maeda, K., Takefuji, M., Kikuchi, R., Morishita, Y., Hirashima, M., & Murohara, T. (2017). Dynamics of angiogenesis in ischemic areas of the infarcted heart. *Scientific Reports*. https://doi.org/10.1038/s41598-017-07524-x

Kung, G. L., Vaseghi, M., Gahm, J. K., Shevtsov, J., Garfinkel, A., Shivkumar, K., & Ennis, D. B. (2018). Microstructural infarct border zone remodeling in the post-infarct swine heart measured by diffusion tensor MRI. *Frontiers in Physiology*, *9*(1–17). https://doi.org/10.3389/fphys.2018.00826

LaFonte, M. W., Stanek, A., Mueller, C., Zenilman, M. E., Sugawara, A., Alfonso, A. E., & Huan, C. (2013). Identification of Reg1 as a novel stellate cell activator in regenerating pancreas. *Journal of the American College of Surgeons*, *217*(3), S18. https://doi.org/10.1016/J.JAMCOLLSURG.2013.07.025

Lafuse, W. P., Wozniak, D. J., & Rajaram, M. V. S. (2021). Role of cardiac macrophages on cardiac inflammation, fibrosis and tissue repair. *Cells*, *10*(51), 1–27. https://doi.org/10.3390/cells10010051

Laine, G. A., & Allen, S. J. (1991). Left ventricular myocardial edema. Lymph flow, interstitial fibrosis, and cardiac function. *Circulation Research*, *68*(6), 1713–1721. https://doi.org/10.1161/01.RES.68.6.1713

Lê, S., Josse, J., & Husson, F. (2008). FactoMineR: An R Package for Multivariate Analysis. *Journal of Statistical Software*, *25*(1), 1–18. https://doi.org/10.1016/j.envint.2008.06.007

Leancă, S. A., Crișu, D., Petriș, A. O., Afrăsânie, I., Genes, A., Costache, A. D., Tesloianu, D. N., & Costache, I. I. (2022). Left Ventricular Remodeling after Myocardial Infarction: From Physiopathology to Treatment. *Life*, *12*(8), 1111. https://doi.org/10.3390/life12081111

Lehotzkya, R. E., Partchb, C. L., Mukherjeea, S., Casha, H. L., Goldman, W. E., Gardner, K. H., & Hooper, L. V. (2010). Molecular basis for peptidoglycan recognition by a bactericidal lectin. *Proceedings of the National Academy of Sciences of the United States of America*, *107*(17), 7722–7727. https://doi.org/10.1073/pnas.0909449107

Levick, J. R., & Michel, C. C. (2010). Microvascular fluid exchange and the revised Starling principle. *Cardiovascular Research*, *87*(2), 198–210. https://doi.org/10.1093/cvr/cvq062

Li, B., Wang, X., & Liu, J. L. (2010). Pancreatic acinar-specific overexpression of Reg2 gene offered no protection against either experimental diabetes or pancreatitis in mice. *American Journal of Physiology - Gastrointestinal and Liver Physiology*, *299*(2), 413–

421. https://doi.org/10.1152/AJPGI.00500.2009

Li, Q., Wang, H., Zogopoulos, G., Shao, Q., Dong, K., Lv, F., Nwilati, K., Gui, X.-Y., Cuggia, A., Liu, J.-L., & Gao, Z.-H. (2016). Reg proteins promote acinar-to-ductal metaplasia and act as novel diagnostic and prognostic markers in pancreatic ductal adenocarcinoma Qing. *Oncotarget*, *7*(47), 77838–77835. https://doi.org/10.18632/oncotarget.12834

Li, Y. H., Zhang, Y., Pan, G., Xiang, L. X., Luo, D. C., & Shao, J. Z. (2022). Occurrences and Functions of Ly6Chi and Ly6Clo Macrophages in Health and Disease. *Frontiers in Immunology*, *13*(5), 1–9. https://doi.org/10.3389/fimmu.2022.901672

Li, Y., Li, Q., & Fan, G. C. (2021). Macrophage efferocytosis in cardiac pathophysiology and repair. In *Shock* (Vol. 55, Issue 2, pp. 177–188). Lippincott Williams and Wilkins. https://doi.org/10.1097/SHK.0000000000001625

Liao, S., & Von Der Weid, P. Y. (2014). Inflammation-induced lymphangiogenesis and lymphatic dysfunction. *Angiogenesis*, *17*(2), 325–334. https://doi.org/10.1007/s10456-014-9416-7

Liao, Y., Smyth, G. K., & Shi, W. (2014). FeatureCounts: An efficient general purpose program for assigning sequence reads to genomic features. *Bioinformatics*, *30*(7), 923–930. https://doi.org/10.1093/bioinformatics/btt656

Libby, P., Nahrendorf, M., & Swirski, F. K. (2016). Leukocytes link local and systemic inflammation in ischemic cardiovascular disease an expanded cardiovascular continuum. *Journal of the American College of Cardiology*, *67*(9), 1091–1103. https://doi.org/10.1016/j.jacc.2015.12.048

Lieu, H.-T., Simon, M.-T., Nguyen-Khoa, T., Kebede, M., Cortes, A., Tebar, L., Smith, A. J. H., Bayne, R., Hunt, S. P., Bréchot, C., & Christa, L. (2006). Reg2 Inactivation Increases Sensitivity to Fas Hepatotoxicity and Delays Liver Regeneration Post-hepatectomy in Mice. *Hepatology*, *44*(6), 1452–1464. https://doi.org/10.1002/hep.21434

Lörchner, H., Cañes Esteve, L., Góes, M. E., Harzenetter, R., Brachmann, N., Gajawada, P., Günther, S., Doll, N., Pöling, J., & Braun, T. (2023). Neutrophils for Revascularization Require Activation of CCR6 and CCL20 by TNFα. *Circulation Research*, *133*(7), 592–610. https://doi.org/10.1161/CIRCRESAHA.123.323071

Lörchner, H., Hou, Y., Adrian-Segarra, J. M., Kulhei, J., Detzer, J., Gü nther, S., Gajawada, P., Warnecke, H., Niessen, H. W., Pö ling, J., & Braun, T. (2018). Reg proteins direct accumulation of functionally distinct macrophage subsets after myocardial infarction.

Cardiovascular Research, *114*(10), 1667–1679. https://doi.org/10.1093/cvr/cvy126

Lörchner, H., Pöling, J., Gajawada, P., Hou, Y., Polyakova, V., Kostin, S., Adrian-Segarra, J. M., Boettger, T., Wietelmann, A., Warnecke, H., Richter, M., Kubin, T., & Braun, T. (2015). Myocardial healing requires Reg3β-dependent accumulation of macrophages in the ischemic heart. *Nature Medicine*, *21*(4), 353–362. https://doi.org/10.1038/nm.3816

Lörchner, H., Widera, C., Hou, Y., Elsässer, A., Warnecke, H., Giannitsis, E., Hulot, J. S., Braun, T., Wollert, K. C., & Pöling, J. (2018). Reg3β is associated with cardiac inflammation and provides prognostic information in patients with acute coronary syndrome. *International Journal of Cardiology*, *258*(5), 7–13. https://doi.org/10.1016/j.ijcard.2018.01.043

Loukas, M., Shah, S., Bhusnurmath, S., Bhusnurmath, B. S., & Tubbs R. S. (2013). A General Outline of the Cardiac Lymphatic System. In *The Cardiac Lymphatic System: An Overview* (pp. 3–15). https://doi.org/10.1007/978-1-4614-6774-8_1

Love, M. I., Huber, W., & Anders, S. (2014). Moderated estimation of fold change and dispersion for RNA-seq data with DESeq2. *Genome Biology*, *15*(12), 1–21. https://doi.org/10.1186/s13059-014-0550-8

Luengo-Fernandez, R., Walli-Attaei, M., Gray, A., Torbica, A., Maggioni, A. P., Huculeci, R., Bairami, F., Aboyans, V., Timmis, A. D., Vardas, P., & Leal, J. (2023). Economic burden of cardiovascular diseases in the European Union: a population-based cost study. *European Heart Journal*, *44*(45), 4752–4767. https://doi.org/10.1093/eurheartj/ehad583

Ma, Y. (2021). Role of neutrophils in cardiac injury and repair following myocardial infarction. *Cells*, *10*(7), 1–17. https://doi.org/10.3390/cells10071676

Martin, C., Burdon, P. C. E., Bridger, G., Gutierrez-Ramos, J.-C., Williams, T. J., & Rankin, S. M. (2003). Chemokines Acting via CXCR2 and CXCR4 Control the Release of Neutrophils from the Bone Marrow and Their Return following Senescence. *Immunity*, *19*(10), 583–593. https://doi.org/10.1016/s1074-7613(03)00263-2

Martini, E., Kunderfranco, P., Peano, C., Carullo, P., Cremonesi, M., Schorn, T., Carriero, R., Termanini, A., Colombo, F. S., Jachetti, E., Panico, C., Faggian, G., Fumero, A., Torracca, L., Molgora, M., Cibella, J., Pagiatakis, C., Brummelman, J., Alvisi, G., … Kallikourdis, M. (2019). Single-Cell Sequencing of Mouse Heart Immune Infiltrate in Pressure Overload-Driven Heart Failure Reveals Extent of Immune Activation. *Circulation*, *140*(25), 2089–2107. https://doi.org/10.1161/CIRCULATIONAHA.119.041694

Mass, E., Nimmerjahn, F., Kierdorf, K., & Schlitzer, A. (2023). Tissue-specific macrophages: how they develop and choreograph tissue biology. *Nature Reviews Immunology*, *23*(9), 563–579. https://doi.org/10.1038/s41577-023-00848-y

Mathias, J. R., Perrin, B. J., Liu, T.-X., Kanki, J., Look, A. T., & Huttenlocher, A. (2006). Resolution of inflammation by retrograde chemotaxis of neutrophils in transgenic zebrafish. *Journal of Leukocyte Biology*, *80*(6), 1281–1288. https://doi.org/10.1189/jlb.0506346

Mehta, H. M., & Corey, S. J. (2021). G-CSF, the guardian of granulopoiesis. *Seminars in Immunology*, *54*(10), 101515. https://doi.org/10.1016/j.smim.2021.101515

Miao, R., Lim, V. Y., Kothapalli, N., Ma, Y., Fossati, J., Zehentmeier, S., Sun, R., & Pereira, J. P. (2020). Hematopoietic Stem Cell Niches and Signals Controlling Immune Cell Development and Maintenance of Immunological Memory. *Frontiers in Immunology*, *11*(11), 1–13. https://doi.org/10.3389/fimmu.2020.600127

Mitroulis, I., Kalafati, L., Bornhäuser, M., Hajishengallis, G., & Chavakis, T. (2020). Regulation of the Bone Marrow Niche by Inflammation. *Frontiers in Immunology*, *11*(7), 1–8. https://doi.org/10.3389/fimmu.2020.01540

Moskalik, A., Niderla-Bielińska, J., & Ratajska, A. (2022). Multiple roles of cardiac macrophages in heart homeostasis and failure. *Heart Failure Reviews*, *27*(4), 1413–1430. https://doi.org/10.1007/s10741-021-10156-z

Mozaffarian, D., Benjamin, E. J., Go, A. S., Arnett, D. K., Blaha, M. J., Cushman, M., Das, S. R., Ferranti, S. De, Després, J. P., Fullerton, H. J., Howard, V. J., Huffman, M. D., Isasi, C. R., Jiménez, M. C., Judd, S. E., Kissela, B. M., Lichtman, J. H., Lisabeth, L. D., Liu, S., … Turner, M. B. (2016). Heart disease and stroke statistics-2016 update a report from the American Heart Association. *Circulation*, *133*(4), e38–e48. https://doi.org/10.1161/CIR.0000000000000350

Mozaffarian, S., Etemad, K., Aghaali, M., Khodakarim, S., Ghorbani, S. S., & Nazari, S. S. H. (2021). Short and long-term survival rates following myocardial infarction and its predictive factors: A study using national registry data. *The Journal of Tehran University Heart Center*, *16*(2), 68–74. https://doi.org/10.18502/jthc.v16i2.7387

Mozaffarian, S., Etemad, K., Aghaali, M., Khodakarim, S., Ghorbani, S. S., Saeed, S., Nazari, H., & Article, O. (2021). Its Predictive Factors: A Study Using National Registry Data. *The Journal of Tehran University Heart Center*, *16*(2), 68–74. http://jthc.tums.ac.ir

Mukherjee, S., Zheng, H., Derebe, M. G., Callenberg, K. M., Partch, C. L., Rollins, D., Propheter, D. C., Rizo, J., Grabe, M., Jiang, Q. X., & Hooper, L. V. (2014). Antibacterial

membrane attack by a pore-forming intestinal C-type lectin. *Nature*, *505*(7481), 103–107. https://doi.org/10.1038/nature12729

Namikawa, K., Fukushima, M., Murakami, K., Suzuki, A., Takasawa, S., Okamoto, H., & Kiyama, H. (2005). Expression of Reg/PAP family members during motor nerve regeneration in rat. *Biochemical and Biophysical Resarch Communications*, *332*(4), 126–134. https://doi.org/10.1016/j.bbrc.2005.04.105

Namikawa, K., Okamoto, T., Suzuki, A., Konishi, H., & Kiyama, H. (2006). Development/Plasticity/Repair Pancreatitis-Associated Protein-III Is a Novel Macrophage Chemoattractant Implicated in Nerve Regeneration. *The Journal of Neuroscience*, *26*(28), 7460–7467. https://doi.org/10.1523/JNEUROSCI.0023-06.2006

Olszewski, W. L. (2003). The lymphatic system in body homeostasis: physiological conditions. *Lymphatic Research and Biology*, *1*(1), 11–24. https://doi.org/10.1089/15396850360495655

Ortega-Gómez, A., Perretti, M., & Soehnlein, O. (2013). Resolution of inflammation: An integrated view. *EMBO Molecular Medicine*, *5*(5), 661–674. https://doi.org/10.1002/emmm.201202382

Overbeeke, C., Tak, T., & Koenderman, L. (2022). The journey of neutropoiesis: how complex landscapes in bone marrow guide continuous neutrophil lineage determination. *Blood*, *139*(15), 2285–2293. https://doi.org/10.1182/blood.2021012835

Palasubramaniam, J., Wang, X., & Peter, K. (2019). Myocardial Infarction - From Atherosclerosis to Thrombosis: Uncovering New Diagnostic and Therapeutic Approaches. *Arteriosclerosis, Thrombosis, and Vascular Biology*, *39*(8), E176–E185. https://doi.org/10.1161/ATVBAHA.119.312578

Pandey, A. K., Singhi, E. K., Arroyo, J. P., Ikizler, T. A., Gould, E. R., Brown, J., Beckman, J. A., Harrison, D. G., & Moslehi, J. (2018). Mechanisms of VEGF (vascular endothelial growth factor) inhibitor-associated hypertension and vascular disease. *Hypertension*, *71*(2), E1–E8. https://doi.org/10.1161/HYPERTENSIONAHA.117.10271

Petrova, T. V, & Young Koh, G. (2020). Biological functions of lymphatic vessels. *Science*, *369*(6500), 1–11. https://doi.org/10.1126/science.aax4063

Poller, W. C., Nahrendorf, M., & Swirski, F. K. (2020). Hematopoiesis and Cardiovascular Disease. *Circulation Research*, *126*(8), 1061–1085. https://doi.org/10.1161/CIRCRESAHA.120.315895

Prabhu, S. D., & Frangogiannis, N. G. (2016). The biological basis for cardiac repair after myocardial infarction. *Circulation Research*, *119*(1), 91–112. https://doi.org/10.1161/CIRCRESAHA.116.303577

Puhl, S. L., & Steffens, S. (2019). Neutrophils in Post-myocardial Infarction Inflammation: Damage vs. Resolution? *Frontiers in Cardiovascular Medicine*, *6*(3), 1–9. https://doi.org/10.3389/fcvm.2019.00025

Ranjbaran, R., Abbasi, M., Rahimian, E., Dehbidi, G. R., Seyyedi, N., Zare, F., & Behzad-Behbahani, A. (2020). GDF-15 negatively regulates excess erythropoiesis and its overexpression is involved in erythroid hyperplasia. *Experimental Cell Research*, *397*(2), 112346. https://doi.org/10.1016/j.yexcr.2020.112346

Rexius-Hall, M. L., Khalil, N. N., Escopete, S. S., Li, X., Hu, J., Yuan, H., Parker, S. J., & McCain, M. L. (2022). A myocardial infarct border-zone-on-a-chip demonstrates distinct regulation of cardiac tissue function by an oxygen gradient. *Science Advances*, *8*(49), 1–16. https://doi.org/10.1126/sciadv.abn7097

Robertson, A. L., Holmes, G. R., Bojarczuk, A. N., Burgon, J., Loynes, C. A., Chimen, M., Sawtell, A. K., Hamza, B., Willson, J., Walmsley, S. R., Anderson, S. R., Coles, M. C., Farrow, S. N., Solari, R., Jones, S., Prince, L. R., Irimia, D., Ed Rainger, G., Kadirkamanathan, V., … Renshaw, S. A. (2014). A zebrafish compound screen reveals modulation of neutrophil reverse migration as an anti-inflammatory mechanism. *Science Translational Medicine*, *6*(225), 1–24. https://doi.org/10.1126/scitranslmed.3007672

Rockson, S. G. (2021). Advances in Lymphedema. *Circulation Research*, *128*(12), 2003–2016. https://doi.org/10.1161/CIRCRESAHA.121.318307

Rodríguez-Fernández, J. L., & Criado-García, O. (2020). The Chemokine Receptor CCR7 Uses Distinct Signaling Modules With Biased Functionality to Regulate Dendritic Cells. *Frontiers in Immunology*, *11*(4), 1–10. https://doi.org/10.3389/fimmu.2020.00528

Saaristo, A., Veikkola, T., Tammela, T., Enholm, B., Karkkainen, M. J., Pajusola, K., Bueler, H., Ylä-Herttuala, S., & Alitalo, K. (2002). Lymphangiogenic gene therapy with minimal blood vascular side effects. *Journal of Experimental Medicine*, *196*(6), 719–730. https://doi.org/10.1084/jem.20020587

Sager, H. B., Heidt, T., Hulsmans, M., Dutta, P., Courties, G., Sebas, M., Wojtkiewicz, G. R., Tricot, B., Iwamoto, Y., Sun, Y., Weissleder, R., Libby, P., Swirski, F. K., & Nahrendorf, M. (2015). Targeting interleukin-1β reduces leukocyte production after acute myocardial infarction. *Circulation*, *132*(20), 1880–1890. https://doi.org/10.1161/CIRCULATIONAHA.115.016160/-/DC1

Sager, H. B., Hulsmans, M., Lavine, K. J., Moreira, M. B., Heidt, T., Courties, G., Sun, Y., Iwamoto, Y., Tricot, B., Khan, O. F., Dahlman, J. E., Borodovsky, A., Fitzgerald, K., Anderson, D. G., Weissleder, R., Libby, P., Swirski, F. K., & Nahrendorf, M. (2016). Proliferation and Recruitment Contribute to Myocardial Macrophage Expansion in Chronic Heart Failure. *Circulation Research*, *119*(7), 853–864. https://doi.org/10.1161/CIRCRESAHA.116.309001/-/DC1

Sansonetti, M., Waleczek, F. J. G., Jung, M., Thum, T., & Perbellini, F. (2020). Resident cardiac macrophages: crucial modulators of cardiac (patho)physiology. *Basic Research in Cardiology*, *115*(6), 1–15. https://doi.org/10.1007/s00395-020-00836-6

Schwager, S., & Detmar, M. (2019). Inlammation and Lymphatic Function. *Front. Immunol*, *10*(308), 1–11. https://doi.org/10.3389/fimmu.2019.00308

Shalabi, F., Rossant, J., Yamaguchi, T. P., Gertseinstein, M., & Schuh, A. C. (1995). Failure of blood-island formation and vasculogenesis in Flk-1-deficient mice. *Nature*, *376*(7), 62–66.

Shimizu, Y., Polavarapu, R., Eskla, K.-L., Pantner, Y., Nicholson, C. K., Ishii, M., Brunnhoelzl, D., Mauria, R., Husain, A., Naqvi, N., Murohara, T., & Calvert, J. W. (2018). Impact of Lymphangiogenesis on Cardiac Remodeling After Ischemia and Reperfusion Injury. *Journal of the American Heart Association*, *7*(19), 1–14. https://doi.org/10.1161/JAHA.118.009565

Shirazi, L. F., Bissett, J., Romeo, F., & Mehta, J. L. (2017). Role of Inflammation in Heart Failure. *Current Atherosclerosis Reports*, *19*(27), 1–19. https://doi.org/10.1007/s11883-017-0660-3

Silvestre-Roig, C., Braster, Q., Ortega-Gomez, A., & Soehnlein, O. (2020). Neutrophils as regulators of cardiovascular inflammation. *Nature Reviews Cardiology*, *17*(6), 327–340. https://doi.org/10.1038/s41569-019-0326-7

Smolina, K., Wright, F. L., Rayner, M., & Goldacre, M. J. (2012). Long-term survival and recurrence after acute myocardial infarction in England, 2004 to 2010. *Circulation: Cardiovascular Quality and Outcomes*, *5*(4), 532–540. https://doi.org/10.1161/CIRCOUTCOMES.111.964700/-/DC1

Sreejit, G., Abdel-Latif, A., Athmanathan, B., Annabathula, R., Dhyani, A., Noothi, S. K., Quaife-Ryan, G. A., Al-Sharea, A., Pernes, G., Dragoljevic, D., Lal, H., Schroder, K., Hanaoka, B. Y., Raman, C., Grant, M. B., Hudson, J. E., Smyth, S. S., Porrello, E. R., Murphy, A. J., & Nagareddy, P. R. (2020). Neutrophil-derived S100A8/A9 amplify granulopoiesis after myocardial infarction. *Circulation*, *141*(3), 1080–1094. https://doi.org/10.1161/CIRCULATIONAHA.119.043833

Sreejit, G., Nooti, S. K., Jaggers, R. M., Athmanathan, B., Ho Park, K., Al-Sharea, A., Johnson, J., Dahdah, A., Lee, M. K. S., Ma, J., Murphy, A. J., & Nagareddy, P. R. (2022). Retention of the NLRP3 Inflammasome-Primed Neutrophils in the Bone Marrow Is Essential for Myocardial Infarction-Induced Granulopoiesis. *Circulation*, *145*(1), 31–44. https://doi.org/10.1161/CIRCULATIONAHA.121.056019

Sun, C., Wang, X., Hui, Y., Fukui, H., Wang, B., & Miwa, H. (2021). The potential role of REG family proteins in inflammatory and inflammation-associated diseases of the gastrointestinal tract. In *International Journal of Molecular Sciences* (Vol. 22, Issue 13, pp. 1–14). MDPI. https://doi.org/10.3390/ijms22137196

Sun, K., Li, Y.-Y., & Jin, J. (2021). A double-edged sword of immuno-microenvironment in cardiac homeostasis and injury repair. *Signal Transduction and Targeted Therapy*, *6*(79), 1–16. https://doi.org/10.1038/s41392-020-00455-6

Suratt, B. T., Petty, J. M., Young, S. K., Malcolm, K. C., Lieber, J. G., Nick, J. A., Gonzalo, J. A., Henson, P. M., & Worthen, G. S. (2004). Role of the CXCR4/SDF-1 chemokine axis in circulating neutrophil homeostasis. *Blood*, *104*(2), 565–571. https://doi.org/10.1182/blood-2003-10-3638

Swirski, F. K., Nahrendorf, M., Etzrodt, M., Wildgruber, M., Cortez-Retamozo, V., Panizzi, P., Aikawa, E., Mempel, T., Libby, P., Weissleder, R., & Pittet, M. J. (2009). Identification of Splenic Reservoir Monocytes and Their Deployment to Inflammatory Sites. *Science*, *325*(7), 612–616.

Takahashi, D., Fujihara, M., Miyazaki, T., Matsubayashi, K., Sato, S., Azuma, H., Kato, T., Kino, S., Ikeda, H., Takamoto, S., Sato, N., & Torigoe, T. (2017). Flow cytometric quantitation of platelet phagocytosis by monocytes using a pH-sensitive dye, pHrodo-SE. *Journal of Immunological Methods*, *447*(8), 57–64. https://doi.org/10.1016/j.jim.2017.04.009

Tanaka, H., Fukui, H., Fujii, S., Sekikawa, A., Yamagishi, H., Ichikawa, K., Tomita, S., Imura, J., Yasuda, Y., Chiba, T., & Fujimori, T. (2011). Immunohistochemical Analysis of REG Ia Expression in Ulcerative Colitis-Associated Neoplastic Lesions. *Digestion*, *83*(1), 204–209. https://doi.org/10.1159/000321808

Tanno, T., Noel, P., & Miller, J. L. (2010). Growth differentiation factor 15 in erythroid health and disease. *Current Opinion in Hematology*, *17*(3), 184–190. https://doi.org/10.1097/MOH.0b013e328337b52f

Tatin, F., Renaud-Gabardos, E., Godet, A.-C., Hantelys, F., Pujol, F., Morfoisse, F., Calise, D., Viars, F., Valet, P., Masri, B., Prats, A.-C., & Garmy-Susini, B. (2017). Apelin modulates pathological remodeling of lymphatic endothelium after myocardial

infarction. *JCI Insight*, *2*(12), 1–16. https://doi.org/10.1172/jci.insight.93887

Terazono, K., Yamamoto, H., Takasawa, S., Shiga, K., Yonemura, Y., Tochino, Y., & Okamoto, H. (1988). A novel gene activated in regenerating islets. *Journal of Biological Chemistry*, *263*(5), 2111–2114. https://doi.org/10.1016/s0021-9258(18)69176-8

Tie, R., Li, H., Cai, S., Liang, Z., Shan, W., Wang, B., Tan, Y., Zheng, W., & Huang, H. (2019). Interleukin-6 signaling regulates hematopoietic stem cell emergence. *Experimental and Molecular Medicine*, *51*(10), 1–12. https://doi.org/10.1038/s12276-019-0320-5

Trincot, C. E., Xu, W., Zhang, H., Kulikauskas, M. R., & Caranasos, T. G. (2018). Adrenomedullin Induces Cardiac Lymphangiogenesis After Myocardial Infarction and Regulates Cardiac Edema Via Connexin 43. *Circulation Research*, *124*(1), 101–113. https://doi.org/10.1161/CIRCRESAHA.118.313835

Unno, M., Nata, K., Noguchi, N., Narushima, Y., Akiyama, T., Ikeda, T., Nakagawa, K., Takasawa, S., & Okamoto, H. (2002). Production and Characterization of Reg Knockout Mice Reduced Proliferation of Pancreatic-Cells in Reg Knockout Mice. *Diabetes*, *51*(3), S478–S483. http://diabetesjournals.org/diabetes/article-pdf/51/suppl_3/S478/371909/db12t200s478.pdf

Vafadarnejad, E., Rizzo, G., Krampert, L., Arampatzi, P., Arias-Loza, A. P., Nazzal, Y., Rizakou, A., Knochenhauer, T., Bandi, S. R., Nugroho, V. A., Schulz, D. J. J., Roesch, M., Alayrac, P., Vilar, J., Silvestre, J. S., Zernecke, A., Saliba, A. E., & Cochain, C. (2020). Dynamics of Cardiac Neutrophil Diversity in Murine Myocardial Infarction. *Circulation Research*, *127*(9), E232–E249. https://doi.org/10.1161/CIRCRESAHA.120.317200

Van Ba, I. A. T., Marchal, S., François, F., Silhol, M., Lleres, C., Michel, B., Benyamin, Y., Verdier, J. M., Trousse, F., & Marcilhac, A. (2012). Regenerating islet-derived 1α (Reg-1α) protein is new neuronal secreted factor that stimulates neurite outgrowth via exostosin tumor-like 3 (EXTL3) receptor. *Journal of Biological Chemistry*, *287*(7), 4726–4739. https://doi.org/10.1074/jbc.M111.260349

Van Beelen, A., Østvik, A. E., Brenna, Ø., Torp, S. H., Gustafsson, B. I., & Sandvik, A. K. (2013). REG gene expression in inflamed and healthy colon mucosa explored by in situ hybridisation. *Cell Tissue Res*, *352*(3), 639–646. https://doi.org/10.1007/s00441-013-1592-z

Vélez, E. J., Capilla, E., & Lutfi, E. (2023). Editorial: Inter-organ communication beyond mammals: the role of tissue-specific cytokines. *Frontiers in Endocrinology*, *14*(5), 1–2. https://doi.org/10.3389/fendo.2023.1208000

Vieira, J. M., Norman, S., Del Campo, C. V., Cahill, T. J., Barnette, D. N., Gunadasa-Rohling, M., Johnson, L. A., Greaves, D. R., Carr, C. A., Jackson, D. G., & Riley, P. R. (2018). The cardiac lymphatic system stimulates resolution of inflammation following myocardial infarction. *Journal of Clinical Investigation*, *128*(8), 3402–3412. https://doi.org/10.1172/JCI97192

Von Andrian, U. H., & Mempel, T. R. (2003). Homing and cellular traffic in lymph nodes. *Nature Reviews Immunology*, *3*(11), 867–878. https://doi.org/10.1038/nri1222

Vuorio, T., Ylä-Herttuala, E., Laakkonen, J. P., Laidinen, S., Liimatainen, T., & Ylä-Herttuala, S. (2018). Downregulation of VEGFR3 signaling alters cardiac lymphatic vessel organization and leads to a higher mortality after acute myocardial infarction. *Scientific Reports*, *8*, 16709. https://doi.org/10.1038/s41598-018-34770-4

Wang, J., Hossain, M., Thanabalasuriar, A., Gunzer, M., Meininger, C., & Kubes, P. (2017). Visualizing the function and fate of neutrophils in sterile injury and repair. *Science*, *358*(6359), 111–116. https://doi.org/10.1126/SCIENCE.AAM9690

Weil, B. R., & Neelamegham, S. (2019). Selectins and immune cells in aucte mycardial infarction and post-infarction ventricular remodelings: Pathophysiology and novel treatments. *Frontiers in Immunology*, *10*(2), 1–15. https://doi.org/10.3389/fimmu.2019.00300

Wilson, L. F. L., Dendooven, T., Hardwick, S. W., Echevarría-Poza, A., Tryfona, T., Krogh, K. B. R. M., Chirgadze, D. Y., Luisi, B. F., Logan, D. T., Mani, K., & Dupree, P. (2022). The structure of EXTL3 helps to explain the different roles of bi-domain exostosins in heparan sulfate synthesis. *Nature Communications*, *13*(1), 1–15. https://doi.org/10.1038/s41467-022-31048-2

Xie, C., Mao, X., Huang, J., Ding, Y., Wu, J., Dong, S., Kong, L., Gao, G., Li, C. Y., & Wei, L. (2011). KOBAS 2.0: A web server for annotation and identification of enriched pathways and diseases. *Nucleic Acids Research*, *39*(SUPPL. 2), 316–322. https://doi.org/10.1093/nar/gkr483

Xiong, X., Wang, X., Li, B., Chowdhury, S., Lu, Y., Srikant, C. B., Ning, G., & Liu, J. L. (2011). Pancreatic islet-specific overexpression of Reg3β protein induced the expression of pro-islet genes and protected the mice against streptozotoc in induced diabetes mellitus. *American Journal of Physiology - Endocrinology and Metabolism*, *300*(4), 669–680. https://doi.org/10.1152/ajpendo.00600.2010

Xiong, Y., Brinkman, C. C., Famulski, K. S., Mongodin, E. F., Lord, C. J., Hippen, K. L., Blazar, B. R., & Bromberg, J. S. (2017). A robust in vitro model for trans-lymphatic endothelial migration. *Scientific Reports*, *7*(1633), 1–14.

https://doi.org/10.1038/s41598-017-01575-w

Xu, C., Gao, X., Wei, Q., Nakahara, F., Zimmerman, S. E., Mar, J., & Frenette, P. S. (2018). Stem cell factor is selectively secreted by arterial endothelial cells in bone marrow. *Nature Communications*, *9*(1), 1–13. https://doi.org/10.1038/s41467-018-04726-3

Xuan, W., Qu, Q., Zheng, B., Xiong, S., & Fan, G.-H. (2015). The chemotaxis of M1 and M2 macrophages is regulated by different chemokines. *Journal of Leukocyte Biology*, *97*(1), 61–69. https://doi.org/10.1189/jlb.1A0314-170R

Yan, Y., Chen, R., Wang, X., Hu, K., Huang, L., Lu, M., & Hu, Q. (2019). CCL19 and CCR7 Expression, Signaling Pathways, and Adjuvant Functions in Viral Infection and Prevention. *Frontiers in Cell and Developmental Biology*, *7*(10), 1–13. https://doi.org/10.3389/fcell.2019.00212

Yuan, R.-H., Jeng, Y.-M., Chen, H.-L., Hsieh, F.-J., Lee, P.-H., & Hsu, H.-C. (2005). Opposite Roles of Human Pancreatitis-Associated Protein and REG1A Expression in Hepatocellular Carcinoma: Association of Pancreatitis-Associated Protein Expression with Low-Stage Hepatocellular Carcinoma, B-Catenin Mutation, and Favorable Prognosis. *Imaging, Diagnosis, Prognosis*, *11*(7), 2568–2575. https://doi.org/10.1158/1078-0432.CCR-04-2039

Yuan, Z., Syed, A., Panchal, D., Joo, M., Colonna, M., Brantly, M., & Sadikot, R. T. (2014). Triggering Receptor Expressed on Myeloid Cells 1 (TREM-1)-mediated Bcl-2 Induction Prolongs Macrophage Survival. *Journal of Biological Chemistry*, *289*(21), 15118–15129. https://doi.org/10.1074/jbc.M113.536490

Zhu, C., Rajendran, P. S., Hanna, P., Efimov, I. R., Salama, G., Fowlkes, C. C., & Shivkumar, K. (2022). High-resolution structure-function mapping of intact hearts reveals altered sympathetic control of infarct border zones. *JCI Insight*, *7*(3), 1–13. https://doi.org/10.1172/jci.insight.153913

13 SUPPLEMENTARY MATERIAL

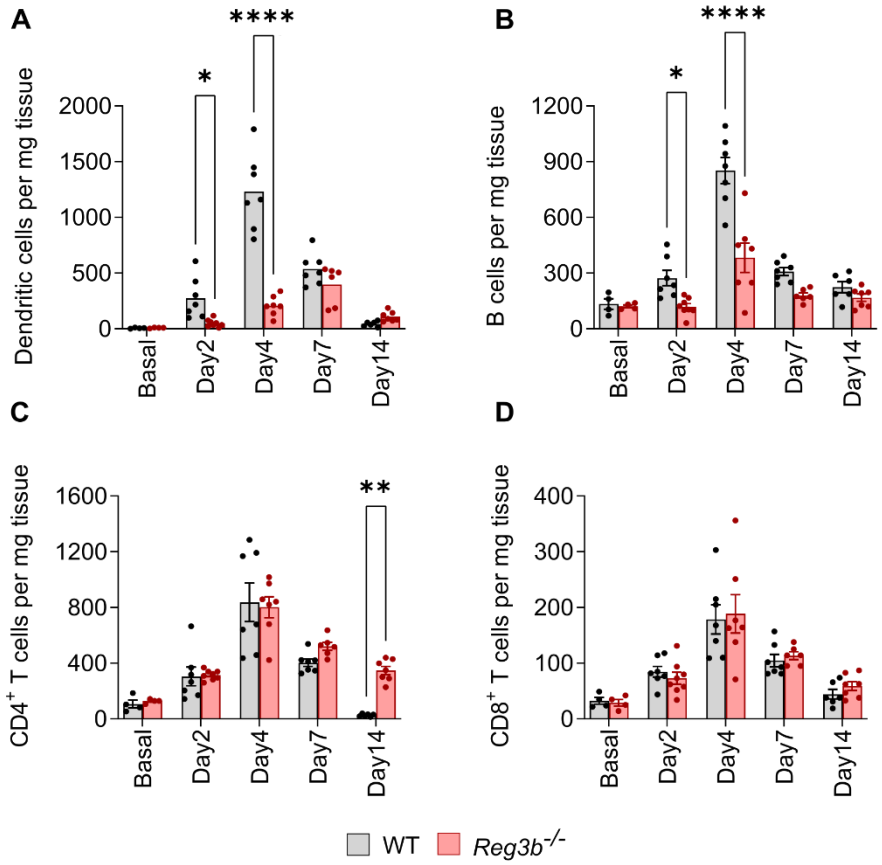

Supplementary Figure 1. Kinetic analysis of immune cells of the adaptive arm of the immune system in WT and *Reg3b*$^{-/-}$ infarcted hearts. Kinetics of **(A)** dendritic cells, **(B)** B cells, **(C)** CD4^{+} T cells and **(D)** CD8^{+} T cells per mg of tissue in WT and *Reg3b*$^{-/-}$ hearts. Data are shown as mean ± SEM. N = 4 (basal), 6 (day 14) or 7 (days 2,4,7). Statistical analysis: Two-way ANOVA followed by Šidák multiple comparisons test. *p ≤ 0,05 ;** p ≤ 0,01 ; *** p ≤ 0,001 ; **** p ≤ 0,0001.

14 LIST OF PUBLICATIONS

Lörchner, H.; Canes, L. E.; **Góes, M.E.**; et al. Neutrophils for revascularization require activation of CCR6 and CCL20 by TNF-a. Cardiovascular Research. 2023.

Lörchner, H.; Adrian-Segarra, J.M.; Wächter, C.; Wagner, R.; **Góes, M.E.**; et al. Concomitant Activation of OSM and LIF Receptor by a Dual-Specific hlOSM Variant Confers Cardioprotection after Myocardial Infarction in Mice. IJMS. 2021.

Cruvinel, E.; Ogusuku, I.; Cerioni, R.; Gonçalves, J.; **Góes, M.E**.; et al. Long-term single-cell passaging of human iPSCs fully supports pluripotency and high-efficient trilineage differentiation capacity. SAGE Open Medicine. 2020.

15 EHRENWÖRTLICHE ERKLÄRUNG

„Hiermit erkläre ich, dass ich die vorliegende Arbeit selbständig und ohne unzulässige Hilfe oder Benutzung anderer als der angegebenen Hilfsmittel angefertigt habe. Alle Textstellen, die wörtlich oder sinngemäß aus veröffentlichten oder nichtveröffentlichten Schriften entnommen sind, und alle Angaben, die auf mündlichen Auskünften beruhen, sind als solche kenntlich gemacht. Bei den von mir durchgeführten und in der Dissertation erwähnten Untersuchungen habe ich die Grundsätze guter wissenschaftlicher Praxis, wie sie in der „Satzung der Justus-Liebig-Universität Gießen zur Sicherung guter wissenschaftlicher Praxis“ niedergelegt sind, eingehalten sowie ethische, datenschutzrechtliche und tierschutzrechtliche Grundsätze befolgt. Ich versichere, dass Dritte von mir weder unmittelbar noch mittelbar geldwerte Leistungen für Arbeiten erhalten haben, die im Zusammenhang mit dem Inhalt der vorgelegten Dissertation stehen, und dass die vorgelegte Arbeit weder im Inland noch im Ausland in gleicher oder ähnlicher Form einer anderen Prüfungsbehörde zum Zweck einer Promotion oder eines anderen Prüfungsverfahrens vorgelegt wurde. Alles aus anderen Quellen und von anderen Personen übernommene Material, das in der Arbeit verwendet wurde oder auf das direkt Bezug genommen wird, wurde als solches kenntlich gemacht. Insbesondere wurden alle Personen genannt, die direkt und indirekt an der Entstehung der vorliegenden Arbeit beteiligt waren. Mit der Überprüfung meiner Arbeit durch eine Plagiatserkennungssoftware bzw. ein internetbasiertes Softwareprogramm erkläre ich mich einverstanden.“

_____ _____

Ort/Datum Unterschrift

16 ACKNOWLEDGMENTS

First and foremost, I would like to thank all my supervisors for guiding me through the each chapters of this thesis. Thank you Prof. Dr. Thomas Braun for inviting me to do the PhD in your laboratory, and for the engaging discussions in all the lab seminars. Thank you for the trust during the long phase when results were paradoxical and we could not understand where they were leading us. Thank you Prof. Dr. Jochen Pöling and Dr. Holger Lörchner for having me in your group and offering unlimited support throughout these years. I recognize all the time, energy and attention you have given to me and to this project since the beginning. I thank you especially for standing next to me during the difficult first 18 months of this journey. I sometimes can still not believe how much our work and personal relations improved so much throughout time. I have to say, this contributed immensely to my well-being here and to the completion of this project. You are great leaders and really complement each other in your work.

I want to acknowledge all the love and support from my family: Carlos, Glória and Maria Clara. I am so lucky to have you next to me during my 32 years of life. You show me the meaning of unconditional love and support every day. I know many times you could not understand what I was doing, or why I was doing this at all, but you have still supported my decisions no matter what. I miss sharing a life with you. It hurts to be far, but we count every single day until we meet again, and this time is not different. I love you.

I thank the members of AG Pöling for creating a great work atmosphere and for the incredible teamwork. We have eaten many delicious cakes together, and although unforgettable, there are other memories that I prefer to mention here. I thank Roxanne Wagner for doing the surgeries in this project. Without you, we would have not finished this project. I wish you all the best with your future plans! Dr. Laia Cañes Esteve, I am incredibly happy you joined this group and my life. You have been the most incredible co-worker I could have asked for. I wish I could have been able to reciprocate all you did for me during these years. You are an amazing scientist and so incredibly good in everything you do. I can only wish you all the success in your career and I hope we will take our friendship for many years still. I thank Nathalie Brachmann for being a great support since the very first day on the lab. You are a great office mate and I really appreciate all the pleasant conversations and technical support you have given us during the years. Thanks to Lucia Camacho Pulido for

taking over the last surgeries of the project, and showing the true meaning of team spirit! I wish you a smooth journey throughout your own PhD.

Antonella Carozzi, Magnus Andresen and Sam Hamberger: you also contribute(d) a lot to the great atmosphere in the group. I am so happy to have co-workers who are always in a good mood and want to learn and participate. I wish you good luck with your theses. May your journeys be smooth and successful! I thank Sam and Linda Hannak for all the nice conversations and all your help sectioning hearts. You helped in a moment when I needed the most and I will never forget it. Indeed, Linda, it has been an unforgettable pleasure to have you as my first student, and I will always vibrate for your success! I also thank the former lab members for their continuous support and contribution to a great work environment: Johanna Schubert, Sophia Schlattner, Dr. Christian Wächter, Dr. Juan Segarra, Dr. Praveen Gawajada and Jutta Wetzel. Also special thanks to Dr. Julia Detzer for showing me how to prepare samples for light sheet microscopy and teaching me how to use the microscopes where I sat for so many hours of my life.

I have to dedicate a paragraph for three friends that Max Planck brought to my life, and have been always open ears and stood next to me during all these years. Ágatha Ribeiro, my twin from another mother: sometimes it is hard to believe we lived in the same city for a full decade and only met each other in Bad Nauheim. You have been the most amazing friend I could ever ask for. Friends like you are unique in a lifetime. Chiara Mura, what an amazing pleasure have I had to share an apartment with you. You brought joy to my life on a daily basis for two years. What an incredible personality and company! I wish we had had even more time together. Adriana Vucetic, you were my first friend in Bad Nauheim, and together we explored and learned so much. I will not forget all our adventures together and how our personalities clicked so fast. I wish we will take this friendship for many years to go.

I also acknowledge the technical support I had from many incredible and competent colleagues in the institute. Dr. Kenny Mattonet and Dr. Srinath Ramkumar, thanks for all the help in the Imaging facility. You built something great and you should be proud of it! I deeply acknowledge the work of the RNAseq facility and Bioinformatics facility, special Dr. Stefan Günther and Dr. Carsten Kuenne. Thanks Susanne Martin to all the organizational support and listening attentive to all our needs. Thanks to all technicians, IT team and staff in MPI Bad Nauheim who make this laboratory function so well. Thanks to Karin Laurentius for

illuminating our days with the warmest good mornings, even on the rainiest days. Very special thanks to all the animal caretakers who take so good care of our mice and enable us to do this work.

Thanks for friends with whom I shared so many good moments during the years: Gabrielius Jakutis, Pooja Sagvekar and Mário Ferreira, it has been great to share an apartment and life with you. You have been great friends and company! Poonam, Shahriar, Salma, thanks for integrating me in the AG Braun and for the nice conversations. Sissi and Kathy, I am so happy to have you next to me! Ana Paula, Ágatha and Juliana, my amazing friends in three continents. Now we know we can keep oversea friends as long as there is a lot of love involved. Isabella and Taís, I am happy we could meet again in Germany and strengthen our friendships even more.

I have had the pleasure to be involved in Max Planck-wide initiatives and met very engaged people with whom I brought several nice projects forward: Sabine Ziegler, Anne Grewlich-Gerke, Alicia, Osama, Liza, Franziska and Jaswanth.

I thank Prof. Dr. Ebba Brakenhielm for the engaging conversations in scientific conferences and Prof. Dr. Kari Alitalo for sharing mouse lines and AAV constructs used in this project. I thank the external TAC members, Prof. Dr. Michael Potente and Prof. Dr. Norbert Weissmann for the input and feedback during the TAC meetings.

Finally, I want to mention and acknowledge the fact that animal lives were employed in this project. It is never easy to work with animals, and we have to distance ourselves emotionally from this process in order to do it. I tried to do this with as much respect as I could, but it is still important to make it clear that without the little ones, our scientific progress would be so limited, and we should be very aware and thankful to that.

Maria Elisa Almeida Góes